SENSITIVITY-BASED UPSCALING FOR LARGE SCALE RESERVIOR MODEL HISTORY MATCHING

BY

SAAD MEHMOOD

A Thesis Presented to the
DEANSHIP OF GRADUATE STUDIES

KING FAHD UNIVERSITY OF PETROLEUM & MINERALS
DHAHRAN, SAUDI ARABIA

In Partial Fulfillment of the
Requirements for the Degree of

MASTER OF SCIENCE

In

PETROLEUM ENGINEERING

December, 2013

KING FAHD UNIVERSITY OF PETROLEUM & MINERALS

DHAHRAN- 31261, SAUDI ARABIA

DEANSHIP OF GRADUATE STUDIES

This thesis, written by **SAAD MEHMOOD** under the direction of his thesis advisor and approved by his thesis committee, has been presented and accepted by the Dean of Graduate Studies, in partial fulfillment of the requirements for the degree of **MASTER OF SCIENCE IN PETROLEUM ENGINEERING.**

Dr. Abeeb A. Awotunde
(Advisor)

Dr. Abdullah Sultan
Department Chairman

Dr. Hasan Y. Al-Yousef
(Member)

Dr. Salam A. Zummo
Dean of Graduate Studies

Dr. Roland N. Horne
(Member)

13/1/14
Date

Dedication

To my dear parents for their immense faith and love,

my loving sisters for always being my strength,

and sweet young nephew for his affection

ACKNOWLEDGMENTS

I humbly thank to Almighty ALLAH for His shower of blessings and for making me able to complete this research successfully.

I want to express my gratitude to my thesis advisor Dr. Abeeb A. Awotunde for his continual support, insight and guidance throughout this work. He has helped me overcome numerous problems and obstacles that came during the journey of this work. I would also like to thank the committee members that includes Dr. Hasan Y. Al. Yousef and Dr. Roland N. Horne for their visionary suggestions and recommendations, which has made this project possible.

I would also like to sincerely thank all the faculty members of the Petroleum Engineering Department at KFUPM, particularly the Chairman of the department, Dr. Abdullah S. Sultan. They have helped me in growth of my educational and research attributes, and have extended their support whenever needed.

I want to acknowledge my friends in KFUPM who have always supported me and have made my stay in the university memorable. I want to particularly mention Zaeem Hassan Khan, Sarmad Zafar, Babar Kamal, Zaid Zaffar, Mobeen Murtaza, Yousuf Jabbar, Abdul Hafeez, Arbab Latif, Haider Ali, Hassaan Ahmed and last but in no way the least Asim Akhter, for their encouragement and help.

At last, I would like to thank all my teachers from my school to this level of professional education, because all of them have their contribution in whatever I have achieved so far in my life.

TABLE OF CONTENTS

LIST OF TABLES

LIST OF FIGURES

NOMENCLATURE

Variables

A	=	area of the polygon used for centroid calculation
$\vec{c}$	=	wavelet coefficients
C_D	=	data covariance
C_M	=	model covariance
c_o	=	isothermal compressibility of oil
c_w	=	isothermal compressibility of water
C_x	=	*x*-coordinate of the centroid
C_y	=	*y*-coordinate of the centroid
$\tilde{D}_{cal}$	=	matrix of calculated data
$\tilde{D}_{cal,w}$	=	2D wavelet transform of calculated data matrix
$\vec{d}_{cal}$	=	calculated data
$\tilde{D}_{meas}$	=	matrix of measured data
$\tilde{D}_{meas,w}$	=	2D wavelet transform of measured data matrix

$\vec{d}_{meas}$ = measured data

$\dot{f}$ = probability density function

$\vec{f}$ = vector of residual for flow equations

$\vec{g}$ = gradient of objective function

H = Hessian matrix

J = Jacobian matrix

$\vec{k}$ = permeability distribution

N = number of time steps

p_c = capillary pressure

p_o = pressure of oil phase

p_{wf} = wellbore pressure

$q_{ph,j}^{well}$ = volumetric well rate of phase *ph* at the j^{th} completion

$\vec{s}$ = Newton direction

S = sensitivity matrix

S_w = water saturation

$\vec{u}$ = vector of state variables

$\vec{v}$ = vector of known reservoir properties

W = wavelet matrix

WI = well index

Greek Symbols

$\vec{\alpha}$ = reservoir parameters

Φ = objective function

κ = iteration index

λ_{ph} = mobility of any phase *ph*

$\dot{\lambda}$ = Levenberg-Marquardt parameter

γ_{ph} = specific gravity of any phase *ph*

φ = porosity

Subscripts

cal = calculated

D = data space

ini = initial

M = model space

meas = measured

o	=	oil
ph	=	phase (water or oil)
pri	=	prior
w	=	water

Superscripts

n	=	time step index
T	=	transpose

Other Symbols

$\mathfrak{N}$	=	Normal distribution

ABSTRACT

Full Name : [Saad Mehmood]

Thesis Title : [Sensitivity-based Upscaling for Large-Scale Reservoir Model History Matching]

Major Field : [Petroleum Engineering]

Date of Degree: [December, 2013]

Simulation of reservoir flow processes at the finest scale is computationally expensive and in some cases impractical. Consequently, upscaling of several fine scale grid blocks into fewer coarse-scale grids has become an integral part of reservoir simulation for most reservoirs. This is because as the number of grid blocks increases, the number of equations increases and this increases, in large proportions, the time required for solving flow problems. Even though we can adopt parallel computations to share the load, still a large number of grid blocks poses significant computational challenges. Thus, upscaling acts as a bridge between the reservoir scale and the simulation scale. However as the upscaling ratio is increased the accuracy of the numerical simulation is reduced, hence the need to keep a balance between the two.

The objective of this thesis is to present a sensitivity-based upscaling during history-matching. This work involves the introduction of an upscaling technique and evaluation of its application in different scenarios. The technique that will be adopted in this study is based on the wavelet transformation and reduction of the data and model spaces as presented in the 2Dwp-wk approach. In the 2Dwp-wk approach, a set of wavelets of

measured data is first selected and then a reduced model space composed of important wavelets is gradually built during the first few iterations of nonlinear regression. The building of the reduced model space is done by thresholding the full wavelet sensitivity matrix. In our work, the distribution of permeability in the reservoir after thresholding of the full wavelet sensitivity matrix would be used to determine the neighboring grids that would be upscaled. Neighboring grid blocks having the same permeability values due to model space reduction would be combined into single grid block in the simulation model, thus integrating upscaling with wavelet multi-scale inverse modeling.

The history matching results obtained using sensitivity-based upscaling are reasonably good. They are also found to be in very close agreement of the match provided by fine-scale inverse analysis. The reliability of the technique is evaluated using various scenarios and almost all the cases considered have shown good results.

ملخص الرسالة

الاسم الكامل: سعد محمود

عنوان الرسال: تكبير حجم التجزئة في عملية توافق تواريخ الإنتاج في محاكاة الخزانات الكبيرة بناء على دراسة حساسية المتغيرات

التخصص: هندسة البترول

تاريخ الدرجة العلمية: ديسمبر 2013

إن محاكاة عمليات تدفق السوائل على مستوى دقيق جداً تستهلك جهداً كبيراً في حسابها وتصبح أحياناً غير عملية أو مجدية. ولذلك أصبح تجزئة الخزان إلى أجزاء أكبر بأعداد أقل جزءاً رئيسياً في محاكاة معظم الخزانات. وذلك لأنه كلما زاد عدد أجزاء الخزان، كلما زادت المعادلات الرياضية المطلوبة وبالتالي يزيد الوقت المطلوب لحلها واتمام عملية المحاكاة. حتى وإن استخدمنا نظام المعالجة المتوازي لتوزيع أحمال الحسابات، فإنه يظل العدد الكبير لأجزاء الخزان يشغل وقت وتحدي كبيرين. تعمل عملية تكبير أجزاء الخزان (وتقليل عددها) كجسر يصل بين مقياس الخزان الحقيقي والمقياس المستخدم في عملية المحاكاة. ولكن كلما زادت النسبة المستخدمة في تكبير حجم أجزاء الخزان، كلما قلت دقة عملية المحاكاة. وهنا تبرز أهمية حفظ التوازن بين النقطتين.

تهدف هذه الدراسة إلى تقديم دراسة مبنية على حساسية المتغيرات في عملية تكبير أجزاء الخزان أثناء تنفيذ عملية تطابق التواريخ. يتضمن العمل تقديم أسلوب للقيام بعملية تكبير أجزاء الخزان وكذلك تقييم استخداماته في صور وحالات مختلفة ومتنوعة. الأسلوب المستخدم في هذه الدراسة يعتمد على عملية تحويل الموجات، وكذلك على تقليل فضاءات البيانات والنموذج كما هو مستخدم في اسلوب (2Dwp-wk). في اسلوب (2Dwp-wk)، يتم في البداية اختيار مجموعة من الموجات الخاصة ببيانات تم قياسها، ثم يتم تدريجياً استخدام الموجات المهمة منها في بناء فضاء أبسط للنموذج، وذلك خلال المراحل الأولى من عملية التكرار الخاصة بالمعالجة الغير خطية. تتم عملية بناء الفضاء المبسط الخاص بالنموذج عن طريق تنقيح المصفوفة الكاملة الخاصة بحساسية الموجات. في هذا العمل، بعد إتمام عملية تنقيح المصفوفة الكاملة الخاصة بحساسية الموجات، يتم استخدام قيم النفاذية الموزعة في الخزان لتحديد الأجزاء المجاورة التي سيتم تكبيرها. يتم دمج الأجزاء المجاورة والتي لها نفس قيم النفاذية (نتيجة انشاء فضاء النموذج المبسط) في جزء واحد، وبهذا يتم دمج عملية تكبير أجزاء النموذج مع النموذج العكسي الخاص بالموجات متعددة القياس.

النتائج التي حصلنا عليها في عملية مطابقة التواريخ باستخدام تقنية تكبير أجزاء الخزان بالاعتماد على دراسة حساسية المتغيرات تعتبر جيدة جداً. وهي تعطي نتائج قريبة جداً من تلك التي نحصل عليها عند العمل على أجزاء صغيرة (ولكن تلك الأخيرة تستخدم وقت وجهد معالجة أكثر بكثير). تم تقييم إمكانية الاعتماد على هذه الطريقة باستخدام ظروف وحالات متعددة، وقد أعطت الطريقة نتائج جيدة في معظم الحالات.

CHAPTER 1

INTRODUCTION

Upscaling is the process of reducing large number of the fine-scale grid blocks to fewer number of coarse-scale grid blocks. This is required because it is often impractical to perform simulation at finest scale of the reservoir. Therefore, upscaling is one of the most important component of reservoir simulation. The last few decades have seen significant advancements in upscaling which include development of single-phase and multi-phase upscaling as well as upscaling in the near wellbore and away from wellbore regions. Single-phase upscaling involves the upscaling of permeability distribution only. The technique is simple and can be used for structurally complex reservoirs but it neglects the multiphase flow effects (Durlofsky, 1991; Ringrose, 2007). In multiphase flow upscaling, relative permeability curves are also upscaled in addition to absolute permeability upscaling. This approach is computationally expensive and as such its use is limited to simple reservoir models (Ekrann and Dale, 1992; Ringrose, 2007).

One method of upscaling involves averaging the data and including it directly into the simulation flow grid. Most of the averaging techniques (arithmetic, harmonic, geometric, power law, pressure solver) are only appropriate under the circumstances of perfectly layered or heterogeneous distributions that is perfectly random, which is seldom observed in realistic reservoir descriptions. A relatively new averaging technique first computes the lower and upper bounds of the effective properties, based on geology, and then uses a

new correlation and scaling technique to estimate the effective properties for the upscaled grid (Li, Beckner and Kumar, 2001). The issue with simple averaging is that it may provide upscaled fluid and reservoir properties that are not representative of fine-scale properties. It also ignores the data sampling effects that can lead to gross errors (Ringrose, 2007). Purely local upscaling methods consider only those fine-scale grids that are combined in the target coarse-scale grid (Durlofsky, 1991; King and Mansfield, 1999). Extended local procedure includes few of the adjacent grids in the local problems (Gómez-Hernández and Journel, 1994; Wu et al., 2002). However both of these procedures can lead to inaccurate results in some scenarios, as they need assumptions regarding the boundary conditions to be applied. Specifically, in local and extended local methods, usually the boundary conditions that are applied on the local well model can affect the upscaled parameters and these boundary conditions depend on global flow and are not, therefore known a priori. In global upscaling methods, the flow solution utilized to calculate the upscaled parameters is performed over the entire domain (White and Horne, 1987; Pickup et al., 1992; Holden and Nielson, 2000). This technique can provide high level of accuracy, but it has a shortfall of requiring global fine-scale solutions.

In local-global upscaling approach, global coarse-scale simulations are performed to obtain the local boundary conditions that are utilized for upscaling computations (Chen and Durlofsky, 2006a; Gerritsen and Lambers, 2008). The original local-global procedure was applied to single-phase upscaling, but Chen and Li (2009) extended the approach to multiphase oil-water system. An adaptive local-global procedure has also been proposed for multiphase near-well problems (Nakashima, 2009). Adaptive means that the actual boundary conditions are applied for global coarse-scale simulations rather than the

generic set of boundary conditions. Adaptive local-global upscaling technique involves global coarse-scale simulation with initial estimates for well-block parameters which provides the coarse-block pressure and saturations. This resultant pressure and saturation distribution is then interpolated onto the local well model to obtain boundary conditions for the near-well upscaling computations. The purpose of all these researches is to capture the physics of single-phase flow, multi-phase flow and the effects of various regions in the modeling of reservoir response upon coarsening the simulation models. The established upscaling techniques require the coarse-scale permeabilities to be determined separately and this requires an additional computational time. However, there has been no forward model upscaling method combined with history matching that is based-on wavelet sensitivity thresholding.

History matching has long been used to estimate reservoir parameters from dynamic production history data. However, a limitation of this procedure is that it is often the case that the information content of the production histories not enough to resolve the model parameters at the finest scale. Thus, different methods of model space reduction have been proposed in the literature to reduce the number of model parameters to be estimated from the production history, thereby reducing the non-uniqueness associated with the inverse modeling. One such model reduction method is wavelet multiscale inverse analysis such as those proposed by Lu and Horne, 2000; Sahni and Horne, 2005 & 2006; Awotunde and Horne, 2012 & 2013. In parameter estimation involving model space reduction the actual model parameter field often combined to form smaller parameter space comprising fewer model coefficients than the original space. This procedure is a form of upscaling but in the sense of inverse analysis. The various methods of model

space reduction often automatically produce some level of smoothening (homogenization) of the reservoir model parameters such as gridblock permeabilities. This smoothening creates a scenario in which several adjacent gridblocks have same permeability values. However, during such history matching procedures, forward simulation run are still done at the finest scale (Lu and Horne, Sahni and Horne, Awotunde and Horne). In this way, a huge time of time is spent on forward simulation. The purpose of this thesis is to utilize the pattern of smoothening in the permeability field created by model space reduction during history matching, to upscale the forward simulation model with an ultimate goal of reducing the total time required for history matching.

In this study we propose and evaluate an upscaling procedure based on wavelet sensitivity thresholding. Sensitivity-based thresholding has been used in the literature to reduce model parameter space during history matching (Sahni and Horne, 2006; Awotunde and Horne, 2012). Sensitivity computation is required for computing the Hessian matrix in the Gauss-Newton and Levenberg-Marquardt algorithms (Gill et al., 1981; Nocedal and Wright, 2006; Griva et al., 2009). In addition, sensitivity matrix has been used for reducing the model space. One of the features of such model reduction is the emergence of several neighboring grids with similar values of reservoir model parameter; in this case the permeability.

The upscaling methods proposed in the literature involve the computation of the upscaled permeability field which should be representative of the fine scale permeability distribution. In most cases, however, the upscaled permeability field does not accurately represent the fine-scale permeability distribution. The major objective of this thesis is to

propose use of the wavelet sensitivity thresholding to obtain the pattern in which reservoir gridblocks should be combined during inverse modeling. This process will avoid the requirement of coarse-scale permeability calculations because the areas of homogeneous permeability distribution would be determined by the sensitivity of production data to model parameters. This is important, because in conventional upscaling techniques substantial time is required for obtaining the coarse-scale gridblock permeabilities. Basically the method is based on the identification of the adjacent grids with similar permeabilities obtained from the model space reduction. The upscaling ratio will be based on the number of neighboring grids with equal permeability values.

The approach uses the thresholding of wavelet sensitivity matrix computed in early iterations of the 2Dwp-wk approach, to determine the reduced model space. The back-transformation of this obtained model space would identify the regions of homogeneity in the upscaled reservoir model. Combining the gridblocks based on the pattern obtained from the model reduction would result in a coarse-scale unstructured grid system. The method is expected to be more consistent as it predetermines the areas of the reservoir with homogeneous permeability distribution based on sensitivity analysis. To improve the accuracy of simulation results, gridblocks having wells completed in them will not be combined with any neighboring gridblock. Further, two scenarios would be tested; one in which all neighboring gridblocks with equal permeabilities but without any well would be combined. In the second scenario, the number of neighboring grids that can be combined into one simulation gridblock will be restricted regardless of pattern of homogenization. The second scenario is enforced to reduce the upscaling ratio and thereby improving the accuracy of results.

In order to investigate the effectiveness of this method, the proposed method would be applied to history matching two synthetic two-dimensional reservoir models with multiphase flow. The accuracy of the technique would be evaluated by comparing the results of the upscaled model to that obtained from fine scale model, with no history matching carried out in this case. Also, the actual history matching will be performed using the fine-scale forward simulation model as well as the coarse-scale forward simulation model proposed in this work and results from these two would be compared to check the reliability of the proposed technique.

1.1 Statement of the Problem

Reservoirs are often very large and performing simulation at the finest scale is usually not feasible as it would require huge computational time. Therefore, upscaling fine grids into manageable coarse grids has become an integral part of reservoir simulation. Although upscaling reduces the computational time required for simulation, it impacts negatively on the accuracy of simulation results. Thus, there is a trade-off between upscaling ratio and the reliability of simulation results.

Upscaling can be categorized into single-phase upscaling and multiphase upscaling. Single-phase upscaling involves only the upscaling of permeability distribution; while conventional approaches for multiphase scale-up, have in addition to absolute permeability upscaling, upscaling of relative permeabilities in order to capture the effects of geological heterogeneities. There are numerous procedures utilized: data averaging directly incorporated into the simulation flow grid or geological model, adaptive local-global upscaling, integration of renormalization and nonuniform coarsening with

upscaling of absolute and relative permeabilities and variable compact multipoint flux schemes. However in almost all the approaches, the upscaled permeability is also required to be calculated, and that upscaled gridblock permeability should be representative of the permeabilities of associated fine-scale gridblocks. This process of obtaining coarse-scale permeabilities requires an additional effort and computational time.

To the best of our knowledge, there has been no forward model upscaling method based-on wavelet sensitivity thresholding. In this work, sensitivity-based upscaling would be used during parameter estimation to reduce simulation time. The proposed method depends on the identification of neighboring grids with equal permeability values arising from the reduction of the model space during history matching. This reduction in model space is obtained by thresholding the wavelet sensitivity matrix computed as part of the 2Dwp-wk technique. After thresholding, the reduced model space (permeability) would be used to determine the pattern of coarsening the gridblocks. One advantage of this technique is that the computation of permeabilities for the upscaled gridblocks becomes unnecessary as the unique permeability for each coarse grid has already been determined by the wavelet sensitivity thresholding. This is an important point to note because in conventional upscaling significant time is devoted to determining the coarse-scale permeabilities. The technique is expected to be more reliable as it predetermines the regions of the reservoir with homogeneous permeability distribution based on the sensitivity of production data to reservoir permeability. To show the effectiveness of this method, a fine scale reservoir model would be considered for history matching and the proposed upscaling technique would be applied to reduce the number of gridblocks. The

reliability of the technique would be evaluated by comparing the results of the upscaled model with that obtained from fine scale model.

1.2 Research Objectives

The aim of this thesis is to devise an upscaling technique for reservoir model, based on wavelet sensitivity thresholding. The integration of the upscaling technique, forward modeling and history matching process is the focus of this work.

There has been much research work done related to upscaling but not based on wavelet sensitivity upscaling. The earlier works involve the calculation of upscaled permeability with the objective that it should be representative of the fine scale permeability. The objective of this work is to use the wavelet sensitivity thresholding to determine the manner of coarsening reservoir grid blocks during history matching. The procedure adopted will avoid the problem of computing coarse-scale permeabilities as the regions with homogeneous permeability distribution will be predetermined by wavelet sensitivity thresholding, an integral part of our history matching process. The homogeneous permeability patches determined by the wavelet sensitivity thresholding is expected to produce unstructured coarse-scale grids which will lead to the replacement of the structured fine-scale simulation.

CHAPTER 2

LITERATURE REVIEW

2.1 Upscaling

There are various levels of scale that are dealt in reservoir engineering: pore scale, core scale, geocellular scale, and flow simulation scale. Upscaling of the reservoir properties based on their grid structure is one of the prime steps in reservoir simulation. Upscaling techniques can be categorized in several ways as:

- Number of parameters (permeability, rock & fluid properties etc.)
- Reservoir regions (global, near-well)
- Domains employed for upscaling calculations (local, extended local, global)

The techniques developed so far for near-well upscaling, do not account for well-block pressure differences between fine and coarse scale models. Durlofsky (2005) has done a detailed classification of upscaling techniques. In broader perspective it can be divided into single-phase and multiphase upscaling.

2.1.1 Single-phase Upscaling

Basically it involves the upscaling of permeability distribution only. It is the general method of flow-based upscaling that includes calculation of fluxes from the fine simulation results and post-processing based on Darcy's law. In single-phase upscaling away from wells, the simplest set of boundary conditions is constant pressure-no flow but

also periodic boundary conditions can be applied to calculate full tensor coarse scale permeability (Durlofsky, 1991), and those tensors are always symmetric and positive definite. The extended local region can be used instead of the region only conforming to a single coarse block, while the comparison of purely local and extended local permeability upscaling procedures show that extended local techniques generally provided better accuracy. But in case of heterogeneous permeability, local and extended local both may not provide satisfactory coarse scale permeability, instead global fine-scale single-phase solutions with analytical relative permeability upscaling provide good results for this system (Holden and Lia, 1992; Wen et al., 2003; Zhang et al., 2008). It is also observed that transmissibility upscaling is more accurate and robust than permeability upscaling. Even though global upscaling provides high degree of accuracy but it is expensive in terms of computation and can be regarded as impractical for large reservoir models. The local-global approach proposed for upscaling addressed some of limitations of previous techniques and it has applications for two-phase relative permeabilities as well (Chen et al., 2003; Chen and Li, 2009).

The pressure distribution in well's vicinity is not linear, so an extended local region in wells' vicinity for the fine scale computations is needed for near-well upscaling. Also an averaging and flow based approach for well index upscaling with the utilization of flexible grids can be used (Durlofsky et al., 2000; Chen and Wu, 2008).

2.1.2 Multiphase Upscaling

The primary difference is that alongwith permeability distribution; it also includes the upscaling of relative permeability curves. Single phase upscaling primarily focusses on pressure equation while multiphase parameter upscaling is required when transport

phenomena are important. Two major approaches, dynamic-pseudo approaches and effective-property can be used for averaging flow properties (Ekrann and Dale, 1992). Dynamic pseudo approaches are based on fine scale simulation results of multiphase flow in whole (global) or a representative (local or extended local) portion of model. The effective property methods assume that the actual physical conditions can be approximated by limiting cases such as viscous-dominated and capillary dominated flow, in which case simplified solution procedures can be applied.

Transmissibility potential weighted method can be applied to simulation models for multiphase upscaling away from wells, and also steady state upscaling based on diffusion-convection-gravity equation can be implemented. Effective flux boundary conditions (EFBCs) in which a flux is assigned to each fine grid on the boundary of the target coarse block based on fine-cell and average or global permeability, are also found suitable (Darman et al., 1999; Stephen et al., 2001; Wallstrom et al., 2002). For the near-well upscaling, a mobility correction function that separates coarse grid effects and heterogeneity effects should be used. Also an optimization procedure for the computation of coarse scale relative permeability for oil-water system can be implemented but the drawback of the approach was in efficiency and robustness (Hui, 2005; Hui and Durlofsky, 2005).

2.1.3 Unstructured Grid System

The unstructured grids can be used with the utilization of control volume finite difference (CVFD) technique in order to deal with coning issues in both vertical and horizontal wells. A near-well upscaling procedure for single phase flow parameters can be

implemented for distorted grid systems as corner point geometry (Consonni et al., 1993; Ding, 2004).

2.1.4 Adaptive Local-Global Upscaling

Usually the boundary conditions that are applied on the local well model can affect the upscaled parameters. These boundary conditions depend on global flow and are not, therefore known a priori. In order to avoid this issue, an adaptive local-global procedure can be used that includes the global coarse-scale simulation with initial estimates for well-block parameters. The resultant pressure and saturation distribution is then interpolated onto the local well model to obtain boundary conditions for the near-well upscaling computations (Nakashima, 2009).

2.2 Reservoir Parameter Estimation

The process to determine the spatial distribution of reservoir properties particularly porosity and permeability (simply to generate a reservoir model) is known as reservoir characterization. The history matching is the process of modifying the reservoir model by matching the simulation production results with the actual field data. Earlier the process of reservoir characterization was done by hand, then progress was made and the industry shifted to analog computers. Nowadays with much more advancements and research, it's done with the utilization of high performance, high storage capacity computers. Also parallel processing is used to speed up the process and reduce the computational time.

Several researchers have worked in this area. Network and variational analysis (from electrical engineering) can be implemented for data integration during history matching and parameter estimation process. With more advancement the concept of gradient-based

techniques was expended for history-matching which involves the calculation of derivatives of pressure data with respect to reservoir parameters, these derivatives are known as sensitivity coefficients (Jacquard and Jain, 1960; Carter, Pierce, Kemp and William). It is followed by use of optimal control theory for directly computing the gradient of the objective function. The method was based on using the reservoir flow and adjoint equations (Chen, Gavalas, Seinfeld and Wasserman, 1974; Chavent, Dupuy and Lemonnier, 1975).

With further research, the technique known as gradient simulator came up for the computation of sensitivity coefficients. The technique found useful when applied to couple of cases and it was further utilized for calculating the sensitivity coefficients from an implicit numerical simulator. The scope of this method was expanded with its implementation to object modeling, and a parallelized gradient simulator using wavelet reparameterization was also developed for history matching. (Anterion, Eymard and Karcher, 1989; Tan and Kalogerakis, 1991; Bissel, Sharma and Killough, 1994; Tan, 1995; Bissel, 1996; Landa and Horne, 1997; Lu, 2000 & 2001). Streamline simulation is another method and is capable for fast integration of dynamic data into reservoir models and production scenarios. It minimizes the numerical diffusion as compared to conventional finite-difference techniques which ultimately makes it computationally efficient. (Datta-Gupta, Vasco and Long, 1995; Thiele, Batycky and Blunt, 1997; Vasco, Yoon and Datta-Gupta, 1998).

Optimization algorithm is the most important facet of history matching process. There are plenty of optimization procedures available as gradient-based techniques, and non-gradient or global optimization techniques. They can be utilized depending on the

requirement and applicability. The gradient-based techniques are much cheaper in terms of computational time but global methods can yield better results.

The gradient-based methods are computationally more efficient and produce good convergence rates; however the calculation of gradient is quite expensive. But, these techniques also often suffer the issue of convergence to local minima instead of obtaining global optimum parameter values. Gradient-based techniques employ an iterative procedure that involves the computation of Hessian matrix. Different gradient-based algorithms actually differ in a way they approximate the Hessian.

The steepest descent is one of such method (Gill et al., 1981; Nocedal and Wright, 2006; Griva et al., 2009). Its major assumption is to consider Hessian to be an identity matrix which in turns avoids its computation and storage. The search direction is opposite to that of gradient of objective function and it is also the direction of steepest decent. As identity matrix is positive definite, this method always converges.

The method which finds the minimum of quadratic function from the information of gradient only is known as nonlinear conjugate (Gill et al., 1981; Nocedal and Wright, 2006; Griva et al., 2009). This algorithm starts with a direction opposite to the gradient and subsequently takes directions that are conjugate to each other (with respect to the Hessian). The convergence rate of this approach is linear but it is generally faster that steepest decent method.

Newton, Gauss-Newton and Levenberg-Marquardt methods are the most commonly used ones. The Newton approach requires the exact Hessian to be computed. In order to use Newton method successfully, Hessian must be positive-definite at each iteration. But as

Hessian is the second derivative matrix, it is very expensive to compute it. So we need to search for some alternative to Hessian. In Gauss-Newton method (Gill et al., 1981; Nocedal and Wright, 2006; Griva et al., 2009) the approximation is made for Hessian to eliminate the third term from its equation because it is the most expensive part, but this assumption is good if the current guess is close to the true solution. Levenberg-Marquardt method (Levenberg, 1944; Marquardt, 1963) replaces the third term with a diagonal matrix (λI). This diagonal perturbation in the Gauss-Newton Hessian matrix shifts every eigenvalue of it, thus ensuring a positive-definite Hessian matrix. The λ is often selected by trial and error (Gill et al., 1981; Nocedal and Wright, 2006). In Levenberg-Marquardt, the initial guess of λ is made. If residual is reduced, a decay factor of 2 is used but if it fails to decrease then a growth factor of 4 is used.

The Quasi-Newton method (Gill et al., 1981; Nocedal and Wright, 2006; Griva et al., 2009) is usually implemented to inverse problems having large number of control variables. It avoids the computation of sensitivity coefficient matrix which makes it computationally very efficient. The Hessian or its inverse is approximated using the information obtained from the gradient.

In practical scenarios we can have more than one localized minimum which can affect the results obtained through gradient-based techniques. Non-gradient or global techniques mostly reach the global minima for cases in which objective function has several minima. The prime disadvantage of these techniques is that they are numerically very expensive. There are several methods available such as genetic algorithm, simulated annealing, particle swarm optimization, CMAES, differential evolution and ant colony optimization.

In simple, an inverse problem can be divided in three steps:

1) Parameterization of the system

2) Forward Modeling

3) Inverse Modeling

2.2.1 Parameterization

Parameterization is basically determination of minimal subset that can characterize the reservoir accurately. Broadly there are two spaces: model space and data space. Reservoir parameter or reservoir model is regarded as model space (permeability distribution). The choice of model parameter for the system is called parameterization of the system. Data space is classified in two groups: measurement space and observation space. Observation space is a subset of measured data. It contains actual data matched during inverse modeling. The observation space can be constructed by linear transformation of measured data into frequency domain.

One of the parameterization techniques is zonation, in which reservoir is divided into larger blocks as compared to simulation grid blocks. A variation of this method in which reservoir is divided into high sensitivity zones can also be implemented. (Jacquard and Jain, 1965; Bissel et al., 1994). The eigenvectors corresponding to highest eigenvalues of covariance matrix as the model parameters can also be used, and singular values decomposition (SVD) can be used to choose the set of basic vectors (Gavalas et al., 1976; Shah et al., 1978; Oliver, 1996; Reynolds et al., 1996). Sequential Self-Calibration (SSC) methods can also be implemented for this purpose. It is an iterative geostatistically-based inverse method which is found effective in constructing multiple equiprobable reservoir

models while honouring the single-phase pressure data. The production data can be integrated and SSC technique can be implemented to the problem of single-phase multiple well pressure and rate data, and also to joint inversion of multiple well pressure and multiphase fractional flow data (Gomez-Hernandez et al., 1998; Wen et al., 1998).

2.2.2 Forward Modeling

It is the prediction of the production data from the given reservoir model that includes the observable parameters and given values of model parameters. It utilizes the single-phase or multiphase flow equations to estimate the required properties and data. It involves the computation of basic phase properties, utilization of analytical correlations, descretized finite-difference equations, and Newton-Raphson iterative procedure to obtain the converged solution.

2.2.3 Inverse Modeling

Inverse analysis is the determination of model parameters using actual production data and other available information. As the direct measurement of reservoir quantities is impossible, the inverse analysis using observed data (well pressure, water-cut etc.) can be used to estimate these properties. The inverse process for obtaining the reservoir parameters using indirect measurements is referred as parameter estimation. The main steps are as follows:

1) Construct a mathematical reservoir model.

2) Define the objective function.

3) Apply the minimization technique.

After these steps, the inversion process is carried out in following manner:

1) Unknown set of parameters should be assigned with some arbitrary but reasonable values.

2) Compute the response of system using mathematical model.

3) Calculate the objective function. It compares the calculated response with actual data. Terminate the procedure if objective function is less than the predetermined criterion.

4) Use minimization algorithm for calculating the change in parameter values. Again check the change, if it is less than the predetermined criterion, terminate.

5) Go back to step 3.

2.3 Wavelet Analysis and Its Implementation in Petroleum Engineering

Wavelets transformation and multiresolution analysis have become very useful. Few decades back, many of the complex and time consuming engineering problems which seemed to be almost impossible to solve, have now been transformed with the implementation of wavelet into relatively simpler and time efficient ones. Thus it has given new dimension and scope to the research work. Wavelets have found applications in signal and image denoising, compression, thresholding, and data mining (Mallat, 1989; Chui, 1992; Daubechies, 1992; Donoho and Johnstone, 1994; Mallat, 1999; Guangming et al., 2002; Fuhr, 2005; Percival, 2006).

But the technique is not limited to other disciplines only and has found numerous applications in petroleum engineering as well. During the initial phase in this industry, wavelet basis functions were implemented to nonlinear partial differential equations for their numerical solution in one-dimension, two-phase flow. It was used as weighted residuals to obtain solution of Buckley-Leverett partial differential equation. With further advancement wavelet found its application for two-phase upscaling in which fine-scale effects are transformed to coarse-scale using wavelet transforms, thus eliminating the requirement of fine-scale simulation and saving considerable amount of time (Moridis et al., 1995; Chu et al., 1996). Wavelet transform can be used to denoise and scale-up permeability data, as well as to identify local discontinuities. Another important application is its utilization for finding interwell relationships. The production data is decomposed into wavelet coefficients and the coefficients are analysed to obtain the relationship. Basically it uses the time localizing ability of the transform. In the same way, it can also be utilized for integrating multiscale data. It deals with the spatial information in frequency domain and decomposes both the coarse-scale and fine-scale data in wavelet coefficients and evaluates it to obtain a correlation between coefficients of different resolutions. This correlation is then used to produce coefficients at interwell positions (Jansen and Kelkar, 1997; Panda et al., 2000).

The Haar wavelet transform can be utilized for time series indexing and a spatially adaptive method can be used for denoising through thresholding in wavelet expansion (Chan and Fu, 1999; Chang et al., 2000). The multiresolution technique can also be implemented for reservoir parameter estimation. Basically the wavelet analysis is utilized for parameterizing the reservoir properties spatial distribution which results in

thresholded wavelet coefficients that provide the parameter space (Lu and Horne, 2000; Lu, 2001). Not only this, it has also established its utilization for improvement of computational efficiency of krigging. In this an orthogonal wavelet basis function can be implemented to refine the covariance matrix of the krigging equation so that matrix becomes sparse and can be inverted easily (Yunowo et al., 2005).

One very significant advantage of wavelets is that they can identify the important events, changes and discontinuities in the data which are not easily distinguishable. This allows capturing the effects that result due to wellbore, reservoir or spurious data. Although there has been many advancements and modification in the downhole tools, still the data obtained from permanent downhole gauges contains noise due to wellbore environment. Haar wavelet transform allows us to denoise the data and acquire important information from it for interpretation (Athichanagorn et al., 2002; Soliman et al., 2003; Shi-Yi and Xiao-Gang, 2007).

Another important breakthrough with the use of wavelets is to produce multiple equiprobable history-matched reservoir models. Wavelets allowed the reservoir models to conform to all available production data and geological uncertainty alongwith varying level of trust. Different subsets of wavelet coefficients are constrained simultaneously for honouring production data and geostatistical information. A bit of modification is done to this work with integration of history-matched model with other geologic data using heuristic methodology. It also avoids the gradient-based methods of inverse problems, and obtains a wavelet subset based on ancillary variable that relates the important descriptions of permeability field and flow patterns simultaneously (Sahni, 2006; Sahni and Horne, 2006, Kind and Quinteros, 2007).

Wavelet transformation is helpful to extract important information from both time and spatial signals, thus it can be used effectively to transform both the model space and the time dependent data (such as well pressure and water-cut). The coupling of wavelet transformation with adjoint sensitivity method marks an important development, as it not only simplifies the problem but also improves the computational efficiency. It has found useful applications not only to single-phase flow problems but also for multiphase analysis (Awotunde, 2010).

2.4 Computation of Sensitivity Matrix

There exists a complex relationship between fluid parameters, reservoir parameters and production from it. It is nonlinear problem which also depends on different set of equations. The fundamental physical laws that govern the fluid flow in porous media are:

- Material Balance (mass conservation)
- Energy Conservation
- Darcy's Law (for flow through porous media)
- Equation of State
- Relative Permeability and Capillary Pressure

It is not possible to obtain an analytical form of solution due to complexity and nonlinearity of the function that connect these physical laws with the reservoir system. In petroleum engineering, the function is the set of physical equations that govern the flow and production data is the output. The system parameters include porosity and permeability of each gridblock and fluid properties etc.

Sensitivity can be defined as the derivative of production data with respect to reservoir parameter (permeability) in each gridblock. The computation time and cost is one of the determining criteria for choosing the appropriate optimization method for parameter estimation. The major techniques for calculation of sensitivity coefficients are: finite difference or substitution method, forward sensitivity method, modified generalized pulse-spectrum technique and adjoint-state method.

The finite difference or substitution method involves the perturbation of each model parameter (separately, one at a time) to obtain the sensitivities of state variables to that parameter. It requires M+1 simulation runs. Even though the technique seems to be simple, but it can become tedious in case of large model space.

Gradient simulator or forward sensitivity technique has been found very beneficial when the number of model parameters is small. Basically, it requires the solution of a linear system with multiple right-hand side vectors and the number of right hand side vectors is equal to the number of model parameters. It becomes inefficient because it needed the computation of sensitivities of all grid block variables although only sensitivities at measurement location are needed. The method has been applied for computation of sensitivity coefficients for history matching of single-phase flow problems and estimation of permeability distribution from pressure data (Jacquard and Jain, 1965; Carter et al., 1974; Sun and Yeh, 1985; Yeh, 1986; Tang et al., 1989; Bissel et al., 1994; Chu et al., 1995; Sun et al., 2001).

Firstly generalized-pulse-spectrum technique was proposed for history matching process but it did not involve the computation of sensitivity coefficients (Chen et al., 1974; Tang

et al., 1989). With advancements, the modified version of generalized-pulse-spectrum technique came up which emerges to be suitable for two-dimensional, two-phase black oil models and involves the computation of sensitivity coefficients (He et al., 1997; Landa et al., 2000).

The adjoint-state method for computation of sensitivity is mainly important when the amount of data is relatively small. This method can be used to compute the gradient of objective function. In this method a linear system is solved with the number of right hand side vectors equal to amount of observed data (well pressure, water-cut) available. The sensitivities are evaluated for the amount of data but the technique is not dependent of number of parameters (Shah et al., 1978; Anterion et al., 1989; Sun and Yeh, 1990; Wu et al., 1999; Li and Petzold, 2004; Michlalak and Kitanidis, 2004; Sun and Sun, 2005; Plessix, 2006).

Optimal control theory is one of other methods which can be used to compute the gradient of objective function for single-phase flow with respect to model parameters. It can also be expanded for multiphase reservoir to perform the automated history matching. It calculates the adjoint variables for the pressure equation and uses an objective function which depends only on the pressure variance term. The technique has also been implemented to groundwater flow problem for parameter estimation (Chen et al., 1974; Chavent et al., 1975; Wasserman et al., 1975; Carrera and Neuman, 1986; Yeh, 1986; Sun and Yeh, 1990).

CHAPTER 3

FUNDAMENTAL CONCEPTS

This chapter presents the fundamental concepts and methods that are used in this work, for the analysis of physical system. The mathematical models and techniques that are required for this research work are discussed here.

3.1 Modeling of Physical System

Modeling of a system is performed in various disciplines of engineering. Forecasting the observed data is the forward problem while using the actual observed data to estimate the model parameters is an inverse problem. Model parameters are the physical properties of the system that remain the same for different problems, and the properties that change are the variables. The purpose of inverse analysis is to obtain such parameters, under which, the performance of the system imitates the actual observed behavior.

Practically, petroleum reservoirs are large which makes the direct measurement of reservoir quantities, impossible. Thus in reservoir characterization, the inverse analysis using observed data (well pressure, water-cut etc.) can be used to estimate these properties becomes important. Inverse problems can be divided into three parts as: parameterization of the system, forward model and inverse model. Inverse problems are difficult because their solutions are usually non-unique. Also the uncertainties play a very significant part in inverse modeling and are described mathematically using probability theory.

3.1.1 Parameter Space and Data Space

The set of parameters that can completely characterize the physical system can be referred to as parameter or model space. The physical system i.e. reservoir can be represented by S, model space with M and model parameter with $\vec{\alpha}$. It is assumed that the reservoir system can be completely characterized by the porosity and permeability distribution.

Data space contains all the data measured from a system or its transformation. The data space consists of two groups: measurement space and observation space. In case of petroleum reservoirs, measurement space comprises of both static (geological and geophysical measurements) and dynamic (production data such as well pressure, water-cut) data. Observation space is a subset of measured data. It contains actual data matched during inverse modeling. The observation space can be constructed by linear transformation of measured data into frequency domain. The measurement data primarily contains the production data, and it is denoted by D_{meas} in this study. It also includes measurement errors from the wells and the reservoir which can be denoted as $\vec{d}$. The observation space often denoted as D_{obs} is constructed in this research work, by transformation of measured data using wavelets followed by its thresholding.

3.1.2 Transformation of Parameter and Data Spaces

There have been various researches performed on model parameter and data decomposition which focuses on denoising of the data or data compression (Kikani and He, 1998; Soliman et al., 2003; Zheng and Li, 2007). Important advancement was made which involves the transformation of the two spaces into wavelet coefficients. The subset

of the wavelet transformed time-series data space is used in the solution of the inverse problem (Awotunde, 2010). Thus, careful selection of important wavelet coefficients is required in dimensionality reduction. The subset of parameter space should comprise of entries that can adequately characterize the reservoir, and similarly the coefficients of data subset must contain the important information of the data in order to produce the correct model from it.

3.2 Probability Model

In practical scenarios, both the forward model used for simulation of the measurement data, and the data space data, have theoretical and measurement errors respectively.

We need a probalistic model to account for them. The Bayes' formula (Bayes, 1763) can be given as,

$$\frac{\dot{f}_{M|D}\left(\vec{\alpha}\,|\,\vec{d}_{meas}\right)}{\dot{f}_{M}\left(\vec{\alpha}\right)} = \frac{\dot{f}_{D|M}\left(\vec{d}_{meas}\,|\,\vec{\alpha}\right)}{\dot{f}_{D}\left(\vec{d}_{meas}\right)} \tag{3.1}$$

where $\dot{f}_{M|D}\left(\vec{\alpha}\,|\,\vec{d}_{meas}\right)$ is *a posteriori*, $\dot{f}_{M}\left(\vec{\alpha}\right)$ is the prior and $\dot{f}_{D|M}\left(\vec{d}_{meas}\,|\,\vec{\alpha}\right)$ is the likelihood estimate. A common assumption is that error in measurement to be independent of true data while error in theoretical predictions (forward model) to be independent of model parameter values. The Bayes' formula in terms of Gaussian density function can be written as,

$$\dot{f}_{M|D}\left(\vec{\alpha}\,|\,\vec{d}_{meas}\right) = \dot{f}_{M}\left(\vec{\alpha}\right)\frac{\mathfrak{N}_{\vec{d}_{meas}}\left(\vec{d}_{cal}, C_D\right)}{\dot{f}_{D}\left(\vec{d}_{meas}\right)} \tag{3.2}$$

and Gaussian probability density function with mean $\vec{\mu}$ and covariance $C_{\vec{x}}$ can be given as,

$$\Re_{\vec{x}}\left(\vec{\mu}, C_{\vec{x}}\right) = \frac{1}{\sqrt{(2\pi)^{N_x} \det\left(C_{\vec{x}}\right)}} \exp\left[-\frac{1}{2}\left(\vec{x}-\vec{\mu}\right)^T C_{\vec{x}}^{-1}\left(\vec{x}-\vec{\mu}\right)\right] \tag{3.3}$$

where N_x is the length of $\vec{x}$.

If in case the model parameters also have normal distribution, we can have,

$$\dot{f}_M\left(\vec{\alpha}\right) = \Re_{\vec{\alpha}}\left(\vec{\alpha}_{pri}, C_M\right) \tag{3.4}$$

So the equation (3.2) becomes,

$$\dot{f}_{M|D}\left(\vec{\alpha} \mid \vec{d}_{meas}\right) = \text{const}.\ \exp\left(-\Phi\left(\vec{\alpha}\right)\right) \tag{3.5}$$

The aim of inverse problem under the probabilistic uncertainty model is to find the maximum likelihood estimate for a given $\vec{d}_{meas}$.This is equivalent to minimizing the function $\Phi(\vec{\alpha})$. Hence it can be referred as the objective function which is defined as,

$$\Phi\left(\vec{\alpha}\right) = \frac{1}{2}\left[\left(\vec{d}_{cal}-\vec{d}_{meas}\right)^T C_D^{-1}\left(\vec{d}_{cal}-\vec{d}_{meas}\right)+\left(\vec{\alpha}-\vec{\alpha}_{pri}\right)^T C_M^{-1}\left(\vec{\alpha}-\vec{\alpha}_{pri}\right)\right] \tag{3.6}$$

3.3 Solution to Inverse Problem

The parameter estimation problems can be expressed in form of minimization of discrepancy (objective function of unknown parameters to be estimated); thus parameter estimation problems can be reduced to optimization problems. Objective function of model parameters is non-linear in nature, so optimization algorithm should be iterative.

All optimization techniques require the objective function that can describe the measure of optimality of solution. The definition given for objective function in equation (3.6) has an assumption that measurement and model errors have zero mean and Gaussian distributions. The forward model can be represented as,

$$\vec{d}_{cal} = f(\vec{\alpha}) \tag{3.7}$$

$f(\vec{\alpha})$ is a function of model parameter $\vec{\alpha}$. If forward model is linear and priori (probability density function) is Gaussian then $\dot{f}\left(\vec{\alpha}+\vec{d}_{meas}\right)$ i.e. the posterior probability density function is Gaussian with its center at the estimate $\vec{\alpha}$, and it represents both the mean value of $\dot{f}\left(\vec{\alpha}+\vec{d}_{meas}\right)$ and its maximum *a posteriori* estimate. But if forward model $(\vec{\alpha})$ is non-linear then posterior probability density function is not Gaussian and analysis becomes more complex.

The second-order approximation using Taylor series expansion of a function $f(\vec{\alpha})$ can be written as,

$$f(\vec{\alpha}+\vec{s}) \approx \hat{f}(\vec{s}) = f(\vec{\alpha}) + \vec{s}^T \vec{g}(\vec{\alpha}) + \vec{s}^T H(\vec{\alpha})\vec{s} \tag{3.8}$$

The approximation $f(\vec{\alpha}+\vec{s})$ is valid, if step $\vec{s}$ is small. Now, differentiate $\hat{f}(\vec{s})$ with respect to $\vec{s}$ and equating it to zero gives,

$$\vec{g} + H\vec{s} = 0 \tag{3.9}$$

At any iteration κ we can compute the vector $\vec{s}_{\kappa}$ as,

$$H_\kappa \vec{s}_\kappa = -\vec{g}_\kappa \tag{3.10}$$

Now the parameter $\vec{\alpha}$ can be updated as,

$$\vec{\alpha}_{\kappa+1} = \vec{\alpha}_\kappa + \vec{s}_\kappa \tag{3.11}$$

Equations (3.10) and (3.11) represent the standard Newton technique for inverse problem solution. This method requires the exact computation of Hessian matrix. The Hessian matrix H can be defined as the second derivative of the objective function. So, the Hessian of the objective function given in Equation (3.6) can be written as,

$$H(\vec{\alpha}) = S^T C_D^{-1} S + C_M^{-1} + \nabla S^T C_D^{-1} \left(\vec{d}_{cal} - \vec{d}_{meas} \right) \tag{3.12}$$

where ∇S is the second derivative matrix and it can be given as,

$$\nabla S = \frac{\partial S}{\partial \vec{\alpha}^T} = \frac{\partial^2 \vec{d}_{cal}}{\partial \vec{\alpha} \partial \vec{\alpha}^T} \tag{3.13}$$

Thus for Newton method, the exact Hessian $H(\vec{\alpha})$ can be computed using Equation (3.12). However, for proper convergence the Hessian matrix should be positive-definite at each iteration; because when it is positive-definite the Newton approach produces a downhill direction and provides a quadratic convergence in the neighborhood of the actual solution $\vec{\alpha}$.

$$0 < \vec{s}^T H \vec{s}^T < -\vec{g}^T \vec{s} \tag{3.14}$$

If Hessian matrix is not positive-definite or if it is singular then we may not go downhill or may fail to have a solution.

In order to solve Equation (3.10) for $\vec{s}_\kappa$, we need to compute gradient and Hessian at each iteration, κ. The gradient for the objective function defined in equation (3.6) can be represented as,

$$\vec{g}(\vec{\alpha}) = S^T C_D^{-1}\left(\vec{d}_{cal} - \vec{d}_{meas}\right) + C_M^{-1}\left(\vec{\alpha} - \vec{\alpha}_{pri}\right) \tag{3.15}$$

where S is the sensitivity matrix and is given as,

$$S = \frac{\partial \vec{d}_{cal}}{\partial \vec{\alpha}} \tag{3.16}$$

The computation of exact Hessian is computationally very expensive. There are various gradient-based methods and each differs uniquely in a way it approximates the Hessian which is required to solve Equation (3.10).

Steepest descent is one of the simplest algorithms for obtaining the solution (Gill et al., 1981; Nocedal and Wright, 2006; Griva et al., 2009). The approach has major assumption that considers Hessian to be an identity matrix, which ultimately avoids its computation and storage. Therefore, Equation (3.10) can be written as,

$$I\vec{s}_\kappa = -\vec{g}_\kappa \tag{3.17}$$

which gives,

$$\vec{s}_\kappa = -\vec{g}_\kappa \tag{3.18}$$

It can be inferred from Equation (3.18) that the search direction is opposite to that of the gradient of objective function. Basically the direction of the gradient is that of steepest

ascent, thus opposite to the direction of gradient is that of steepest descent. Since identity matrix is positive-definite, this technique certainly converges but often takes a lot of time.

Gauss-Newton technique (Gill et al., 1981; Nocedal and Wright, 2006; Griva et al., 2009) provides another approximation for the exact Hessian by neglecting the most expensive third term of the equation (3.12). Thus the $H(\vec{\alpha})$ can be approximated as,

$$H_{GN}(\vec{\alpha}) = S^T C_D^{-1} S + C_M^{-1} \tag{3.19}$$

However, the third term will only be small if we are close to the actual solution and can be neglected. But if the guess is away from the true solution then the residuals in equation (3.12) fails to be small. This results in bad Gauss-Newton direction and the third term becomes significant.

Instead of excluding the third term of the equation (3.12), the **Levenberg-Marquardt** method (Levenberg, 1944; Marquardt, 1963) assumes it to be equal to the diagonal matrix $(\dot{\lambda} I)$. So the equation becomes,

$$H_{LM}(\vec{\alpha}) = H_{GN}(\vec{\alpha}) + \dot{\lambda} I \tag{3.20}$$

A scalar quantity is multiplied with the identity matrix of the Hessian which makes it to be always positive definite. This diagonal perturbation will shift every eigenvalue of the Gauss-Newton Hessian (H_{GN}) by the value of $\dot{\lambda}$. Any eigenvalue that is negative or too close to zero, becomes positive, using this diagonal perturbation. This also improves the condition number of matrix. This perturbation is not limited to Gauss-Newton Hessian, but can even be applied to exact Hessian if it is close to singular. Levenberg-Marquardt is

basically a combination of Steepest Descent (slow but sure convergence) and Newton's method (fast convergence close to optimum).

3.4 Wavelet Transform and Analysis

A wavelet can be described as a real-valued function. Basically, wavelet transform provides a unique way of storing and analyzing the data set using averages and differences. Wavelet analysis (Chui, 1992; Daubechies, 1992; Graps, 1995; Mallet, 1999) has been developed during last two decades. It is fairly recent but a very useful mathematical concept that has become useful for variety of applications as numerical analysis, fractals and multifractal analysis, signal and image processing and estimation of model parameters. Wavelet analysis is similar to Fourier analysis, but in this the target function over a given interval is represented by orthonormal basis function.

The data integration algorithm depends on the reparameterization of model space using wavelet coefficients. Permeability being a Jeffreys parameter, its logarithmic value yields a Cartesian parameter. In wavelet analysis, this has an additional benefit because parameter evaluation in wavelet domain can produce positive or negative values.

3.4.1 Discrete Wavelet Transform (DWT)

Usually the data is sampled as discrete values, so we require a wavelet transform that can incorporate the discrete quantities. Discrete wavelet transform can be considered as dyadic slices of the continuous wavelet transform which makes it possible to take subsamples from the wavelet transform.

A discrete representation for the wavelet coefficients in form of linear transformation using an orthogonal wavelet matrix W can be defined as,

$$\vec{c} = W\vec{d} \tag{3.21}$$

where W represents an N x N matrix that is applied to input data of size N and transforms the input data from time domain to wavelet domain. Equation (3.21) seems to be simple in its application, but realistically, maneuvering and storing of transformation matrices for large amount of input values may not be appropriate. Thus some periodic form of filtering is normally utilized for computation of discrete wavelet coefficients (Mallet, 1989, 1999; Percival and Walden, 2000).

3.4.2 Haar Wavelet Transform

The Haar sequence is considered as the first known wavelet basis. Haar is the simplest discrete wavelet transform. This provides an advantage for its usage in the analysis of signals with abrupt alterations. (Haar, 1910; Chui, 1992)

Properties

1. Haar transform only require additions and differences.
2. Haar matrix consists of many elements with zero values, which reduces computational time.
3. The length of the Haar wavelet should be of the order 2^n. Also the input and output size remains the same.
4. Its orthogonal characteristic allows the analysis for frequency components of input signals.

CHAPTER 4

RESERVOIR MODELING AND UPSCALING

4.1 Reservoir Modeling

Petroleum reservoirs have large structures which makes it impractical to obtain measurements at every location. Mostly reservoir properties depend upon insufficient and indirect measurements taken at well locations. Thus it is quite difficult to characterize the reservoir with appropriate properties and structure, but it is required for better reservoir management.

4.1.1 Reservoir Model

Combination of physical laws, reservoir boundary conditions, the reservoir system and assumptions can be characterized by a set of mathematical equations which is known as *reservoir model*.

4.1.2 Reservoir Simulator

The reservoir model is usually solved by the numerical approach due to its complex nature. The fine-scale simulator; used in this work is a three-dimensional, oil-water, black oil, finite-difference reservoir simulator. The upscaling simulator is also purposely built for this work using the same governing equations for the reservoir model. Both simulators have a built-in functionality of computing sensitivity of data to reservoir parameters using Adjoint-State approach.

Fine-scale Simulator

A three-dimensional reservoir system with total number of *M* grid blocks is considered with total number of wells to be *Nwells*. The general residual equation can be given as,

$$\vec{f}^{\,n+1}\left(\vec{u}^{\,n+1},\vec{u}^{\,n},\vec{v},\Delta t;\vec{\alpha}\right)=\vec{0}, \tag{4.1}$$

where vector $\vec{v}$ consists of known reservoir properties and vector $\vec{u}$ contains state variables and can be written as,

$$\vec{u}=[p_{o,1},S_{w,1},....,p_{o,M},S_{w,M},p_{wf,1},....,p_{wf,Nwell}]^T \tag{4.2}$$

$\vec{f}_{blk}^{\,n+1}$ contains the residual due to flow in and out of reservoir grid blocks and is given as,

$$\vec{f}_{blk}^{\,n+1}=\left[\, f_{w,1}^{n+1},\, f_{o,1}^{n+1},\, f_{w,2}^{n+1},\, f_{o,2}^{n+1}...,\, f_{w,M}^{n+1},\, f_{o,M}^{n+1}\right]^T \tag{4.3}$$

whereas $\vec{f}_{well}^{\,n+1}$ represents the residual due to flow into or out of the wells in the reservoir and can be presented as,

$$\vec{f}_{well}^{\,n+1}=\left[\, f_{well,1}^{n+1},\, f_{well,2}^{n+1},...,\, f_{well,Nwell}^{n+1}\right]^T. \tag{4.4}$$

$\vec{f}_{blk}^{\,n+1}$ and $\vec{f}_{well}^{\,n+1}$ both combine to form $\vec{f}^{\,n+1}$ as,

$$\vec{f}^{\,n+1}=\begin{bmatrix}\vec{f}_{blk}^{\,n+1}\\ \vec{f}_{well}^{\,n+1}\end{bmatrix}, \tag{4.5}$$

Now, equation (4.3) suggests that $\vec{f}_{blk}^{\,n+1}$ comprises the residuals of the two phases existing in the reservoir system which can be given as,

$$\vec{f}_w\left(\vec{p}_o^{\,n+1}, S_w^{n+1}, \vec{p}_{wf}^{\,n+1}, \vec{p}_o^{\,n}, S_w^n, \vec{\phi}_{ini}, \Delta t; \vec{k}\right) = \vec{0}, \tag{4.6}$$

and

$$\vec{f}_o^{\,n+1}\left(\vec{p}_o^{\,n+1}, S_w^{n+1}, \vec{p}_{wf}^{\,n+1}, \vec{p}_o^{\,n}, S_w^n, \vec{\phi}_{ini}, \Delta t; \vec{k}\right) = \vec{0}. \tag{4.7}$$

whereas the well residual for $\vec{f}_{well}^{\,n+1}$ of equation (4.4) can be written as,

$$\vec{f}_{well}^{\,n+1}\left(\vec{p}_o^{\,n+1}, S_w^{n+1}, \vec{p}_{wf}^{\,n+1}, \vec{p}_o^{\,n}, S_w^n, \vec{\phi}_{ini}, \Delta t; \vec{k}\right) = \vec{0}, \tag{4.8}$$

where $\vec{\phi}_{ini}$ represents initial porosity distribution and $\vec{k}$ represents the permeability distribution in the reservoir in all the residual equation presented above.

Consider the constraint of total production rate,

$$f_{well,i}^{n+1} = \sum_{ph=o,w} \sum_{j}^{Ncomp} q_{ph,j}^{well} - q_{t,i} = 0. \tag{4.9}$$

In equation (4.9), $q_{ph,j}^{well}$ represents the flow rate of the phases (oil or water, denoted by *ph*) at the j^{th} completion and it can be defined as,

$$q_{ph,j}^{well} = \lambda_{ph,j}^{n+1} WI_j \left(p_{ph,j}^{n+1} - p_{wf}^{n+1} - \gamma_{ph,j}^{n+1} \Delta z_j\right) \tag{4.10}$$

There is no p_c (capillary pressure) in equation (4.10) because p_{ph} represents both p_o and p_w, so capillary pressure will be incorporated in p_{ph} in case of water phase. The mobility ratio and specific gravity of any phase *ph* at the completion *j* are represented by $\lambda_{ph,j}^{n+1}$ and $\gamma_{ph,j}^{n+1}$ respectively, while WI_j denotes the well index at the j^{th} completion. The

Newton-Raphson iterative method is used in order to solve the nonlinear system of equations at every iteration; so we have at any iteration κ,

$$J^{n+1,\kappa}\delta\vec{u}^{n+1,\kappa} = -\vec{f}^{n+1,\kappa}, \tag{4.11}$$

Where $J^{n+1,\kappa}$ is known as Jacobian matrix and can be written as,

$$J^{n+1,\kappa} = \frac{\partial\vec{f}^{n+1,\kappa}}{\partial\vec{u}^{n+1,\kappa}}. \tag{4.12}$$

the solution is then updated as,

$$\vec{u}^{n+1,\kappa+1} = \vec{u}^{n+1,\kappa} + \delta\vec{u}^{n+1,\kappa}. \tag{4.13}$$

Upscaled Simulator

The basic governing equations in the upscaled simulator are the same as that used for the fine-scale simulator. The principal difference is in the manner of calculating the transmissibility between the upscaled grid blocks. The central idea in this research work involves the upscaling of the reservoir grid blocks based on homogenization of the system parameters. This would result in upscaled grid blocks that have different structures. Also the neighboring grid blocks will not be structured as in the rectangular grid system. Thus we need to find an appropriate way of computing the transmissibility between the interacting grid blocks. The detailed description of the whole upscaling procedure and its calculations is presented in the later section.

4.2 Upscaling Based on Homogeneity of Reservoir System

Petroleum reservoirs have large structures and sizes. This large extent makes it computationally very expensive to imitate the behavior of reservoir at the fine-scale level.

Thus we need to upscale the system to reduce the total number of reservoir grid blocks and make simulating it computationally feasible. Numerous upscaling techniques have been proposed in the literature which involves averaging of fine-scale properties to upscale the system; local and global upscaling; and adaptive local-global upscaling procedures (White and Horne, 1987; Durlofsky, 1991; Li, King and Mansfield, 1999; Beckner and Kumar, 2001; Wu et al., 2002; Chen and Durlofsky, 2006a; Nakashima, 2009).

The purpose of this research is to perform upscaling of the reservoir system based on the sensitivity of production data to the model parameter. The sensitivity computation is primarily a part of inverse analysis. In principle, this provides us the information of the grid blocks that are less sensitive to the changes of production data. These less sensitive grid blocks can be considered as a homogenous section and may then be combined to form an upscaled grid block.

Therefore the pattern of upscaling is based on the pattern of homogenous patches obtained through sensitivity analysis during history matching. The adjacent grid blocks that have low sensitivity are supposed to have similar permeability trend and are merged to form an upscaled grid block. The combination of fine-scale grid blocks into larger ones, based on permeability distribution, ultimately reduces the number of grid blocks for simulation and this in turn reduces the requirement of computational resources and time. In this work the upscaling of grid blocks with similar permeability values is performed subject to one of two different constraints. The first constraint involves ensuring that grid blocks having wells in them (well-blocks) are not combined with any other grid. The

second constraint involves ensuring that any well-block and the grid blocks adjacent to it are not combined with one other or with any other block in their neighborhood.

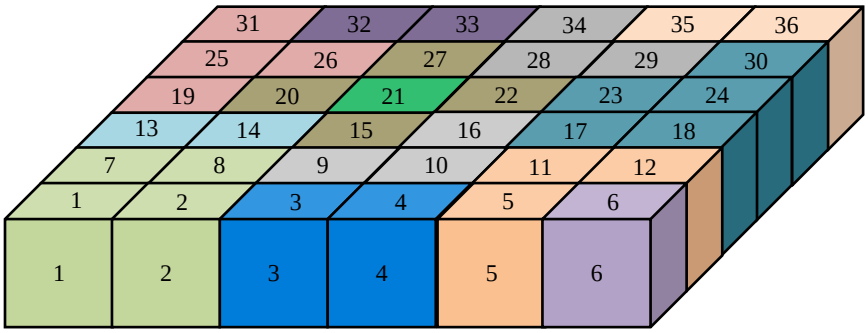

Figure 4.1: Upscaling trend based on homogeneity of reservoir system

Figure 4.1 illustrates an example of a 6x6 reservoir system with the implementation of second constraint. It shows that fine-scale grid blocks are combined based on homogeneity of the system. The grid blocks having the same color have the same permeability value; therefore these fine-scale grid blocks would be combined to form the upscaled system. The transformation from fine-scale to upscale grid blocks can be explained through Table 4.1.

Table 4.1: Combination of fine-scale grid blocks in upscaled system

Upscaled Grid Blocks	**Fine-scale Grids Merged**	**Upscaled Grid Blocks**	**Fine-scale Grids Merged**
1	1, 2, 7, 8	9	19, 25, 26, 31
2	3, 4	10	20
3	5, 11, 12	11	21 (well)
4	6	12	22
5	9, 10, 16	13	27
6	13, 14	14	28, 29, 34
7	15	15	32, 33
8	17, 18, 23, 24, 30	16	35, 36

Table 4.1 gives the description of the fine-scale grid blocks in the 6x6 reservoir system considered that are combined due to homogeneity to form the upscaled system. Figure 4.1 and Table 4.1 also illustrate that the grid block having a well in it (i.e. Grid Block 21) and the grids adjacent to this well-block (Grid Blocks 15, 20, 22 and 27) are not combined with any other grid block. However, because we combine the grid blocks based on permeability distribution, the resulting upscaled grid blocks do not necessarily form well-defined shapes. This can be observed in Figure 4.1. This poses a challenge in calculation of transmissibilities. The transmissibility is performed by first locating the centroid of the irregular (upscaled) grid block and this is discussed later in Section 4.2.1.

The algorithm used for the upscaled simulator is described below:

1. The fine-scale grid blocks are combined to form the upscaled grid blocks based on the permeability distribution having some homogenous patches.
2. The centroid is calculated for each of the upscaled grid block.
3. For all upscaled grid blocks, their interaction is checked and all their neighbors are stored; to be used during the transmissibility calculations.
4. At each simulation time step, the Newton-Raphson iteration is performed.
5. During each iteration, the transmissibility between an upscaled grid block and each of its neighbors is calculated based on their centroid.
6. The procedure is repeated in each iteration, and each time step, until we reach the end of simulation.

4.2.1 Transmissibility Calculation for the Upscaled System

Transmissibility is the property calculated at the interface of the grid blocks, but the properties used in its calculation are known at the grid center. In a uniform rectangular system, the size of the grid blocks and its center are appropriately defined. However in the type of upscaled system shown in Figure 4.1, the shape of the resulting upscaled grid blocks may not be regular, and for calculating transmissibility we need to define the centers of these grids. Thus the centroid of the upscaled grid blocks are evaluated and used for transmissibility computation.

Centroid Calculation

The resulting upscaled grid blocks can be considered as polygons. Figure 4.2 shows one of such grid block. However the centroid calculation is quite challenging. In order to calculate the centroid of any figure, we should have its vertices arranged in either the clockwise or counter-clockwise direction.

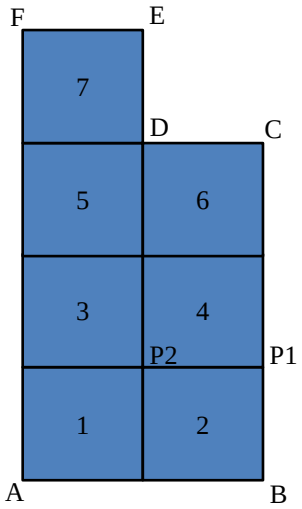

Figure 4.2: Example of an upscaled grid block

Consider that Figure 4.2 shows the grid block that is upscaled based on homogeneous patches obtained as a result of model space reduction. The first step is to define the vertices of the new grid block. Following procedure is followed to determine its vertices:

1. Define and store the vertices of the fine grid blocks that are combined to form this upscaled grid block. This can be done using the dimensions that we have considered for the reservoir system.
2. The algorithm constructed is such that the corner that exist in even number of fine grid blocks should be discarded, while those that occur in odd number of fine grid blocks are the vertices of the upscaled grid block.
3. This can be better understood from Figure 4.2. The vertices of the upscaled grid block are *A*, *B*, *C*, *D*, *E* and *F*. All of these vertices except *D* are part of only one fine-scale grid; as *A* is part of fine-scale Grid 1, *B* is of Grid 2, *C* is included in Grid 6, while *E* and *F* are part of fine Grid 7. On the other hand Vertex *D* is included in three fine-scale grids that are 5, 6 and 7. However all of them are part of odd number of grids.
4. Consider points *P1* and *P2* that are also the vertices of the fine grid blocks that make up this upscaled grid but they are not the vertices of the resulting upscaled grid. The algorithm adopted proves to be viable as these points *P1* and *P2* exists in even number of fine grids. *P1* exist in fine-scale Grid Blocks 2 and 4, while *P2* is part of Grids 1, 2, 3 and 4.
5. Similarly, this is how all other fine grid block vertices (other than *P1* and *P2*, that are not labeled in the figure) are discarded.

This is the first phase in the determination of the centroid. After finding these vertices, they are required to be arranged in clockwise or counter clock-wise order. The algorithm developed for this purpose is explained here:

1. Consider we have a matrix in which all the vertices of an upscaled grid block are stored, and the algorithm used will arrange them in counter-clockwise order. The *x*-coordinates of the vertices are placed in Column 1, while *y*-coordinates are in Column 2 of the matrix.
2. We select the first point i.e. stored in Row 1 of the matrix, let say we start from point *A* mentioned in Figure 4.2.
3. The *y*-coordinate of the point is stored in a variable, and the Column 2 of vertices matrix except Row 1 is searched to locate another same *y*-coordinate. From Figure 4.2 we can see that Point *B* has same y-coordinate as Point *A*. The located point will have different *x*-coordinate than the first point.
4. The point that is being searched can exist either to the right or left of the considered point, means the point *B* in Figure 4.2 can exist on either side but will have same *y*-coordinate.
5. The point can even exist on both sides and also there can be more than one point on any side.
6. When there will be points on both sides, then one of the side will have odd number of vertices and other will have even. This is analyzed by considering several structures.
7. The side having odd number of vertices is the side in which direction we have to move, because it will provide the correct shape.

8. All the points on the selected side are arranged in an ascending or descending order and then the point whose *x*-coordinate is closest to the *x*-coordinate of the point considered is selected to be next point. This selected next point may exist in any row of the vertices matrix, but the matrix is updated by swapping this point with the point stored in Row 2.
9. After moving to this vertex, now the *x*-coordinate of the this vertex that is stored in Row 2 is stored in a separate variable and movement is done in the *y*-direction for which the same procedure is followed as described in step 2 to 7.

This is what we require for the centroid calculation. The arranged points are then used to determine the centroid using following expressions,

$$C_x = \frac{1}{6A}\sum_{i=0}^{n-1}(x_i + x_{i+1})(x_i y_{i+1} - x_{i+1} y_i) \tag{4.14}$$

$$C_y = \frac{1}{6A}\sum_{i=0}^{n-1}(y_i + y_{i+1})(x_i y_{i+1} - x_{i+1} y_i) \tag{4.15}$$

where A is the area of the polygon and is given as,

$$A = \frac{1}{2}\sum_{i=0}^{n-1}(x_i y_{i+1} - x_{i+1} y_i) \tag{4.16}$$

4.3 Inverse Modeling

Parameter estimation is one of the objectives of this work. Within the procedure of parameter estimation, upscaling of the reservoir would be performed to speed up the history matching process. The upscaled system is expected to satisfactorily mimic the performance of the reservoir. The upscaling procedure presented is based on sensitivity

of production data to the reservoir parameter, and the sensitivity computation is performed during history matching. The gradient-based optimization procedure, Levenberg-Marquardt, is used as inverse analysis algorithm.

4.4 Sensitivity Computation

Levenberg-Marquardt method requires the computation of sensitivity coefficients, but these computations are also quite expensive. The time required for these calculations is important in defining the optimization algorithm selected for history matching. Though it provides better results, however if the cost of sensitivity computation is excessively high, then methods such as conjugate-gradient and quasi-Newton that do not require the sensitivity coefficients are used. In this section, we discuss the three methods of sensitivity computation.

4.4.1 Substitution Method

The substitution method is the simplest technique for estimating the sensitivity of production data to the model parameters. It basically involves the perturbation of each model parameter α_m (separately, one at a time) to obtain the sensitivities of state variables $\vec{u}$ to that parameter. Mathematically, it can be mathematically written as,

$$\frac{\partial \vec{u}(\vec{\alpha})}{\partial \vec{\alpha}} = \frac{\vec{u}(\vec{\alpha} + \Delta\vec{\alpha}) - \vec{u}(\vec{\alpha})}{\Delta\vec{\alpha}}. \tag{4.17}$$

This technique requires the forward simulator to run M + 1 times, thus it becomes problematic to implement this approach when the number of model parameters is large. Also the amount of perturbation $\Delta\alpha_m$ should be given prime importance; as too small

values of it can produce numerical errors, while too large values can have significant impact on accuracy of computed sensitivities.

4.4.2 Forward Sensitivity Method

Another technique for computation of sensitivity coefficients is the forward sensitivity method. It is also known as gradient simulator method. It requires the solution of a linear system with multiple right-hand side vectors and the number of right hand side vectors is equal to the number of model parameters. This method is preferred when the number of model parameters selected is less than the number of data to be matched. However this technique computes the sensitivities of all grid block variables, whereas only sensitivities at well locations are necessary for history matching in most cases.

Consider the general residual equation as given in Equation (4.1),

$$\vec{f}^{\,n+1} = \vec{f}\left(\vec{u}^{\,n+1}, \vec{u}^{\,n}, \vec{v}, \Delta t; \vec{\alpha}\right) = \vec{0} \tag{4.18}$$

A perturbation $\delta\vec{\alpha}$ of model parameter $\vec{\alpha}$, induces a perturbation $\delta\vec{u}$ to state variable $\vec{u}$. Thus, the residual can be given as,

$$\vec{f}\left(\vec{u}^{\,n+1} + \delta\vec{u}^{\,n+1}, \vec{u}^{\,n} + \delta\vec{u}^{\,n}, \vec{v}, \Delta t; \vec{\alpha} + \delta\vec{\alpha}\right) = \vec{0} \tag{4.19}$$

which can be written as,

$$\vec{f}^{\,n+1} + \frac{\partial \vec{f}^{\,n+1}}{\partial \vec{u}^{\,n+1}}\delta\vec{u}^{\,n+1} + \frac{\partial \vec{f}^{\,n+1}}{\partial \vec{u}^{\,n}}\delta\vec{u}^{\,n} + \frac{\partial \vec{f}^{\,n+1}}{\partial \vec{\alpha}}\delta\vec{\alpha} + O\left(\delta^2\right) = \vec{0} \tag{4.20}$$

where $\frac{\partial \vec{f}^{n+1}}{\partial \vec{u}^{n+1}}$ represents the Jacobian matrix J^{n+1} that is constructed from the forward simulator at the end of Newton Raphson iteration, $\frac{\partial \vec{f}^{n+1}}{\partial \vec{u}^{n}}$ is the matrix D^{n+1} that contains derivative of accumulation terms with respect to state variables (at timestep *n*), and $\frac{\partial \vec{f}^{n+1}}{\partial \vec{\alpha}}$ is the matrix Y^{n+1} that comprises of the derivative of residual with respect to the model parameters. They can be expressed mathematically as,

$$J^{n+1} = \frac{\partial \vec{f}^{n+1}}{\partial \vec{u}^{n+1}} \tag{4.21}$$

$$D^{n+1} = \frac{\partial \vec{f}^{n+1}}{\partial \vec{u}^{n}} \tag{4.22}$$

$$Y^{n+1} = \frac{\partial \vec{f}^{n+1}}{\partial \vec{\alpha}} = \begin{bmatrix} \frac{\partial \vec{f}_{blk}^{\,n+1}}{\partial \vec{\alpha}} \\ \frac{\partial \vec{f}_{well}^{\,n+1}}{\partial \vec{\alpha}} \end{bmatrix} \tag{4.23}$$

The higher order terms in Equation (4.20) are neglected and $\vec{f}^{n+1} = 0$ gives,

$$J^{n+1}\delta\vec{u}^{n+1} = -D^{n+1}\delta\vec{u}^{n} - Y^{n+1}\delta\vec{\alpha} \tag{4.24}$$

The differentiation of the equation will provide,

$$J^{n+1}\frac{\partial \vec{u}^{n+1}}{\partial \vec{\alpha}} = -D^{n+1}\frac{\partial \vec{u}^{n}}{\partial \vec{\alpha}} - Y^{n+1} \tag{4.25}$$

where $\frac{\partial \vec{u}}{\partial \vec{\alpha}}$ can be defined as sensitivity matrix *S*. So Equation (4.25) can be re-written as,

$$J^{n+1}S^{n+1} = -D^{n+1}S^{n} - Y^{n+1} \tag{4.26}$$

Now, if we take into account wavelets of the model parameter then Equation (4.26) can be expressed as,

$$J^{n+1}S_c^{n+1} = -D^{n+1}S_c^{n} - Y^{n+1}W^{T} \tag{4.27}$$

In Equation (4.27) W is the wavelet matrix, while S_c and $\vec{c}$ can be given as,

$$S_c^{n+1} = \frac{\partial \vec{u}^{n+1}}{\partial \vec{c}} = \frac{\partial \vec{u}^{n+1}}{\partial \vec{\alpha}} W^{T} \tag{4.28}$$

and

$$\vec{c} = W\vec{\alpha} \tag{4.29}$$

4.4.3 The Adjoint Method

The adjoint-state method for computation of sensitivity coefficients becomes suitable when the number of observation data is smaller than the model parameters. Moreover, computationally, it is the most efficient method when only the gradient of objective function is required (Awotunde and Horne, 2012). It is important to note that unlike the forward sensitivity approach, sensitivities of the well variables are only computed at well locations.

The formulation of the adjoint sensitivity method starts by considering a scalar-valued function $\Psi(\vec{\alpha})$ that is dependent on $\vec{u}^{n}(\vec{\alpha})$. This function can be expressed as,

$$\Psi(\vec{\alpha}) = \eta\left(\underset{n=1}{\overset{N}{\Omega}} \vec{u}^{n}(\vec{\alpha}), \vec{\alpha}\right) \tag{4.30}$$

where

$$\underset{n=1}{\overset{N}{\Omega}}\vec{u}^{n}=\left\{\vec{u}^{n}:n=1,2,...N\right\} \tag{4.31}$$

n denotes the time index; and $\eta\left(\underset{n=1}{\overset{N}{\Omega}}\vec{u}^{n}\left(\vec{\alpha}\right),\vec{\alpha}\right)$ in Equation (4.30) is a scalar-valued function that represents the data computed at time index (*n*), for the purpose of sensitivity computation. The augmented functional Ψ_a can be formed as,

$$\Psi_a\left(\vec{u}^{n+1},\vec{\lambda},\vec{\alpha}\right)=\eta+\sum_{n=0}^{N}\left[\left(\vec{\lambda}^{n+1}\right)^{T}\ \vec{f}^{n+1}\right] \tag{4.32}$$

where $\vec{\lambda}^{n+1}$ represents the vector that contains the adjoint variables at *n* + 1 timestep. The dimensions of $\vec{\lambda}^{n+1}$ is same as that of $\delta\vec{u}^{n+1}$. For any appropriate solution $\vec{u}_{sol}^{n+1}$, we can write,

$$\vec{f}^{n+1}\left(\vec{u}_{sol}^{n+1},\vec{u}_{sol}^{n},\vec{\alpha}\right)=0 \tag{4.33}$$

and,

$$\Psi_a\left(\vec{u}_{sol}^{n+1},\vec{\lambda},\vec{\alpha}\right)=\eta\left(\vec{u}_{sol}^{n+1},\vec{\alpha}\right)=\Psi\left(\vec{\alpha}\right) \tag{4.34}$$

The total differential of the above equation can be expressed as,

$$\delta\Psi_a=\delta\eta+\sum_{n=0}^{N}\left[\left(\vec{\lambda}^{n+1}\right)^{T}\frac{\partial\vec{f}^{n+1}}{\partial\vec{u}^{n+1}}\delta\vec{u}^{n+1}+\left(\vec{\lambda}^{n+1}\right)^{T}\frac{\partial\vec{f}^{n+1}}{\partial\vec{u}^{n}}\delta\vec{u}^{n}+\left(\vec{\lambda}^{n+1}\right)^{T}\frac{\partial\vec{f}^{n+1}}{\partial\vec{\alpha}}\delta\vec{\alpha}\right] \tag{4.35}$$

Equation (4.35) can be re-written as,

$$\delta\Psi_a = \delta\eta + \sum_{n=0}^{N}\left[\left(\vec{\lambda}^{n+1}\right)^T \frac{\partial \vec{f}^{\,n+1}}{\partial \vec{u}^{n+1}}\delta\vec{u}^{n+1} + \left(\vec{\lambda}^{n+1}\right)^T \frac{\partial \vec{f}^{\,n+1}}{\partial \vec{\alpha}}\delta\vec{\alpha}\right] + \sum_{n=0}^{N}\left(\vec{\lambda}^{n+1}\right)^T \frac{\partial \vec{f}^{\,n+1}}{\partial \vec{u}^{n}}\delta\vec{u}^{n} \tag{4.36}$$

Separating the terms from the summation, followed by the application of initial conditions $\delta\vec{u}^0 = 0$ and $\vec{\lambda}^{N+1} = 0$ yields,

$$\delta\Psi_a = \delta\eta + \sum_{n=1}^{N}\left[\left(\vec{\lambda}^{n}\right)^T \frac{\partial \vec{f}^{\,n}}{\partial \vec{u}^{n}}\delta\vec{u}^{n} + \left(\vec{\lambda}^{n+1}\right)^T \frac{\partial \vec{f}^{\,n+1}}{\partial \vec{u}^{n}}\delta\vec{u}^{n}\right] + \sum_{n=1}^{N}\left[\left(\vec{\lambda}^{n}\right)^T \frac{\partial \vec{f}^{\,n}}{\partial \vec{\alpha}}\delta\vec{\alpha}\right] \tag{4.37}$$

We can write the total differential of η as,

$$\delta\eta = \frac{\partial\eta}{\partial\vec{\alpha}}\delta\vec{\alpha} + \sum_{n=1}^{N}\frac{\partial\eta}{\partial\vec{u}^{n}}\delta\vec{u}^{n} \tag{4.38}$$

Equation (4.37) can be re-arranged using Equation (4.38) as,

$$\delta\Psi_a = \sum_{n=1}^{N}\left\{\left[\left(\vec{\lambda}^{n}\right)^T \frac{\partial \vec{f}^{\,n}}{\partial \vec{u}^{n}} + \left(\vec{\lambda}^{n+1}\right)^T \frac{\partial \vec{f}^{\,n+1}}{\partial \vec{u}^{n}} + \frac{\partial\eta}{\partial\vec{u}^{n}}\right]\delta\vec{u}^{n}\right\} + \left\{\frac{\partial\eta}{\partial\vec{\alpha}} + \sum_{n=1}^{N}\left[\left(\vec{\lambda}^{n}\right)^T \frac{\partial \vec{f}^{\,n}}{\partial \vec{\alpha}}\right]\right\}\delta\vec{\alpha} \tag{4.39}$$

Consider that the first term of the equation vanishes, so equating it to zero,

$$\left(\vec{\lambda}^{n}\right)^T \frac{\partial \vec{f}^{\,n}}{\partial \vec{u}^{n}} + \left(\vec{\lambda}^{n+1}\right)^T \frac{\partial \vec{f}^{\,n+1}}{\partial \vec{u}^{n}} + \frac{\partial\eta}{\partial\vec{u}^{n}} = 0 \tag{4.40}$$

Equation (4.40) contains J^n and D^{n+1} as previously shown in Equation (4.21) and (4.22). So we may re-write as,

$$\left(J^n\right)^T \vec{\lambda}^{n} = -\left[\left(D^{n+1}\right)^T \vec{\lambda}^{n+1} + \left(\frac{\partial\eta}{\partial\vec{u}^{n}}\right)^T\right] \tag{4.41}$$

$\vec{\lambda}^{N+1}$ is zero at the last timestep, so we have,

$$\left(J^N\right)^T \vec{\lambda}^N = -\left(\frac{\partial \eta}{\partial \vec{u}^N}\right)^T \tag{4.42}$$

The adjoint variables $\vec{\lambda}^n$ are computed using these last two equations. Now as given earlier in Equation (4.23), Y^n can be expressed as,

$$Y^n = \frac{\partial \vec{f}^n}{\partial \vec{\alpha}}$$

Now using this definition along with the above equations, $\delta\Psi_a$ can be written as,

$$\delta\Psi_a = \left\{\frac{\partial \eta}{\partial \vec{\alpha}} + \sum_{n=1}^{N}\left[\left(\vec{\lambda}^n\right)^T Y^n\right]\right\}\delta\vec{\alpha} \tag{4.43}$$

The differentiation of above expression with respect to $\vec{\alpha}$ gives,

$$\frac{\partial \Psi_a}{\partial \vec{\alpha}} = \frac{\partial \eta}{\partial \vec{\alpha}} + \sum_{n=1}^{N}\left[\left(\vec{\lambda}^n\right)^T Y^n\right] \tag{4.44}$$

The function η needs to be replaced by Φ in Equations (4.41), (4.42) and (4.44); in order to calculate the gradient of the objective function (Φ). The matrices J^n, D^{n+1} and Y^n are same for all data points, so it is feasible to group all data points into single vector represented as $\vec{\eta}$, and all solution vectors $\vec{\lambda}^n$ are collected into one single matrix $\tilde{\lambda}^n$. Finally we can simultaneously solve for $\vec{\lambda}^n$. The Equations (4.41), (4.42) and (4.44) can then expressed as,

$$\left(J^n\right)^T \tilde{\lambda}^n = -\left[\left(D^{n+1}\right)^T \tilde{\lambda}^{n+1} + \left(\frac{\partial \vec{\eta}}{\partial \vec{u}^n}\right)^T\right] \tag{4.45}$$

$$\left(J^N\right)^T \tilde{\lambda}^N = -\left(\frac{\partial \vec{\eta}}{\partial \vec{u}^N}\right)^T \tag{4.46}$$

and,

$$\frac{\partial \vec{\Psi}_a}{\partial \vec{\alpha}} = \frac{\partial \vec{\eta}}{\partial \vec{\alpha}} + \sum_{n=1}^{N}\left[\left(\tilde{\lambda}^n\right)^T Y^n\right] \tag{4.47}$$

4.5 Thresholding

The reduction in the dimension of the space can be termed as thresholding. This dimension reduction or determination of wavelets is based on predetermined condition that is subject to the space being thresholded and the available information.

4.5.1 Thresholding of Observation Space

Two methods are available for thresholding of observation space: data-thresholding and sensitivity thresholding.

In this work, the observation space is thresholded using data-thresholding because it has been observed that this method provides more reliable results (Awotunde, 2010). In this technique, the wavelets of measured data that are largest (in terms of absolute value) are chosen as observed data. A predetermined threshold value is used and wavelet coefficients having magnitude greater than this are selected. The reason for using this approach is that the measurement data contains important information related to the model, and it is believed that the best model will provide a good match to this measured data. Usually the number of wavelet coefficients retained for the measured data are quite less than the number of wavelets discarded. In spite of this the number of wavelets

considered contains significant information compared to the discarded coefficients. This is evident from the fact that often the match provided by the fewer number of wavelets is better than obtained from either large number of wavelets or all of them.

4.5.2 Thresholding of Model Space

There are three different methods that can be used for thresholding of model space: sensitivity-based thresholding, gradient-based thresholding and parameter-based thresholding.

The sensitivity-based thresholding is performed for the model space in this work due to the fact that it mostly performs better than other methods (Awotunde, 2010). This technique performs the parameterization based on magnitude of individual entries of the sensitivity matrix. A simple threshold value or a total fractional energy threshold is set, and columns that have at least one entry larger than the preset threshold are selected. There are two costs associated with the approach: one for computing the sensitivities to all coefficients of transformed parameter space and the other for the computation of forward model and sensitivities for new parameter field calculated from selected coefficients.

4.6 Parameterization

The determination of a subset of reservoir model parameters that can adequately characterize the reservoir is known as reservoir parameterization. There are generally two spaces, the model/parameter space and the data space. The parameters of reservoir to be estimated constitute model space; while the data space consists of two sets, the

measurement space and the observation space. The *2Dwp-wk* parameter estimation approach has been used in this work for the parameterization of data and model spaces. The two dimensional transformation and reduction of the data space offers the following advantages (Awotunde, 2010):

- Reduction in storage and computation (sensitivity coefficients) cost.
- Feasibility in integration of different types of production data.
- Helps to decorrelate inter-well data.

4.6.1 Two-dimensional Transformation *2Dwp-wk* Approach

The Two-dimensional wavelet transformation provides a reliable method of data integration. The minimization of the objection function in this approach, in form of Frobenius norm, can be written as,

$$\min_{\vec{\alpha}}\left\{\Phi\left(\vec{\alpha}\right)\right\} = \min_{\vec{\alpha}}\left\{\frac{1}{2}\left\|\tilde{D}_{cal,w} - \tilde{D}_{meas,w}\right\|_F^2\right\} \tag{4.48}$$

where $\Phi\left(\vec{\alpha}\right)$ is the objective function that we need to minimize, $\tilde{D}_{cal,w}$ and $\tilde{D}_{meas,w}$ are wavelet transforms of matrix of calculated and measured data respectively.

In case of wavelet transformation of parameter space, the parameter $\vec{\alpha}$ in Equation (4.48) must be replaced by $\vec{c}_{\vec{\alpha}}$. This two-dimensional wavelet transformation of the data space followed by two-dimensional thresholding outperformed the conventional approach and was also found to be computationally efficient (Awotunde, 2010).

Two-dimensional Data Transformation Procedure

The general procedure is outlined as follows:

- Group all datasets in *N x L* matrix $\tilde{D}_{meas}$.
- Perform two-dimensional wavelet decomposition.
- Find maximum absolute entry $d_{\max}$. Set a threshold values for columns and rows.
- Divide the largest absolute entry of each column by $d_{\max}$ to obtain *cfrac*. Retain all columns that have *cfrac* greater than the threshold value.
- Apply same procedure for rows to get *rfrac* and retain the rows. The final matrix $\tilde{D}_{meas,w}$ will be of dimension N_r x L_r.

4.7 Procedure to Estimate Reservoir Parameters with Sensitivity-based Upscaling

The $\tilde{D}_{meas,w}$ matrix is considered as the final observed data set for inverse analysis. The procedure for reservoir parameter estimation can be given as:

1. Make an initial guess of permeability field $\vec{k}$ and transform into wavelets (wk).
2. Use forward model to obtain calculated data $\tilde{D}_{cal}$ and then compute its reduced wavelets $\tilde{D}_{cal,w}$. These reduced wavelets are to be fitted to observation data $\tilde{D}_{meas,w}$.
3. Compute sensitivity matrix of the reduced wavelets $\tilde{D}_{cal,w}$ to all wavelets of reservoir parameters (wk).

4. Use this sensitivity matrix to threshold the model space from $\vec{\alpha}$ to $\vec{c}_{\vec{\alpha}}$. This reduces the size of model coefficients from *M* to N_{mcoeff}. This is repeated at every iteration while gradually increasing the number of model-space wavelets retained until the desired level of model parameterization has been achieved.
5. Use these thresholded model space coefficients to compute new permeability distribution.
6. The new permeability field is used to run the upscaled forward model to get $\tilde{D}_{cal,w}$, and also compute the model-and-data reduced wavelet sensitivity matrix $\frac{\partial \tilde{D}_{cal,w}}{\partial \vec{c}_{\vec{\alpha}}}$ (the sensitivities of reduced wavelets $\tilde{D}_{cal,w}$ to the thresholded model space $\vec{c}_{\vec{\alpha}}$).
7. Use the calculated data and reduced wavelet sensitivity matrix to compute the gradient and Hessian. This gradient and Hessian are then used to compute the new iterate.
8. Repeat from point 2 to 7 until convergence.

It is to be noted that the adjoint sensitivity computation is integrated into the fine-scale and upscaled simulations. Thus we integrate it with the fine-scale and upscaled simulator used in this work. The computation of sensitivity matrix requires several values including the Jacobian terms, accumulation terms etc. that are calculated during the final Newton-Raphson loop of each time-step of the simulator. Therefore the values are stored in variables during the simulation process and subsequently used to compute the sensitivity matrix. Similar procedure is followed for the calculation of gradient. It is also integrated with the simulator and at the end we obtain the gradient required in the Levenberg-Marquardt algorithm.

4.8 Efficiency of the Proposed Technique

The focus of this work is sensitivity-based upscaling that can be used during history matching. Basically the upscaling is coupled with data and model space reduction and this makes the inverse analysis to be computationally more efficient. The reduction of the two spaces can be better understood with the results presented in Chapter 5.

However the prime objective of reducing these spaces is to make the whole process faster. This reduction is performed through wavelet transformation and thresholding which provide the optimal subset out of the total space that can adequately represent it and can produce good results.

The computational effort of the adjoint method used for sensitivity calculation in this work depends on the number of data points that we use during the history matching process. Thus reducing the data space makes it less expensive. Subsequently reducing the model space makes the size of resulting sensitivity matrix (to be used during calculation of Hessian) to be smaller. These two reductions are same for both fine-scale and upscale history matching process that we have adopted.

However in case of upscaling, the model reduction also reduces the number of simulation grid blocks and by extension the size of the Jacobian matrix used during the Newton-Raphson iteration of the simulation process.

$$\begin{bmatrix} & & \\ & J & \\ & & \end{bmatrix}\begin{bmatrix} \\ \delta\vec{u} \\ \end{bmatrix} = -\begin{bmatrix} \\ \vec{f} \\ \end{bmatrix} \tag{4.49}$$

This represents the equations that we solve to determine the state variable $\vec{u}$. In our simulation it is solved using LU decomposition, thus reduction in Jacobian size has an impact on the computational time.

If we compare the computational time of fine-scale history matching (using complete data and model space) with the upscale history matching (using reduced subset of data and model), we would certainly achieve considerable improvement.

CHAPTER 5

APPLICATION OF SENSITIVITY-BASED UPSCALING DURING HISTORY MATCHING

This chapter presents the application of the sensitivity-based upscaling for the purpose of history matching. First the base results will be presented that will provide the match of fine-scale results to the upscaled results, in which the reservoir is upscaled, based on the provided permeability distribution having homogenous patches. Subsequently the inverse modeling cases will be presented, and the reliability of the technique will be analyzed.

The *2Dwp-wk* approach is used for the transformation of data and model spaces. After transformation and thresholding of the data, a subset of the data is obtained from the actual data. This reduction can be approximated in terms of compression ratio as,

$$CR = \frac{Total\ Amount\ of\ Measured\ Data}{Amount\ of\ Wavelets\ Retained} \tag{5.1}$$

During the inverse modeling, we need to evaluate the permeability and data residuals which can be given as,

$$d_{residual} = \frac{\left\| D_{cal} - D_{meas} \right\|}{n_{data}} \tag{5.2}$$

where D_{cal} is the calculated data, D_{meas} is the measured data and n_{data} is the total amount of data.

The reservoir and fluid properties that have been used for the simulation runs are given in Table 5.1.

Table 5.1: Reservoir and fluid properties used during simulations

Properties	**Values**
Initial Pressure ($p_{initial}$)	5000 psi
Porosity (ϕ)	0.25
c_o	1.2e-5 psi^{-1}
c_w	5e-7 psi^{-1}
S_{wi}	0.1
r_w	0.25 ft
Skin	1.2
Oil Density (ρ_o)	40 lb/ft^3
Water Density (ρ_w)	62.2 lb/ft^3

The capillary pressure (P_c) is neglected during the simulation, while the relative permeability values are calculated using Equations (5.3) and (5.4).

$$k_{rw} = S_w^{1.5} \tag{5.3}$$

$$k_{ro} = (1 - S_w)^{1.5} \tag{5.4}$$

The viscosity for oil and water phases are computed using Equations (5.5) and (5.6) respectively,

$$\mu_o = 5e^{c_{\mu o}(P_o - P_{sc})} \tag{5.5}$$

$$\mu_w = e^{c_{\mu w}(P_o - P_c - P_{sc})} \tag{5.6}$$

where $c_{\mu o}$ is the constant value equal to $2x10^{-6}$, $c_{\mu w}$ is equal to $6x10^{-8}$ and P_{sc} is considered to be 14.7 psi.

During simulations, the total rate constraint has been used for the production wells while water rate constraint is employed for injectors.

5.1 Comparison of Fine-Scale and Upscaled Forward Simulation

First, we considered reservoir models with such permeability distribution that result in some homogenous regions in the reservoir. Three reservoir samples were considered. The samples are (1) a small reservoir discretized into 16x16 grids, (2) another small reservoir discretized into 32x32 grids and (3) a mid-size reservoir discretized into 64x64 grids. Each of these reservoir samples was upscaled based on the homogeneous patches indicated by its inherent permeability distribution. Then a flow simulation was performed on both the fine-scale and upscaled reservoir model. In upscaling, each reservoir sample, the two constraints described in Section 4.2 were imposed. The constraints are that all grid blocks are allowed to be merged during upscaling except:

1. those having wells
2. those having wells and their adjacent transmissibility sharing grid blocks

5.1.1 Results for 16 x 16 Reservoir Model

The reservoir system of size 16x16 is considered and the comparison is made for the results with both constraints. This reservoir contains two producers and two injectors.

The fine-scale and upscaled simulators were run to obtain bottom-hole pressure and water-cut; and the match between the results from the upscaled reservoir model and those from the fine-scale model was used to determine which constraint produced better results. Figure 5.1 presents the permeability distribution and the well location considered for this scenario. Figures 5.2 and 5.3 present the bottom-hole pressure and water-cut matches with Constraint 1, while Figures 5.4 and 5.5 show the matches with Constraint 2.

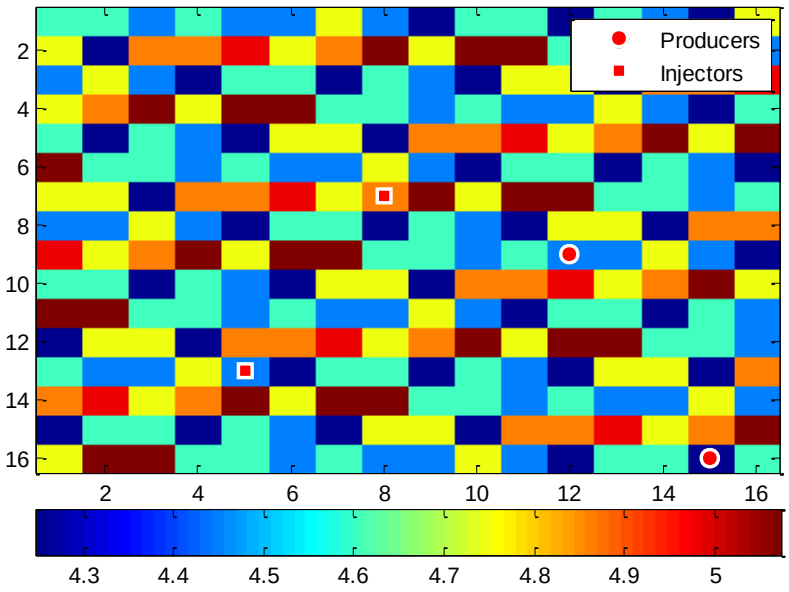

Figure 5.1: *log* permeability distribution and well locations for 16 x 16 system

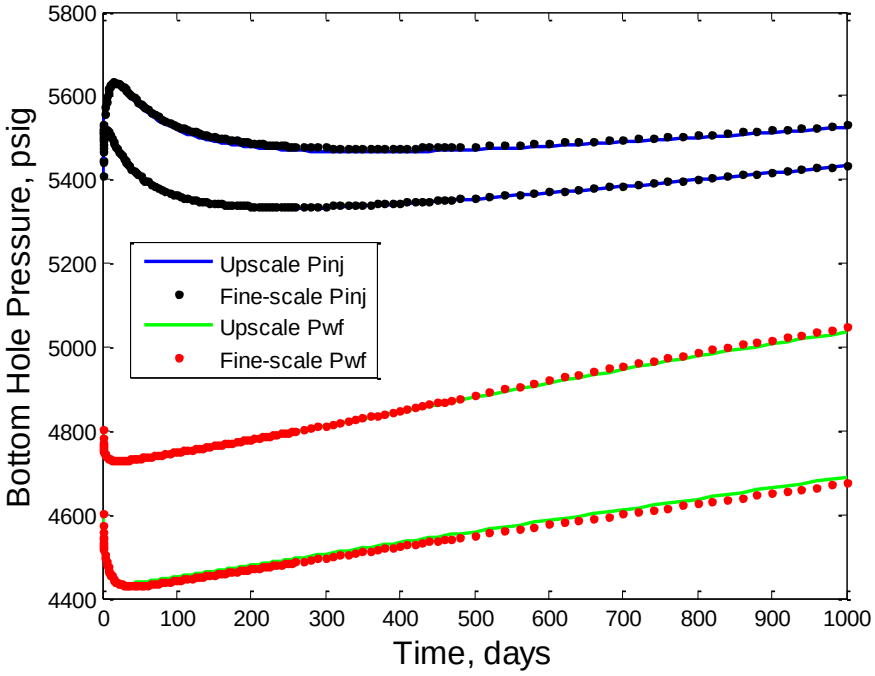

Figure 5.2: Bottom-hole pressures from fine-scale and upscale reservoir models for the 16 x 16 system (Constraint 1)

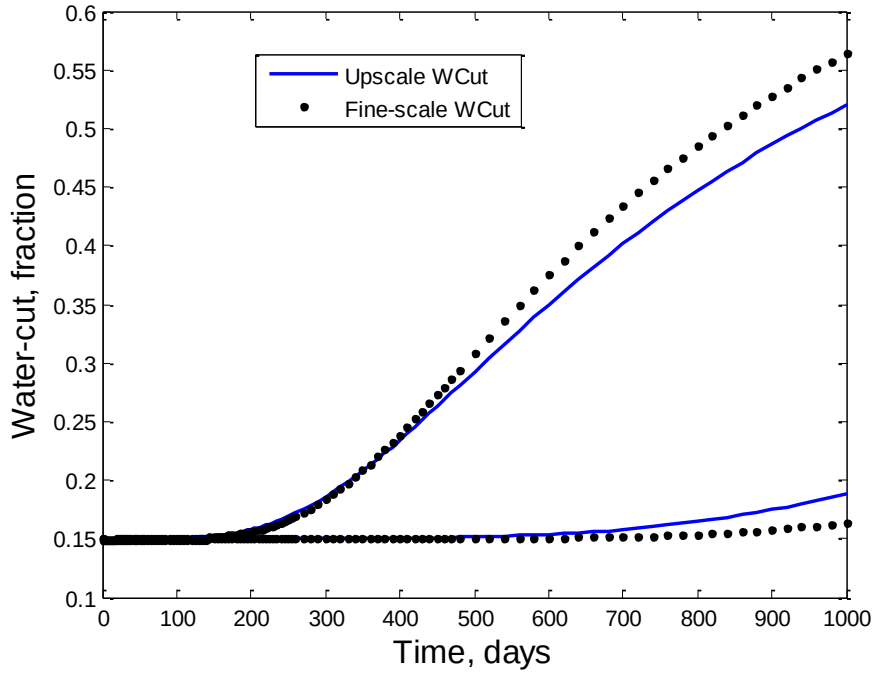

Figure 5.3: Water-cuts from fine-scale and upscale reservoir models for the 16 x 16 system (Constraint 1)

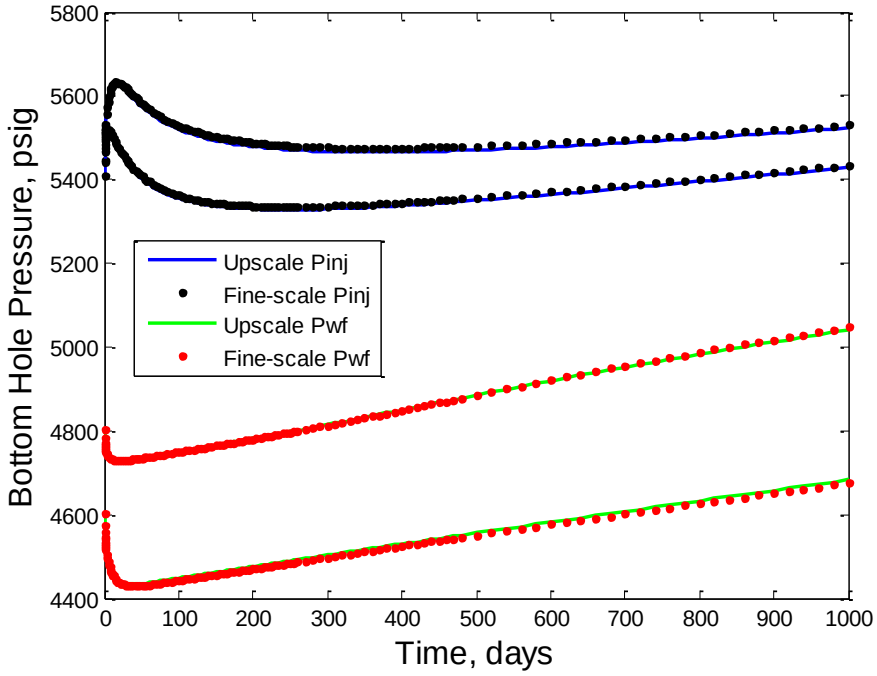

Figure 5.4: Bottom-hole pressures from fine-scale and upscale reservoir models for the 16 x 16 system (Constraint 2)

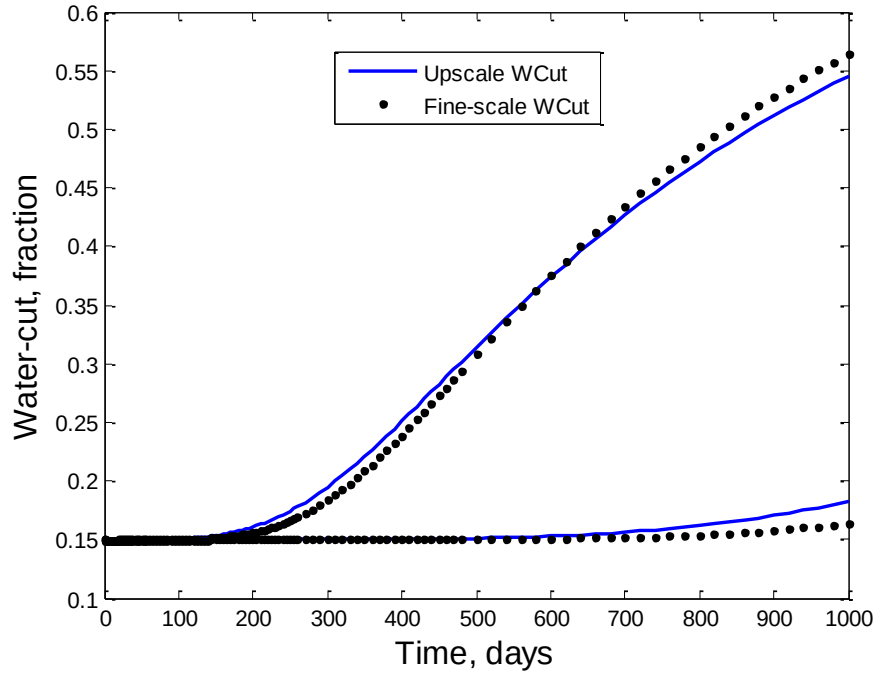

Figure 5.5: Water-cuts from fine-scale and upscale reservoir models for the 16 x 16 system (Constraint 2)

We obtained very good matches of bottom-hole pressure with both constraints. But the water-cut match was not good with any of the constraints. However, the results from Constraint 2 was better than those from Constraint 1.

5.1.2 Results for 32 x 32 Reservoir Model

A similar comparison is made using pressure and water-cut simulated from the 32 x 32 reservoir system shown in Figure 5.6. In this case, the reservoir has three producers and three injectors. The simulated pressure and water-cut from the upscaled model is compared with those from the fine-scale model. Figure 5.6 presents the permeability distribution and well location for this case. The bottom-hole pressure and water-cut match with Constraint 1 are shown in Figures 5.7 and 5.8, while Figures 5.9 and 5.10 provide the match with Constraint 2.

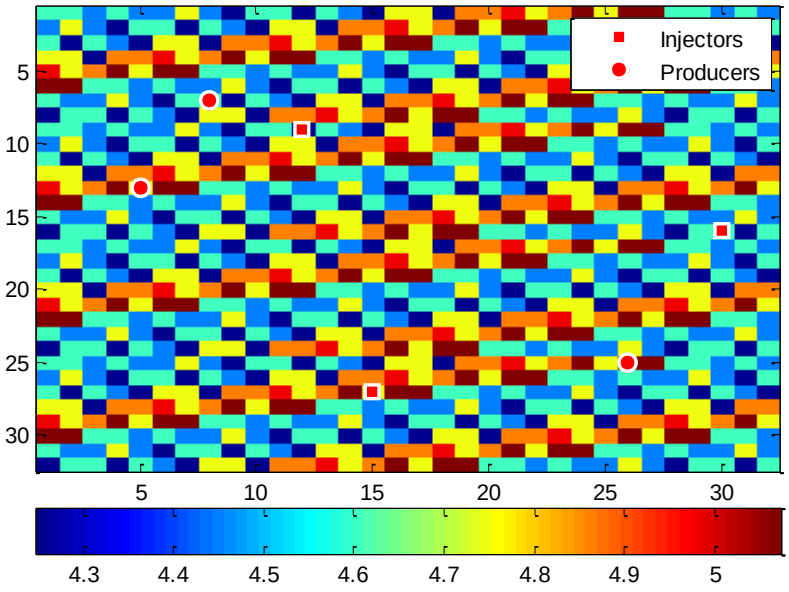

Figure 5.6: *log* permeability distribution and well locations for 32 x 32 system

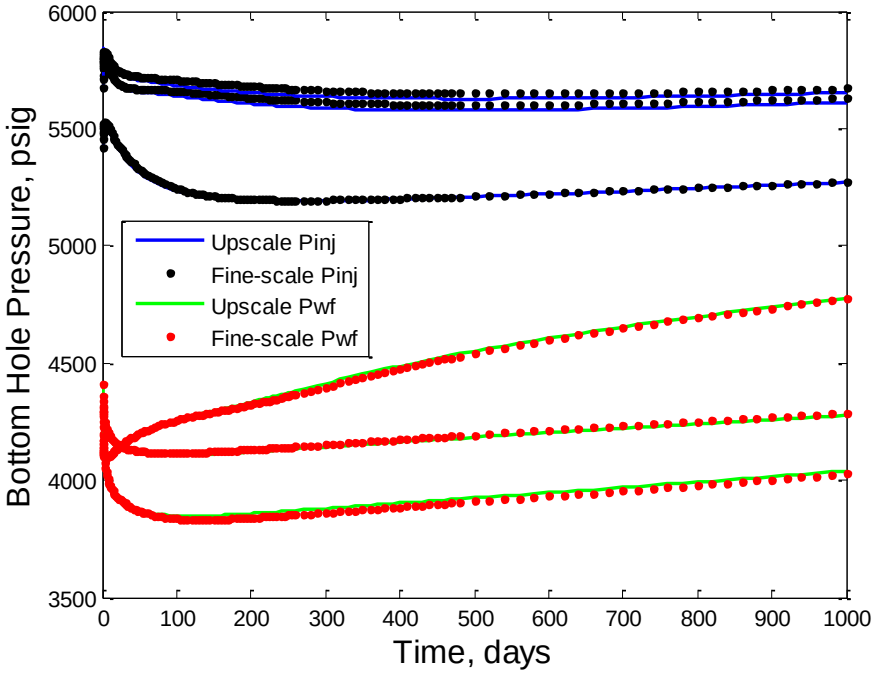

Figure 5.7: Bottom-hole pressures from fine-scale and upscale reservoir models for the 32 x 32 system (Constraint 1)

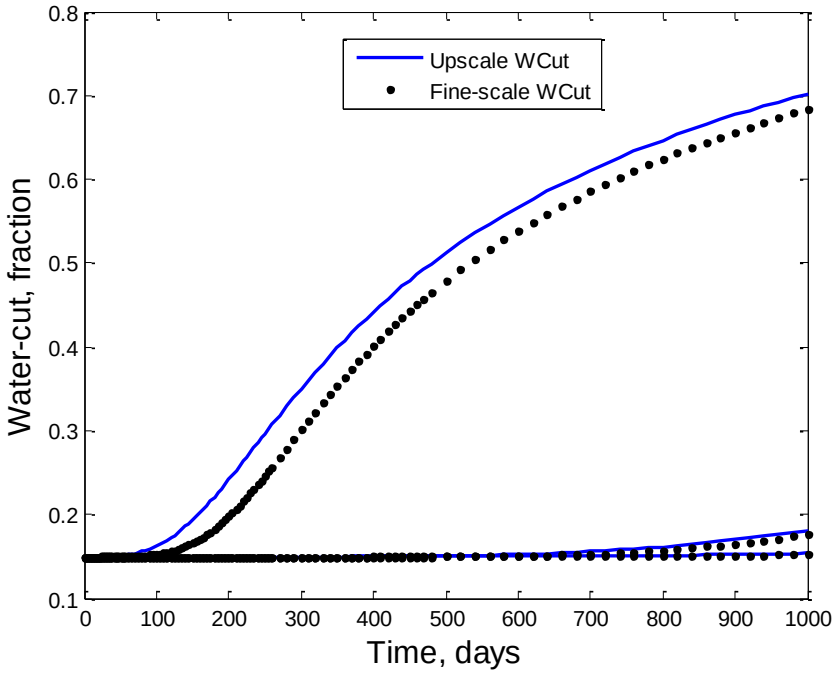

Figure 5.8: Water-cuts from fine-scale and upscale reservoir models for the 32 x 32 system (Constraint 1)

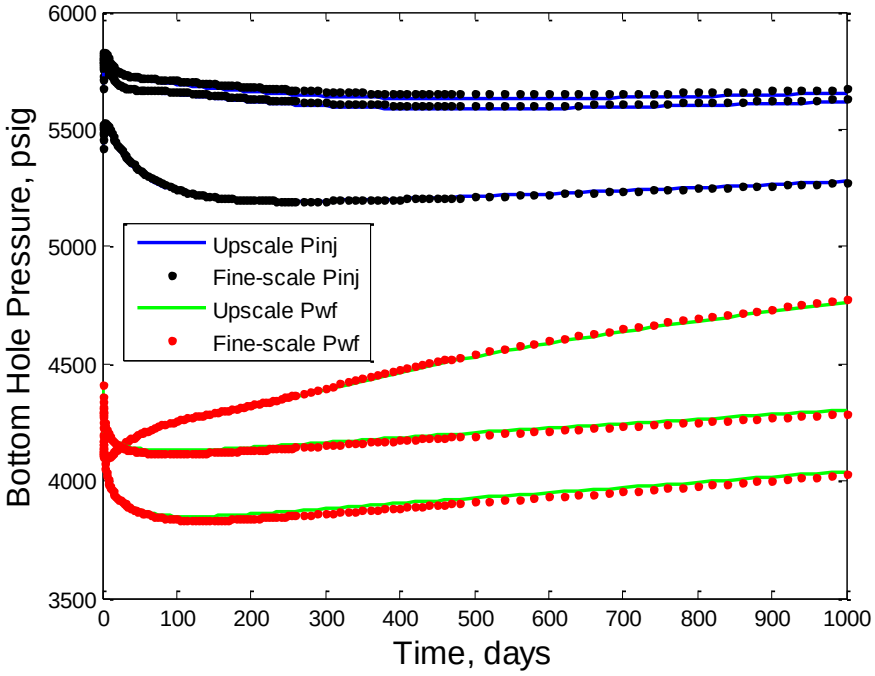

Figure 5.9: Bottom-hole pressures from fine-scale and upscale reservoir models for the 32 x 32 system (Constraint 2)

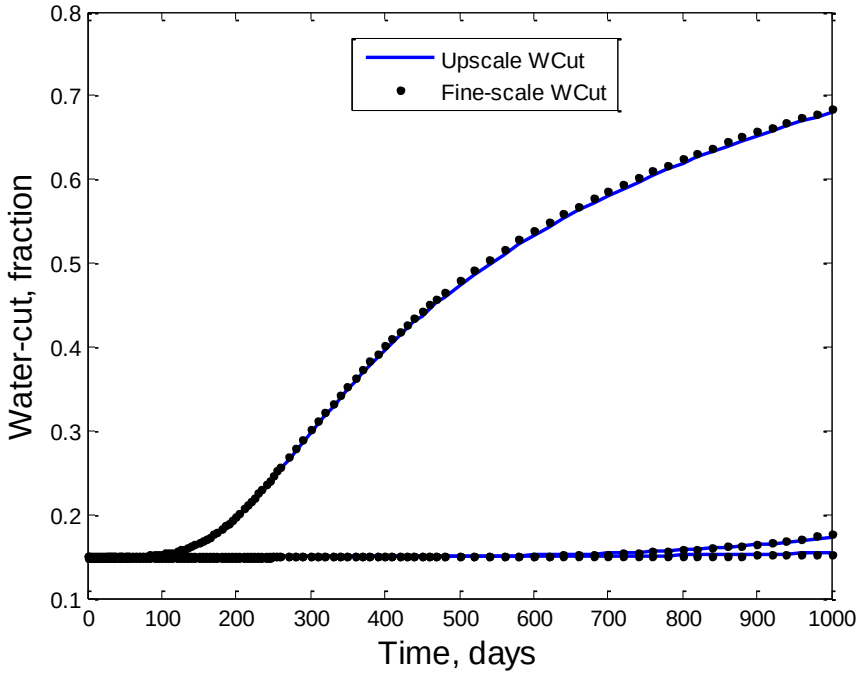

Figure 5.10: Water-cuts from fine-scale and upscale reservoir models for the 32 x 32 system (Constraint 2)

We observe that both constraints provide similar and reasonable matches of pressure of the upscaled model to the pressure of the fine-scale model. However, Figure 5.8 shows that water-cut match with Constraint 1 is poor, particularly for one of the well. On the contrary, Constraint 2 gave a good match for water-cut of all wells.

5.1.3 Results for 64 x 64 Reservoir Model

The 64 x 64 reservoir system is considered with a total of eight wells that include four producers and four injectors. The results from both constraints are compared with the results from fine-scale model. The well locations and the permeability distribution for this system are presented in Figure 5.11. We have again considered few homogenous regions in the reservoirs which are combined during upscaling. Bottom-hole pressure and water-cut matches for Constraint 1 are shown in Figures 5.12 and 5.13, and for Constraint 2 the results are presented in Figures 5.14 and 5.15.

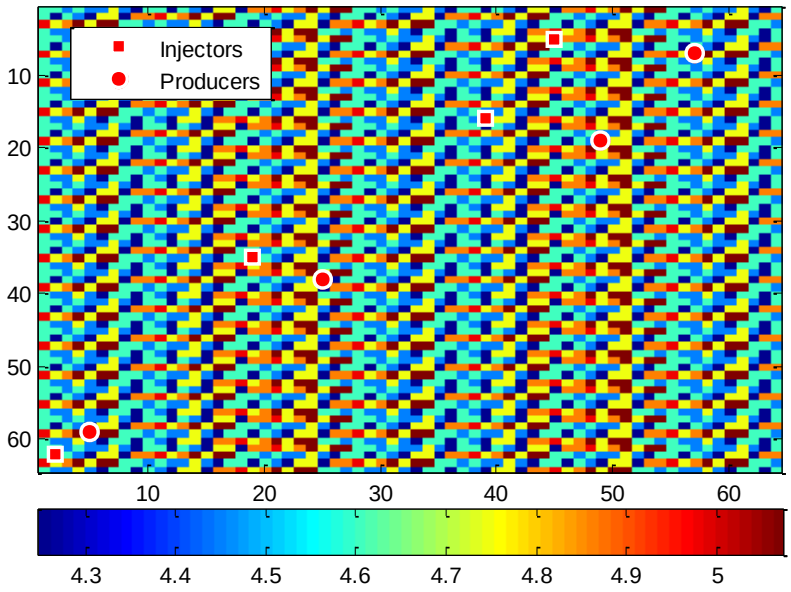

Figure 5.11: *log* permeability distribution and well locations for 64 x 64 system

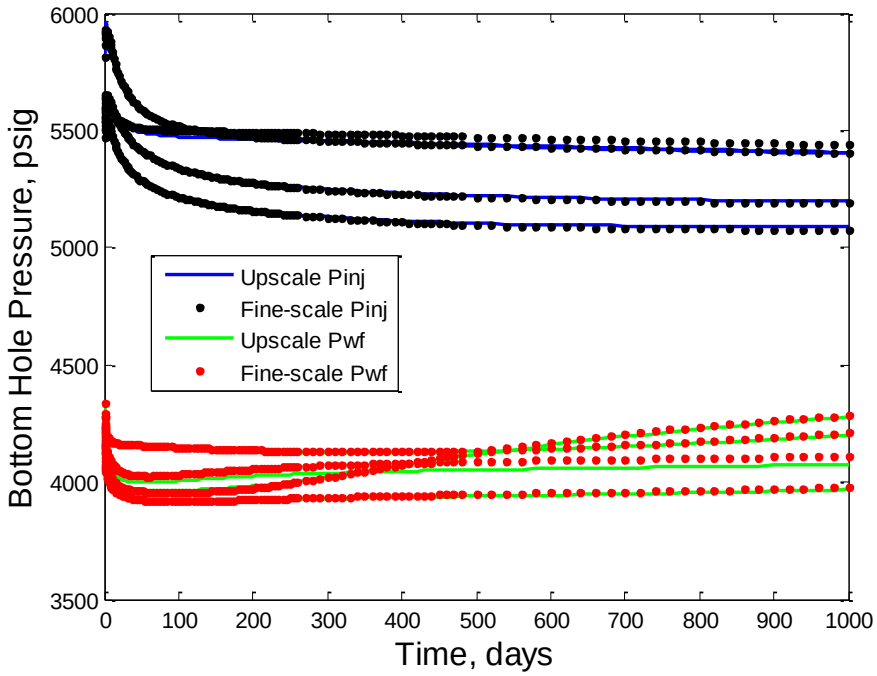

Figure 5.12: Bottom-hole pressures from fine-scale and upscale reservoir models for the 64 x 64 system (Constraint 1)

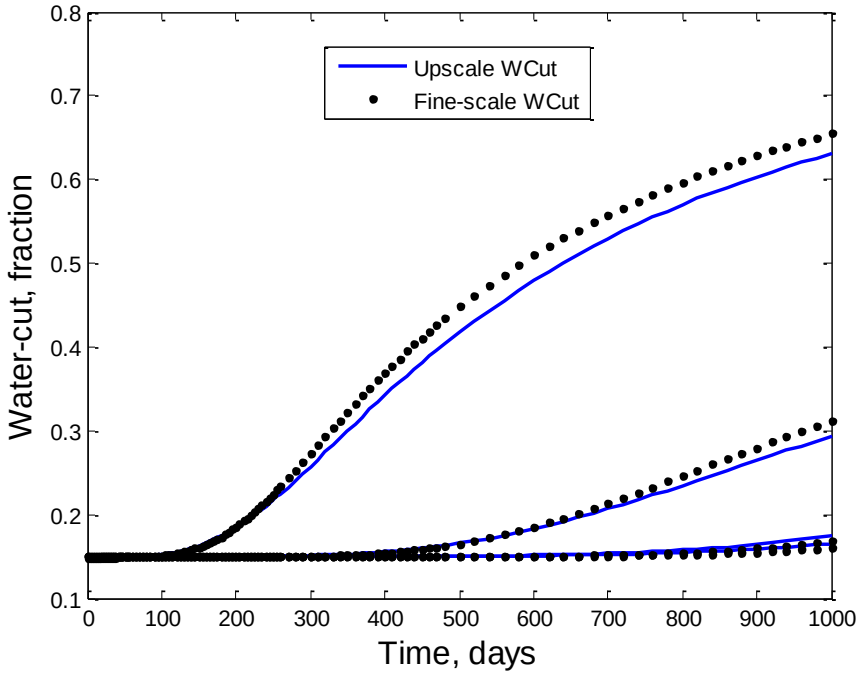

Figure 5.13: Water-cuts from fine-scale and upscale reservoir models for the 64 x 64 system (Constraint 1)

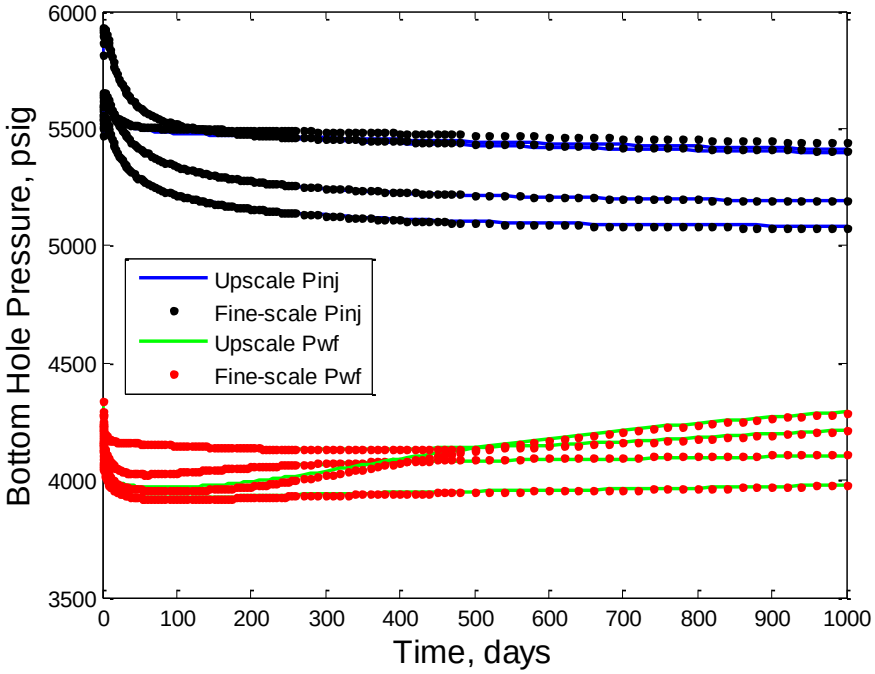

Figure 5.14: Bottom-hole pressures from fine-scale and upscale reservoir models for the 64 x 64 system (Constraint 2)

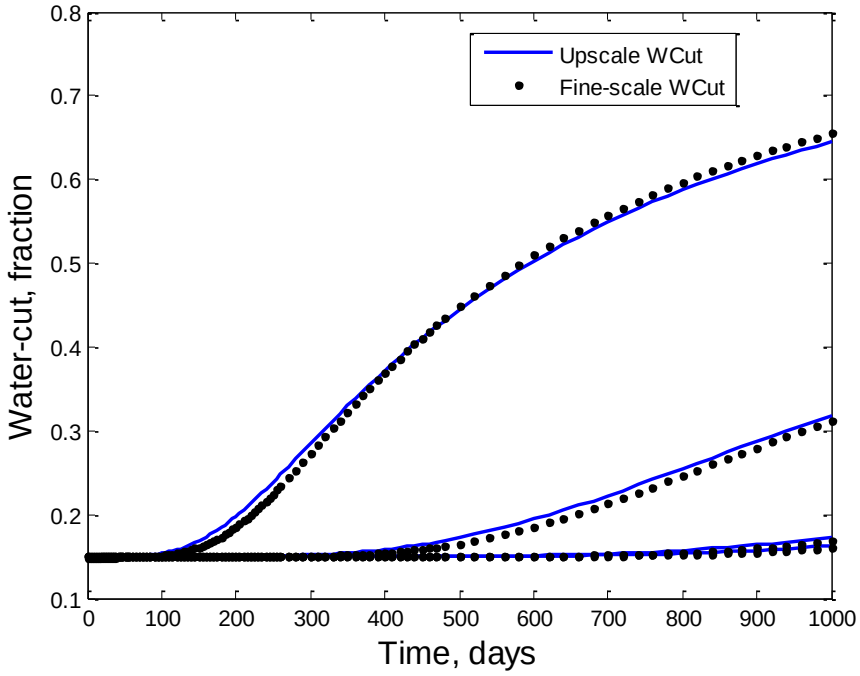

Figure 5.15: Water-cuts from fine-scale and upscale reservoir models for the 64 x 64 system (Constraint 2)

Figures 5.12 and 5.14 indicate that Constraint 2 provides slightly better pressure results than Constraint 1. In case of water-cut; Constraint 1 did not give good results, while Constraint 2 provided reasonably good results for all wells.

Thus, the results from the simulation of the upscaled model suggest that Constraint 2 is better than Constraint 1. Therefore, we chose only Constraint 2 for the history matching.

5.2 Inverse Analysis Using Sensitivity-Based Upscaling

In this section, we present history matching results for three different reservoir models and three model-space thresholding scenarios. For each reservoir model, three

thresholding values were used separately to select the wavelets that make up the model space. The upscaling procedure used in the forward simulations was described in Section 4.7. Furthermore, history matching was performed for the upscaled (this work) and the fine-scale (Awotunde, 2010; Awotunde and Horne, 2010) systems and the results from both of them were compared. We transformed the model space into wavelets and then perform thresholding to reduce the number of model parameters used for describing the system. This is done to reduce the computation time and also the non-uniqueness associated with the estimated results. The three fractions used in thresholding the model space are 0.6, 0.4 and 0.25. Each of these fractions determines the number of wavelets of the parameters we retain for history matching. The wavelet fraction of 0.6 indicates that the problem dimension is reduced to 60% of its original size. That is 60% of the total number of wavelets (of reservoir parameters) are selected. Upon inversion, the selected wavelets results in heterogeneous permeability distribution with some homogeneous patches. These number and size of homogenous patches tend to increase as we reduce the wavelet fraction.

5.2.1 Reservoir System with 16 x 16 Grids

The fine-scale and upscale inverse analyses are performed separately. In each inverse problem, the model space is reduced by selecting 0.6, 0.4 or 0.25 fraction of the total number of wavelets. Two producers and two injectors have been considered for this system.

Fine-scale Inverse Analysis

Fine-scale history matching was performed for the three wavelet fractions as mentioned above. The match of bottom-hole pressure for all the fraction of wavelets considered are shown in Figure 5.16, Figure 5.17 and Figure 5.18, while water-cut match for fraction of 0.6, 0.4 and 0.25 is presented in Figure 5.19, Figure 5.20 and Figure 5.21 respectively.

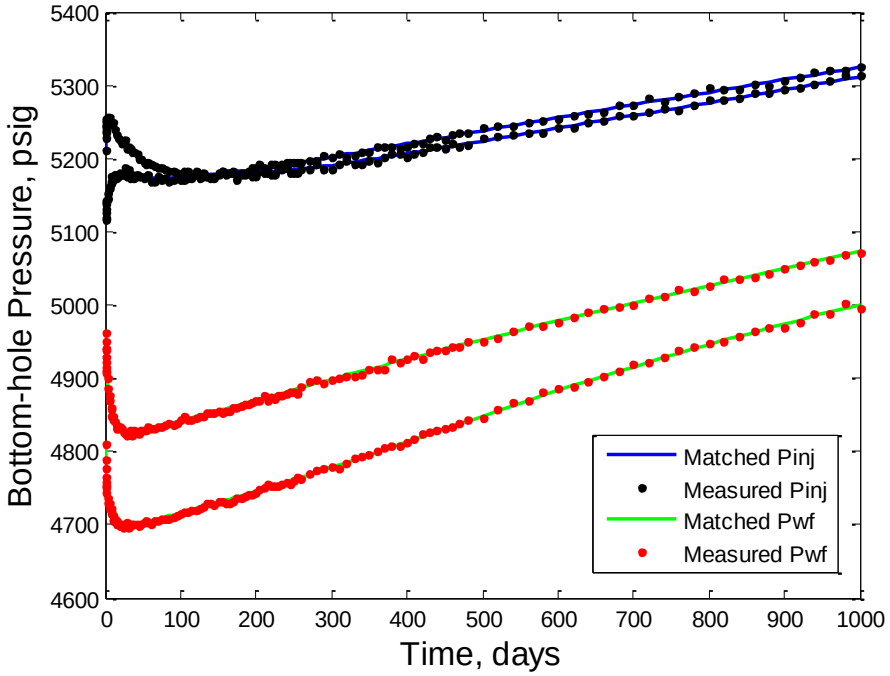

Figure 5.16: Match to measured bottom-hole pressure in all wells for the 16 x 16 reservoir system (wavelet fraction 0.6, no upscaling performed during history matching)

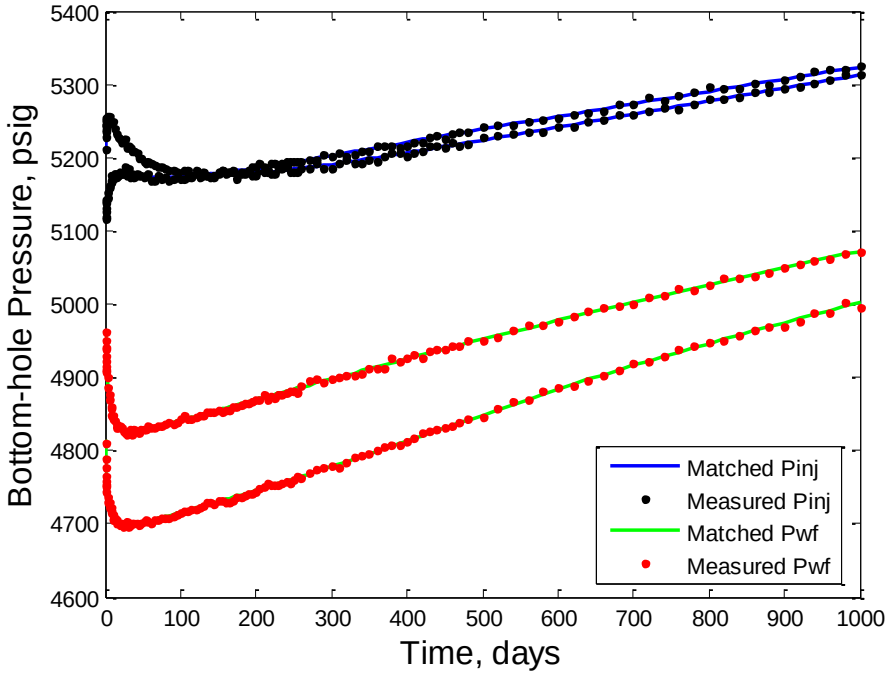

Figure 5.17: Match to measured bottom-hole pressure in all wells for the 16 x 16 reservoir system (wavelet fraction 0.4, no upscaling performed during history matching)

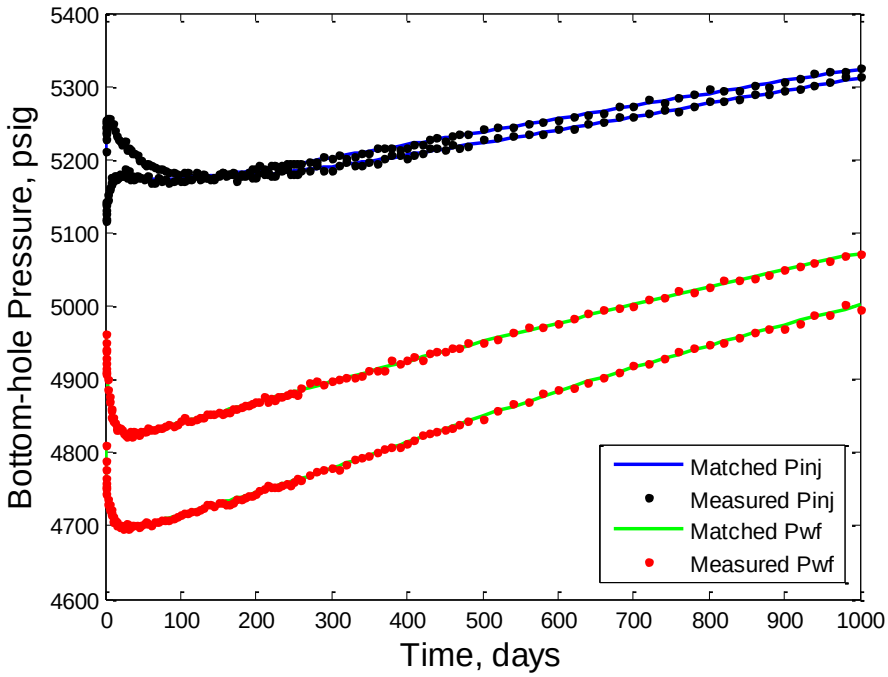

Figure 5.18: Match to measured bottom-hole pressure in all wells for the 16 x 16 reservoir system (wavelet fraction 0.25, no upscaling performed during history matching)

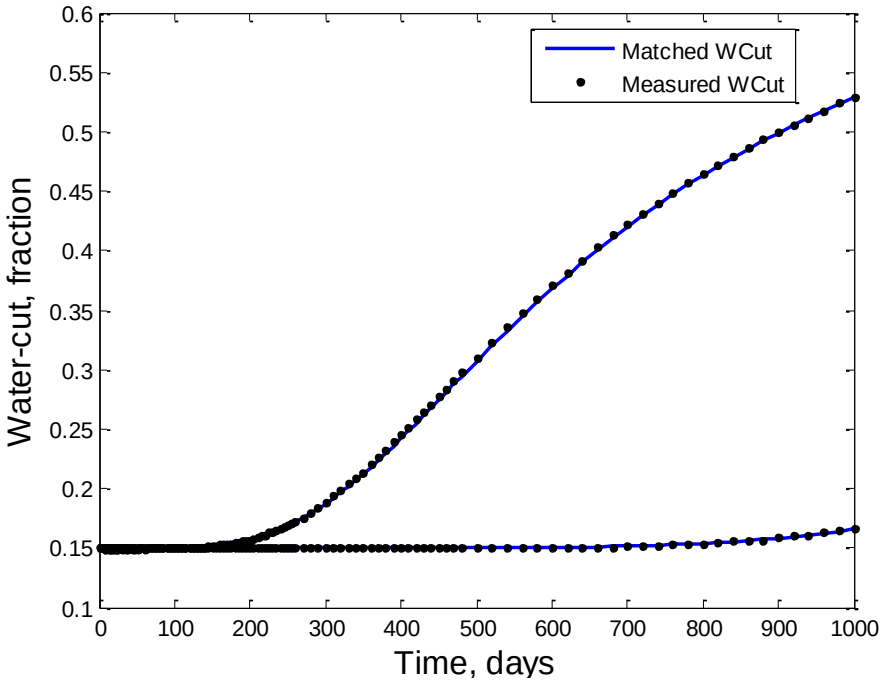

Figure 5.19: Match to water-cut in all producers for the 16 x 16 reservoir system (wavelet fraction 0.6, no upscaling performed during history matching)

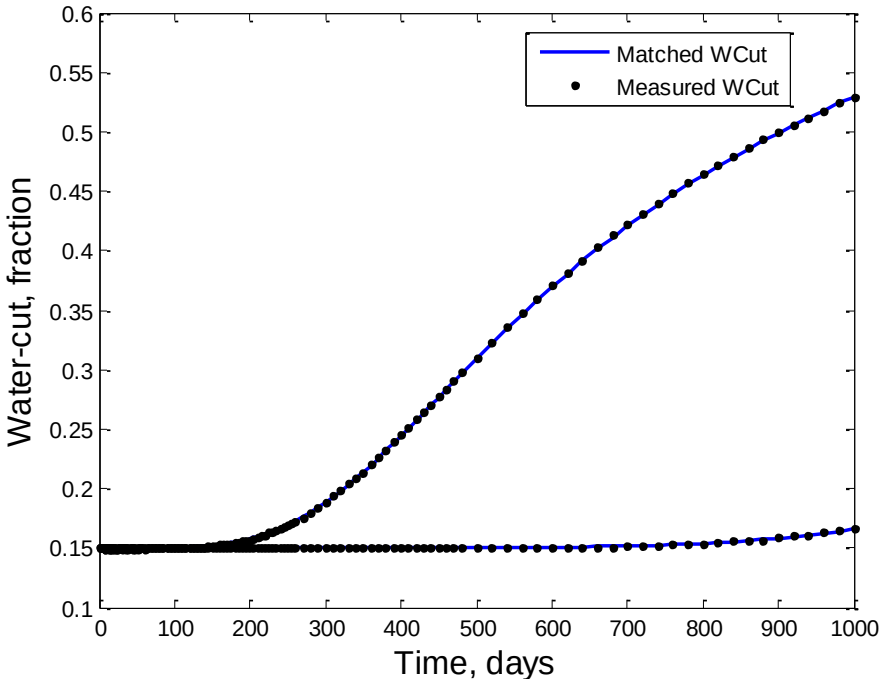

Figure 5.20: Match to water-cut in all producers for the 16 x 16 reservoir system (wavelet fraction 0.4, no upscaling performed during history matching)

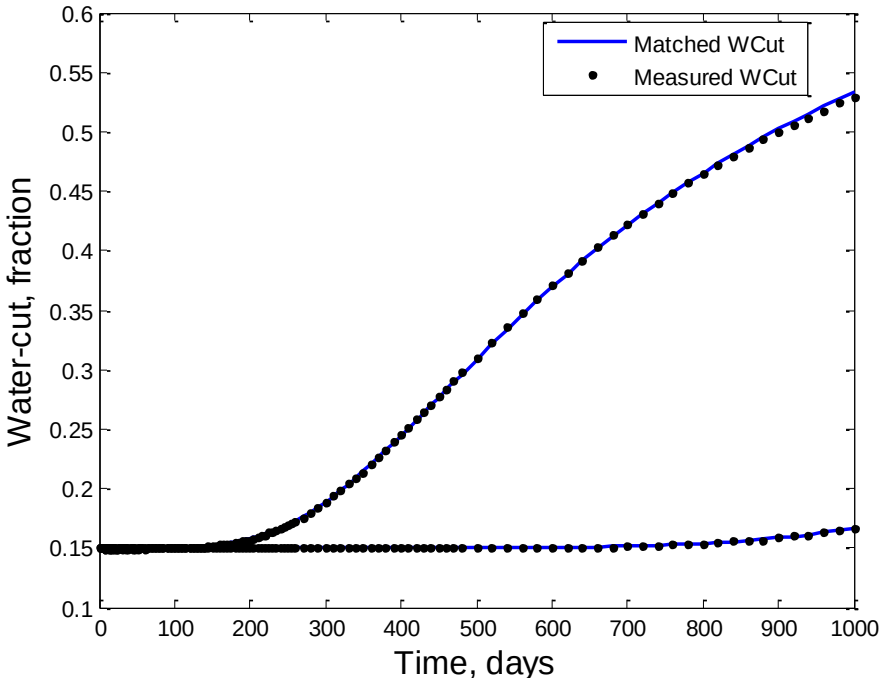

Figure 5.21: Match to water-cut in all producers for the 16 x 16 reservoir system (wavelet fraction 0.25, no upscaling performed during history matching)

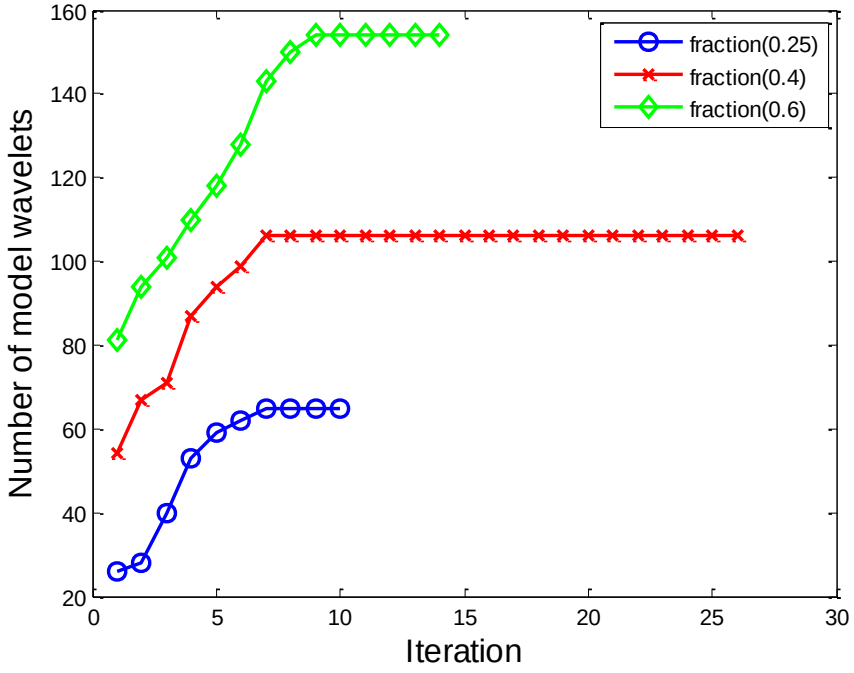

Figure 5.22: Trend of wavelet coefficients for the 16 x 16 reservoir system (all fractions, no upscaling performed during history matching)

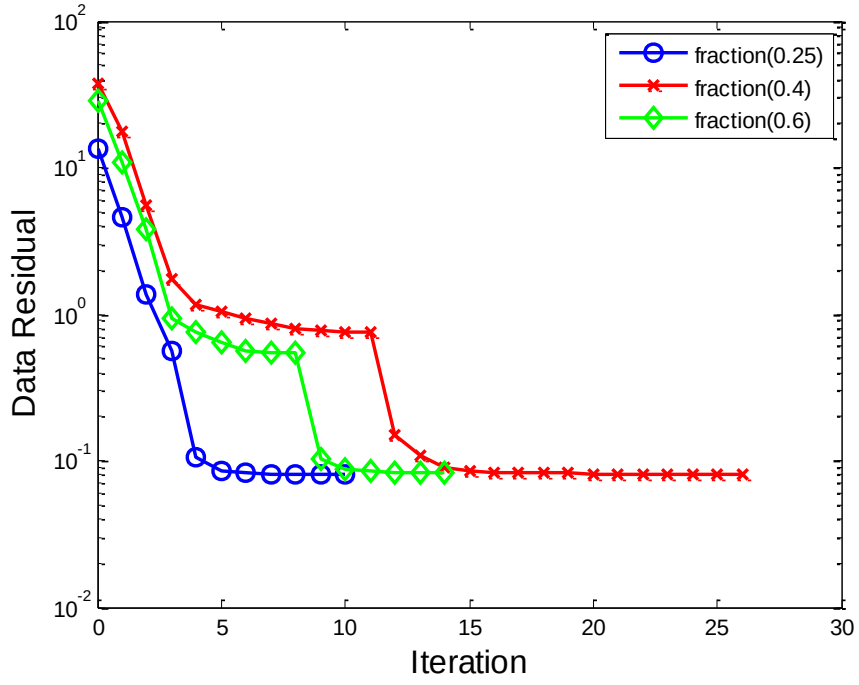

Figure 5.23: Data residual for the 16 x 16 reservoir system (all fractions, no upscaling performed during history matching)

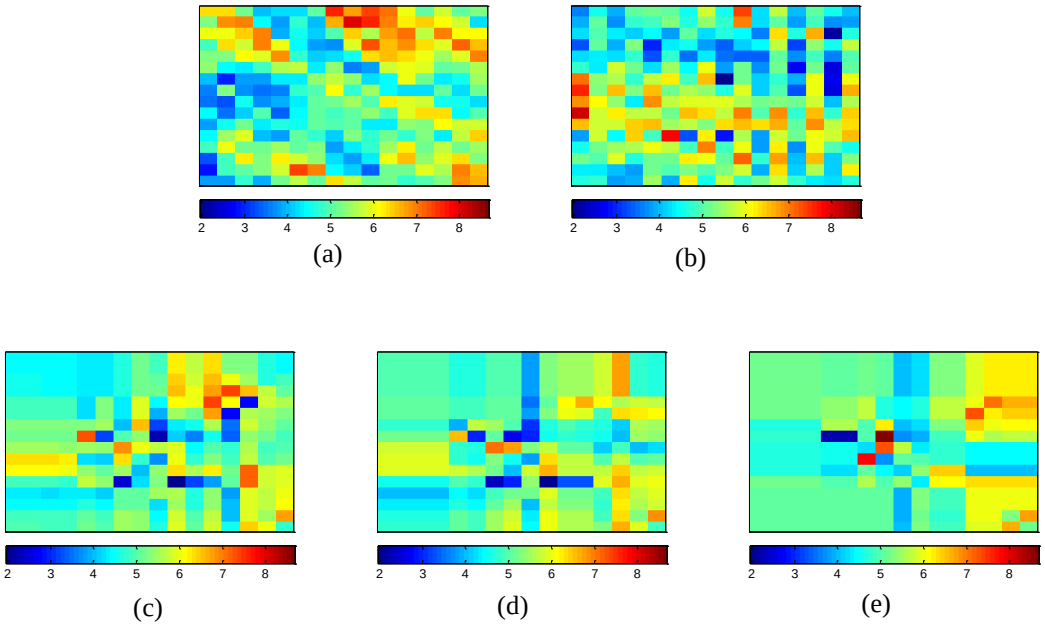

Figure 5.24: *log* permeability distribution for the 16 x 16 reservoir system (a) true (b) initial guess (c) estimate of wavelet fraction 0.6 (d) estimate of wavelet fraction 0.4 (e) estimate of wavelet fraction 0.25 (no upscaling performed during history matching)

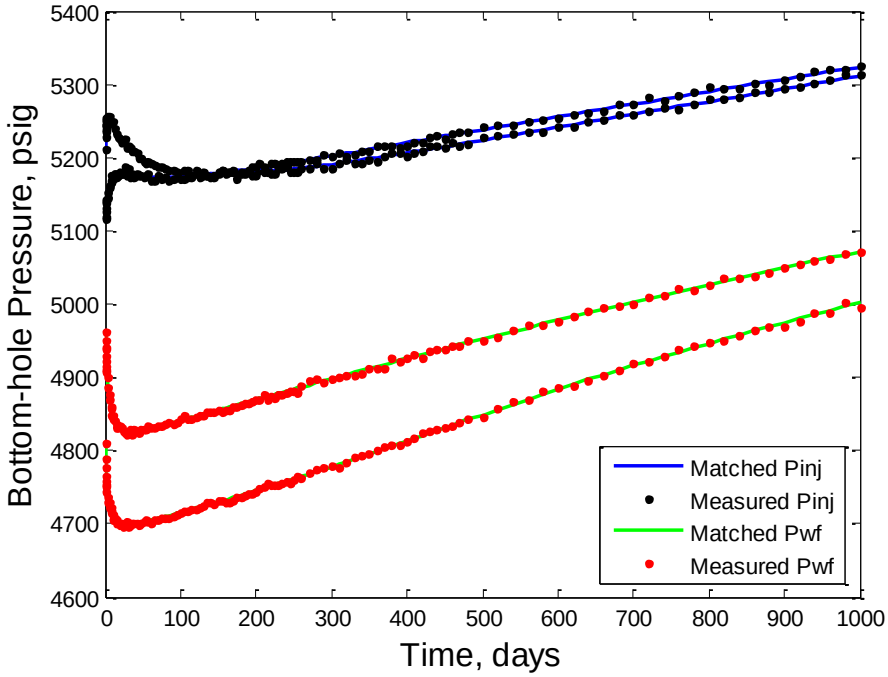

Figure 5.25: Match to measured bottom-hole pressure in all wells for the 16 x 16 reservoir system (wavelet fraction 0.6, upscaling performed during history matching)

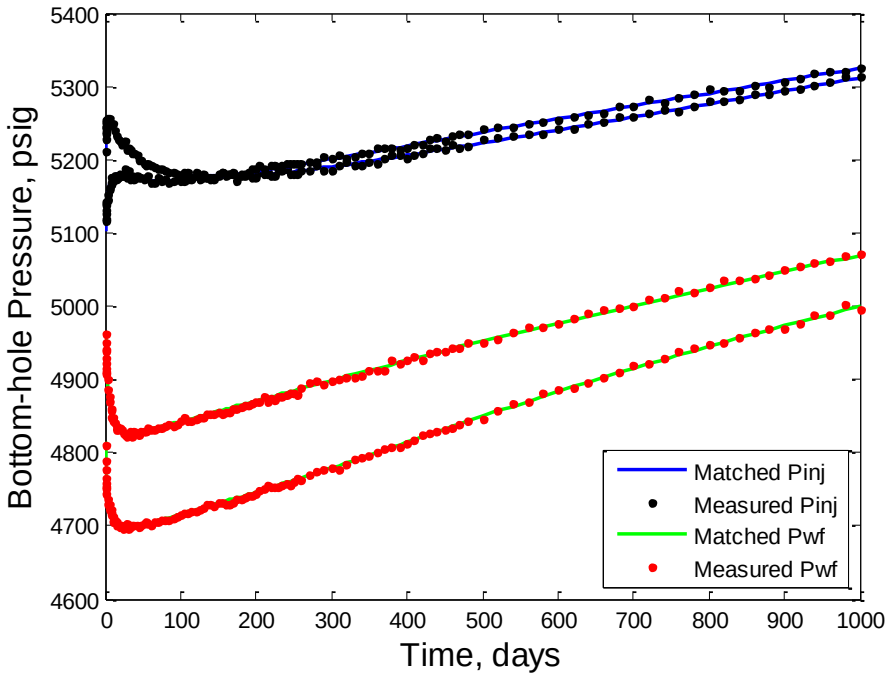

Figure 5.26: Match to measured bottom-hole pressure in all wells for the 16 x 16 reservoir system (wavelet fraction 0.4, upscaling performed during history matching)

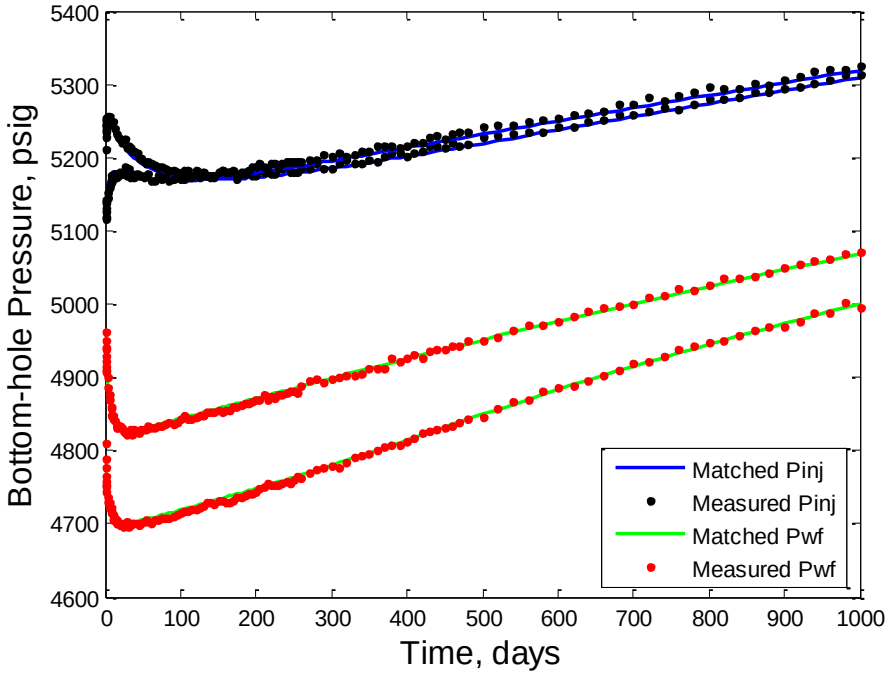

Figure 5.27: Match to measured bottom-hole pressure in all wells for the 16 x 16 reservoir system (wavelet fraction 0.25, upscaling performed during history matching)

A good match is obtained for both pressure and water-cut, in all cases considered. The trend of number of wavelet coefficients selected using each fraction of 0.6, 0.4 and 0.25 is shown in Figure 5.22. Figure 5.23 presents the reduction of error as the iteration is increased; while the true permeability distribution, initial guess and the final distribution obtained for the three scenarios are shown in Figure 5.24.

Upscaled Inverse Analysis

The match of calculated bottom-hole pressure to measured pressure, for the three fractions, using upscaled history matching is presented in Figure 5.25, Figure 5.26 and Figure 5.27, while the water-cut match for each case, using the upscaled reservoir model

is presented in Figure 5.28, Figure 5.29 and Figure 5.30. The pressure match for all fractions is very good, but it is better for fractions of 0.4 and 0.6 than for 0.25. Similarly, excellent matches were obtained to the measured water-cut from all the three fractions. The selection of wavelet coefficients for each fraction is shown in Figure 5.31. The decay of data residual for all the fractions is presented in Figure 5.32. Figure 5.33 shows the true permeability, the initial guess and the resulting permeability field for all the cases. It shows that as the fraction decreases the homogeneity of the system increases. The summary of significant data for all the cases is given in Table 5.2. It represents that we have total of 768 production data points (pressure and water-cut), out of which only 76 have been selected for history matching which gives the compression ratio of 10.1. It is a 16 x 16 grid system that results in 256 reservoir parameter (permeability) values. As discussed earlier that as the wavelet fraction is reduced the number of parameters considered is also reduced. Thus fraction of 0.6 has maximum parameters of 154 which reduce to 65 in case of fraction 0.25. The parameters considered are almost the same in both fine-scale and upscale history matching.

Table 5.2: Important statistics for 16 x 16 reservoir system

Details	**Fine-scale**			**Upscale**		
Number of measured data	768			768		
Number of wavelets of data	76			76		
Compression ratio	10.1			10.1		
Number of reservoir parameters	256			256		
Fraction	0.6	0.4	0.25	0.6	0.4	0.25
Number of wavelets of parameters	81-154	54-106	26-65	81-154	54-107	26-65

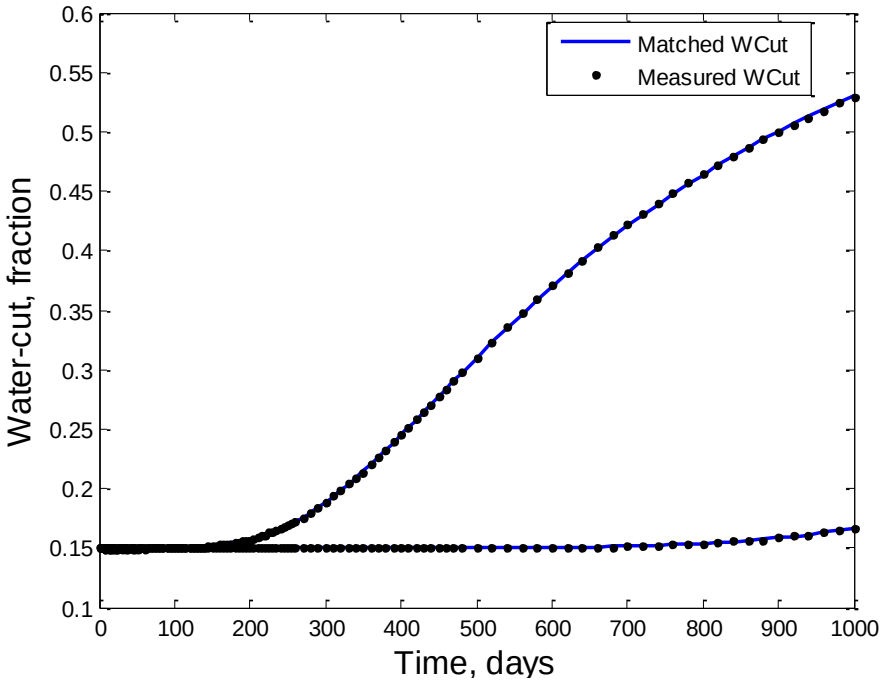

Figure 5.28: Match to water-cut in all producers for the 16 x 16 reservoir system (wavelet fraction 0.6, upscaling performed during history matching)

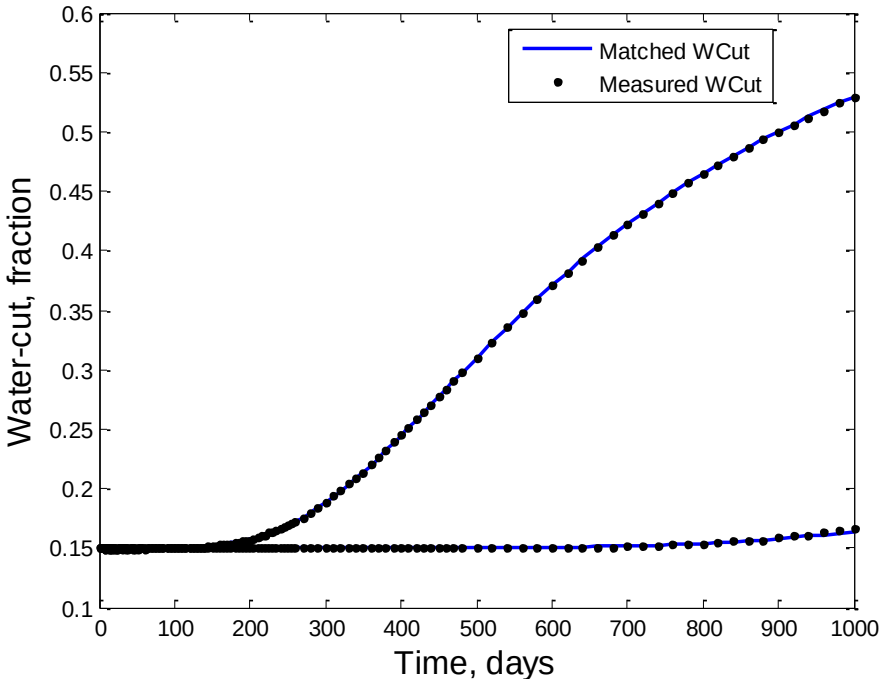

Figure 5.29: Match to water-cut in all producers for the 16 x 16 reservoir system (wavelet fraction 0.4, upscaling performed during history matching)

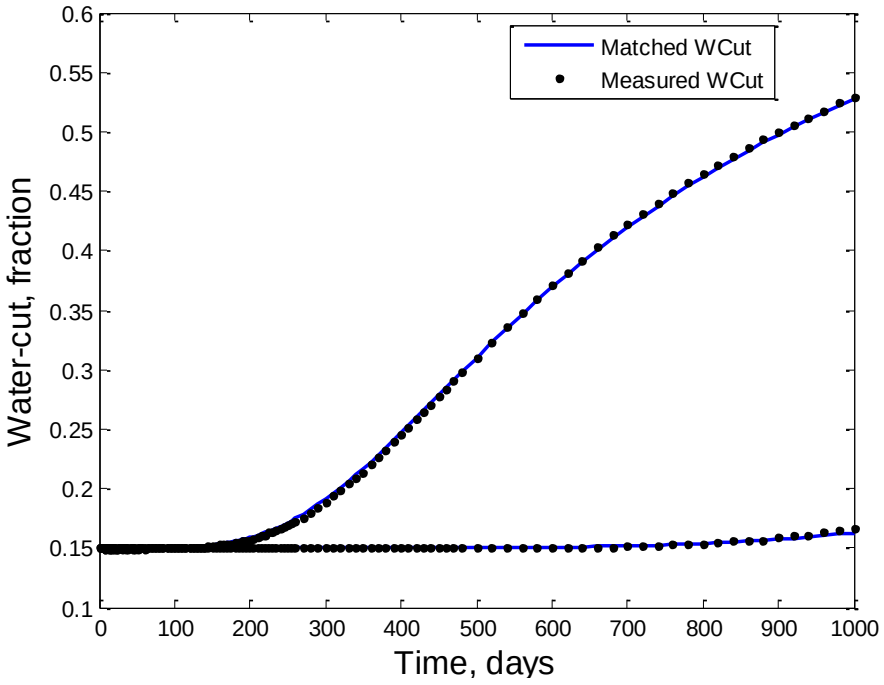

Figure 5.30: Match to water-cut in all producers for the 16 x 16 reservoir system (wavelet fraction 0.25, upscaling performed during history matching)

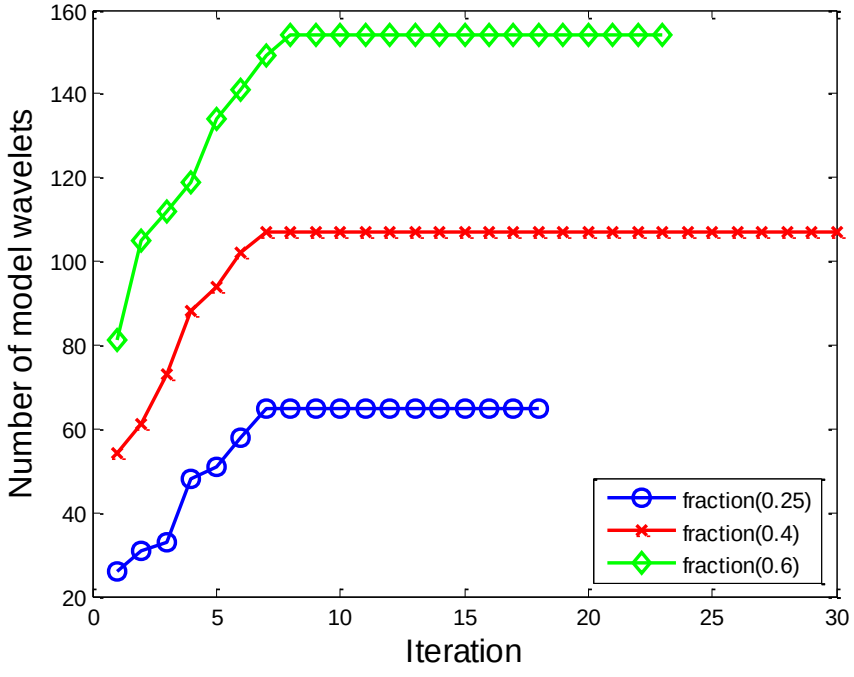

Figure 5.31: Trend of wavelet coefficients for the 16 x 16 reservoir system (all fractions, upscaling performed during history matching)

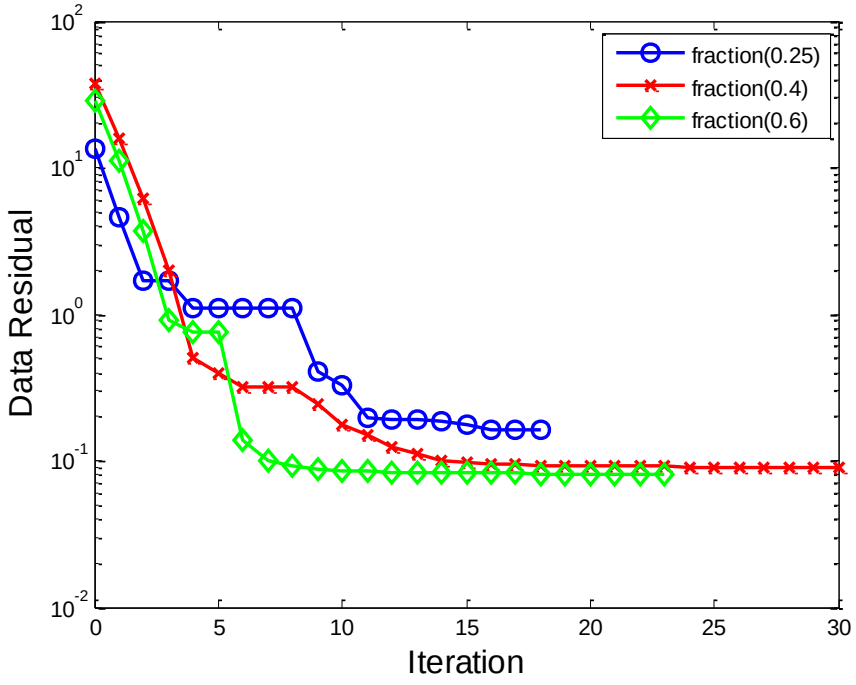

Figure 5.32: Data residual for the 16 x 16 reservoir system (all fractions, upscaling performed during history matching)

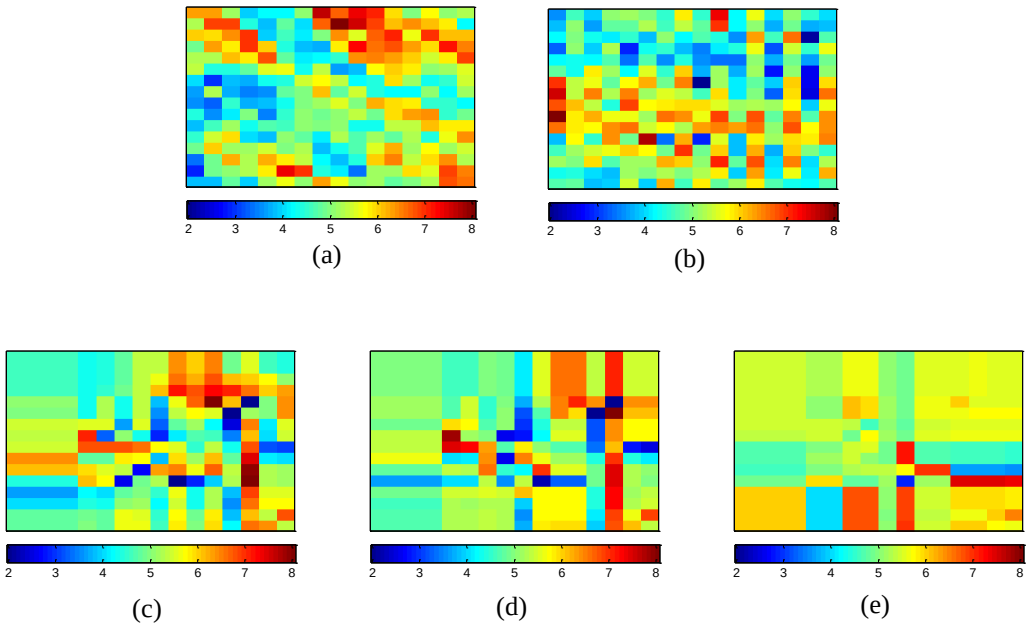

Figure 5.33: *log* permeability distribution for the 16 x 16 reservoir system (a) true (b) initial guess (c) estimate of wavelet fraction 0.6 (d) estimate of wavelet fraction 0.4 (e) estimate of wavelet fraction 0.25 (upscaling performed during history matching)

5.2.2 Reservoir System with 32 x 32 Grids

The fractions of 0.6, 0.4 and 0.25 are used for thresholding the wavelet of model parameters. There are four producing wells and four injecting wells. Both fine-scale and upscaled history matching were performed and the results analyzed. An additional scenario in the upscaled history matching for fraction of 0.4 was performed with a mobility ratio different from that used in primary case. The reason for considering this scenario is to check if this method is valid for different relative permeability values or not. Thus a new data is generated for this with different relative permeability values using Equations (5.7) and (5.8), and then history matched.

$$k_{rw} = S_w^{1.2} \tag{5.7}$$

$$k_{ro} = (1 - S_w)^{1.7} \tag{5.8}$$

Fine-scale Inverse Analysis

The pressure match of all producers and injectors using fine-scale history matching; for all the wavelet fractions are displayed in Figure 5.34, Figure 5.35 and Figure 5.36. The match of water-cut data is given in Figure 5.37, Figure 5.38 and Figure 5.39. An excellent match for pressure is obtained for all the cases, and even good match is obtained for water-cut match of all fractions.

The trend for selection of number of wavelets for each fraction is presented in Figure 5.40. The behavior of the reduction in error between measured and calculated data is shown in Figure 5.41. Figure 5.42 provides the true permeability used for this case; the initial estimate and final permeability obtained for all the fractions considered.

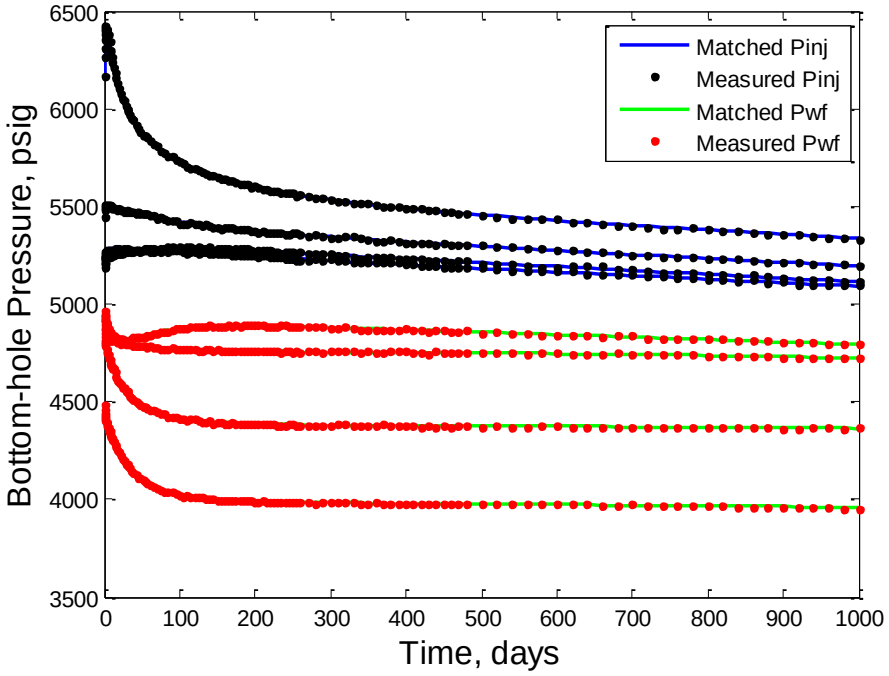

Figure 5.34: Match to measured bottom-hole pressure in all wells for the 32 x 32 reservoir system (wavelet fraction 0.6, no upscaling performed during history matching)

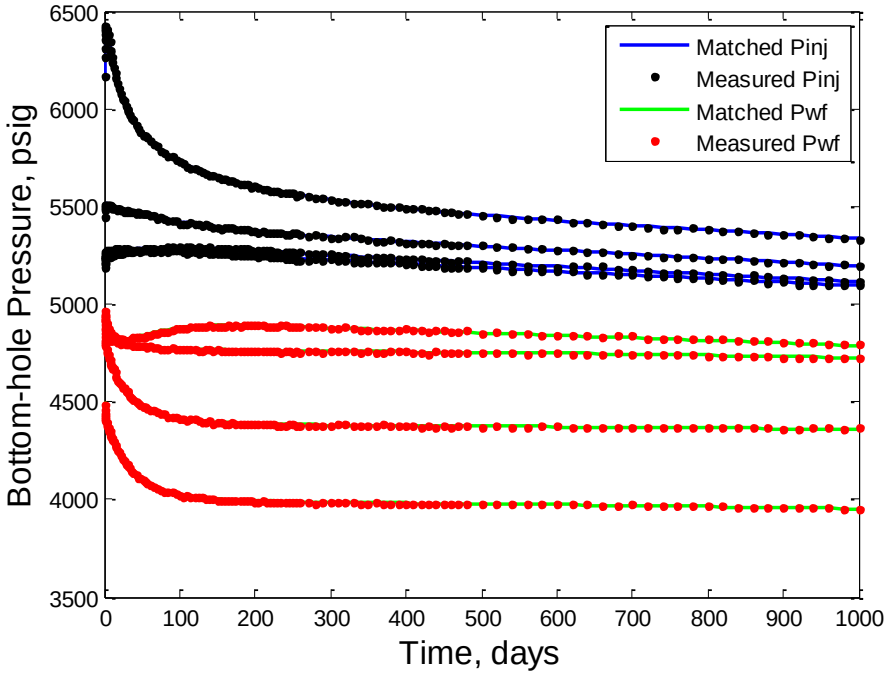

Figure 5.35: Match to measured bottom-hole pressure in all wells for the 32 x 32 reservoir system (wavelet fraction 0.4, no upscaling performed during history matching)

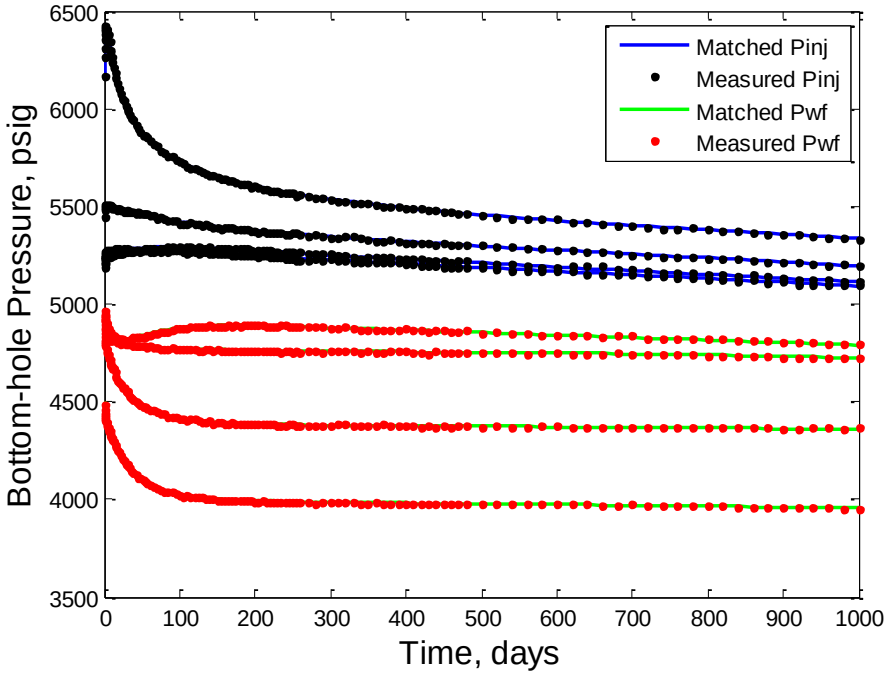

Figure 5.36: Match to measured bottom-hole pressure in all wells for the 32 x 32 reservoir system (wavelet fraction 0.25, no upscaling performed during history matching)

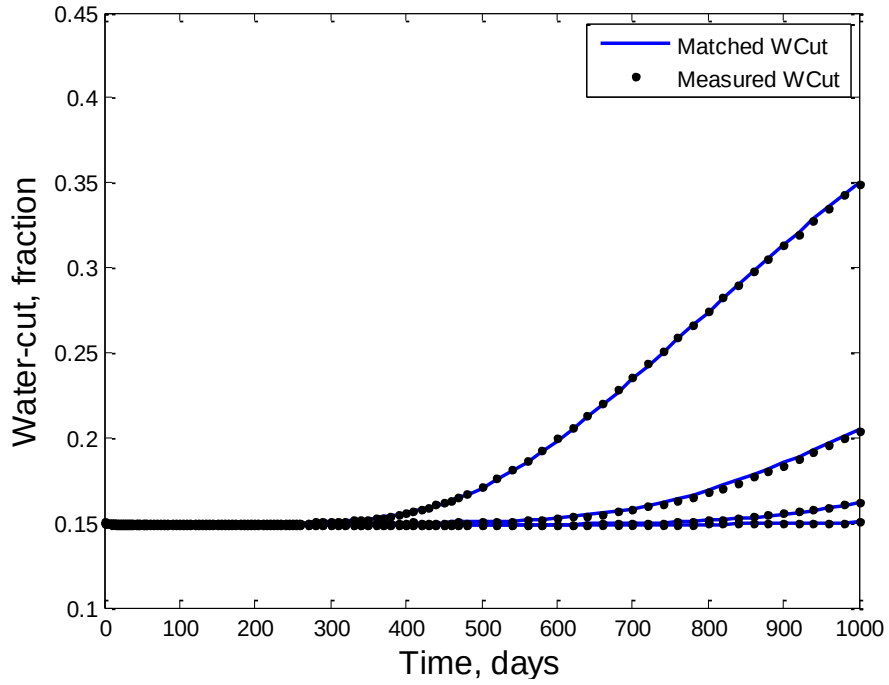

Figure 5.37: Match to water-cut in all producers for the 32 x 32 reservoir system (wavelet fraction 0.6, no upscaling performed during history matching)

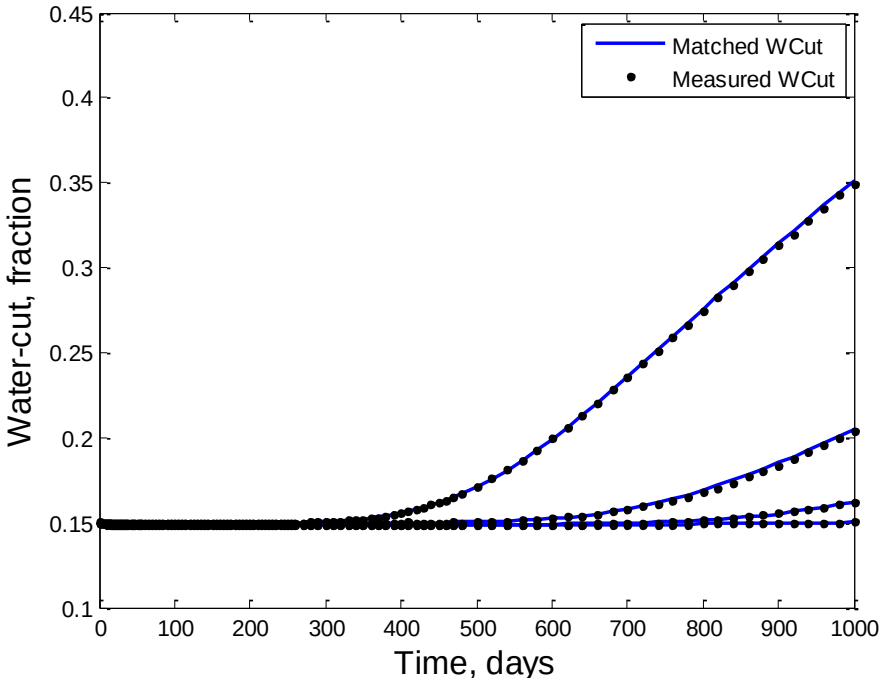

Figure 5.38: Match to water-cut in all producers for the 32 x 32 reservoir system (wavelet fraction 0.4, no upscaling performed during history matching)

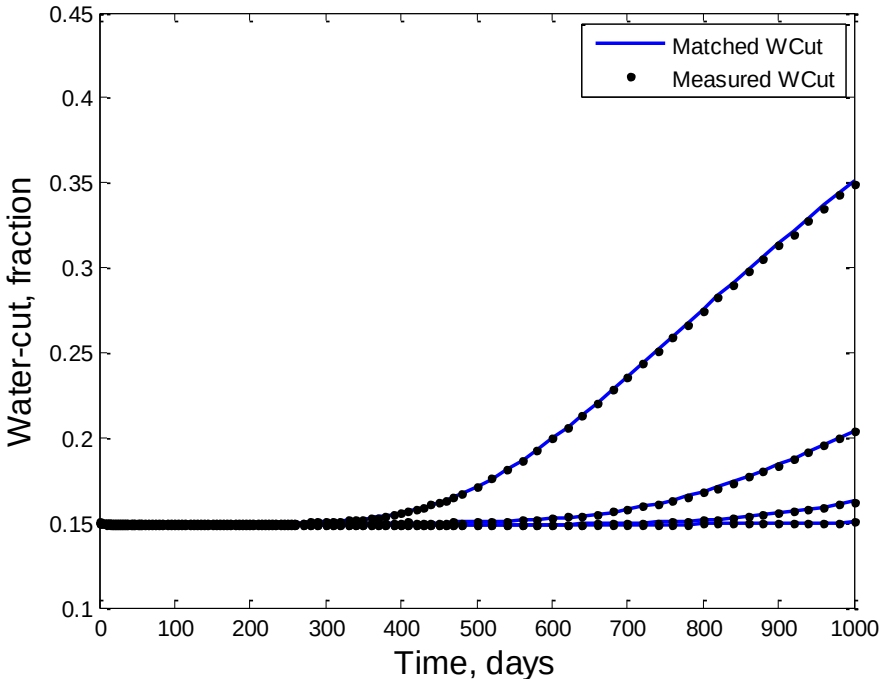

Figure 5.39: Match to water-cut in all producers for the 32 x 32 reservoir system (wavelet fraction 0.25, no upscaling performed during history matching)

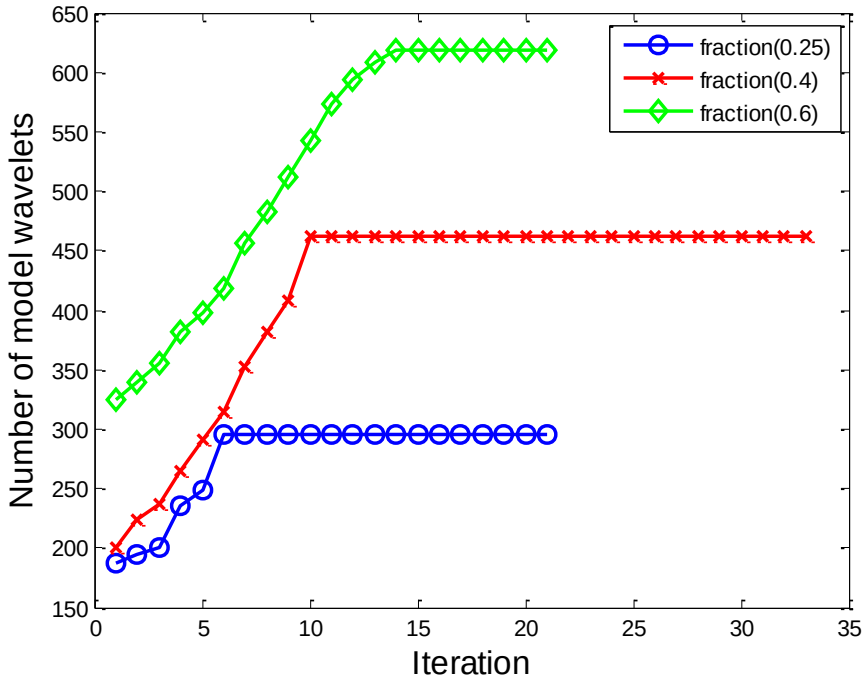

Figure 5.40: Trend of wavelet coefficients for the 32 x 32 reservoir system (all fractions, no upscaling performed during history matching)

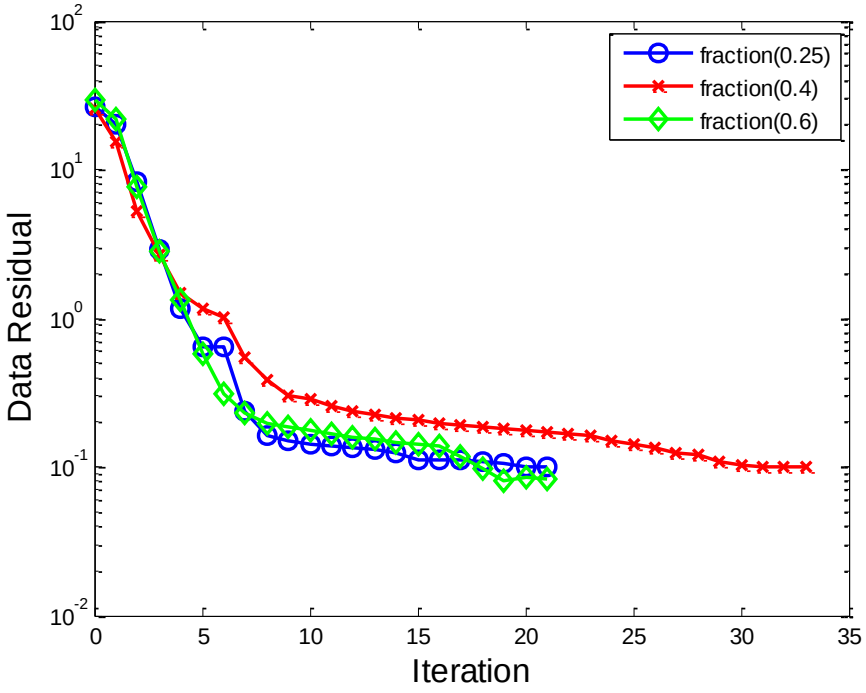

Figure 5.41: Data residual for the 32 x 32 reservoir system (all fractions, no upscaling performed during history matching)

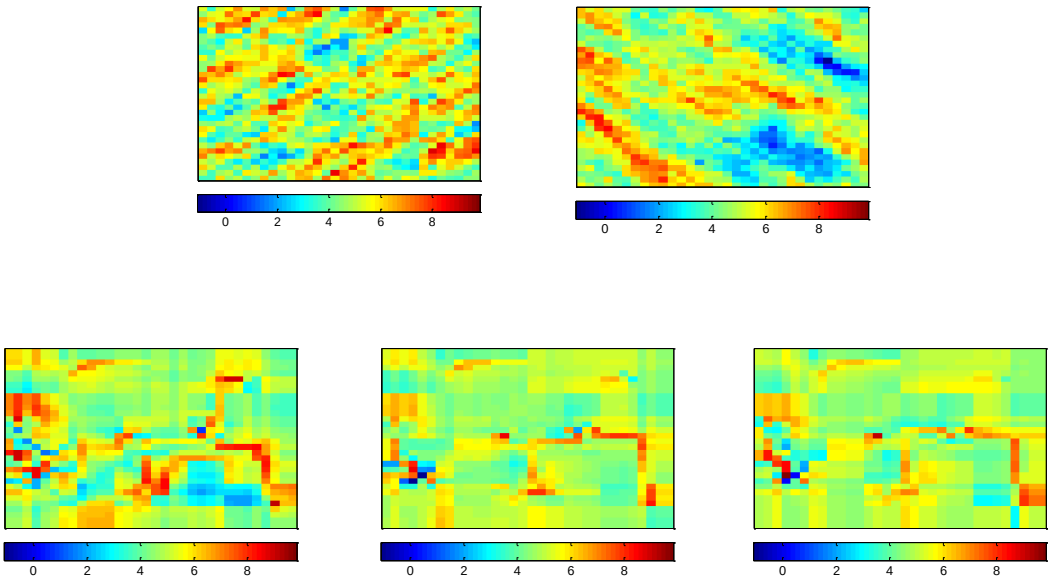

Figure 5.42: *log* permeability distribution for the 32 x 32 reservoir system (a) true (b) initial guess (c) estimate of wavelet fraction 0.6 (d) estimate of wavelet fraction 0.4 (e) estimate of wavelet fraction 0.25 (no upscaling performed during history matching)

Upscaled Inverse Analysis

The upscaled history match between calculated and measured bottom-hole pressure for all the cases are presented in Figure 5.43, Figure 5.44, Figure 5.45 and Figure 5.46. It is observed that the results are very good but in comparison the fine-scale history matching results are slightly better. Almost similar pattern of match is obtained for both scenarios of mobility considered, for fraction of 0.4. The match for water-cut of each fraction is presented in Figure 5.47, Figure 5.48, Figure 5.49 and Figure 5.50; and all the results are appreciably good. The water-cut values have increased for the case of different mobility, as shown in Figure 5.50, due to the reason that the relative mobility of water is increased in this scenario, in comparison to the primary mobility case. However a good match of water-cut is achieved for this example as well. The trend of number of wavelet

coefficients picked for each fraction is displayed in Figure 5.51. The residual between the calculated and measured data for all the scenarios is presented in Figure 5.52. True permeability, initial permeability guess and the permeability distribution obtained for all the fractions are shown in Figure 5.53. The figure signifies that the uniform permeability regions tend to increase with the reduction in fraction of wavelets.

The key values for all the scenarios are given in Table 5.3. It shows that we have 1536 production data points in total. After thresholding, 192 data points have been selected which results in the compression ratio of 8. It is a 32 x 32 grid system that means we have 1024 reservoir parameter (permeability) values. The fraction of 0.6 has maximum parameters of 619 which reduce to 275 as the fraction is reduced to 0.25. The number of parameters selected after reduction are almost same in both fine-scale and upscale inverse analysis.

Table 5.3: Important statistics for 32 x 32 reservoir system

Details	**Fine-scale**			**Upscale**			
Number of measured data	1536			1536			
Number of wavelets of data	192			192			
Compression ratio	8			8			
Number of reservoir parameters	1024			1024			
Fraction	0.6	0.4	0.25	0.6	0.4*	0.4**	0.25
Number of wavelets of parameters	324-619	201-462	187-295	324-600	201-422	205-411	187-275

0.4* - Primary case for fraction 0.4
0.4** - Case for fraction 0.4 with different mobility

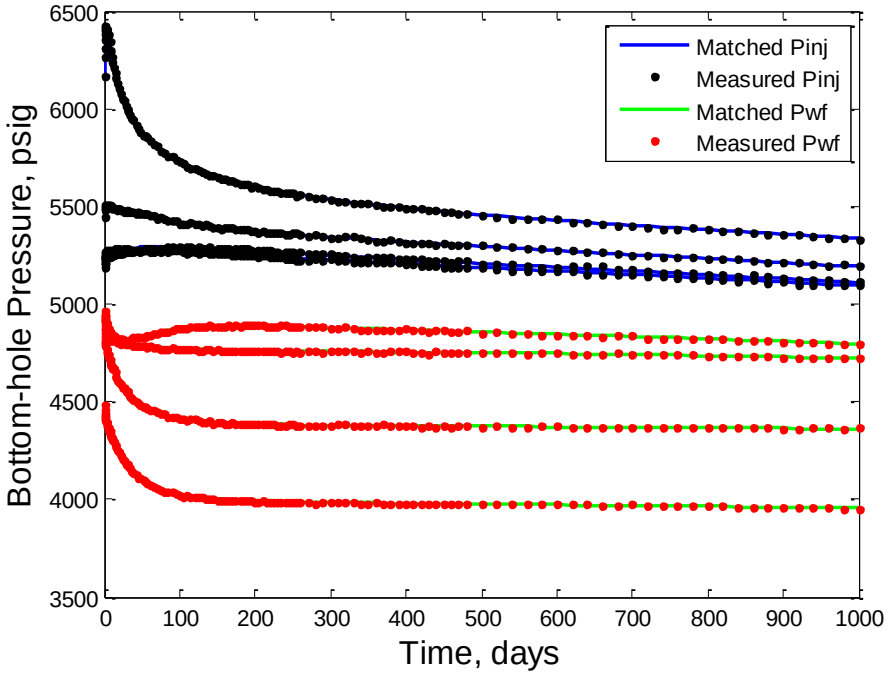

Figure 5.43: Match to measured bottom-hole pressure in all wells for the 32 x 32 reservoir system (wavelet fraction 0.6, upscaling performed during history matching)

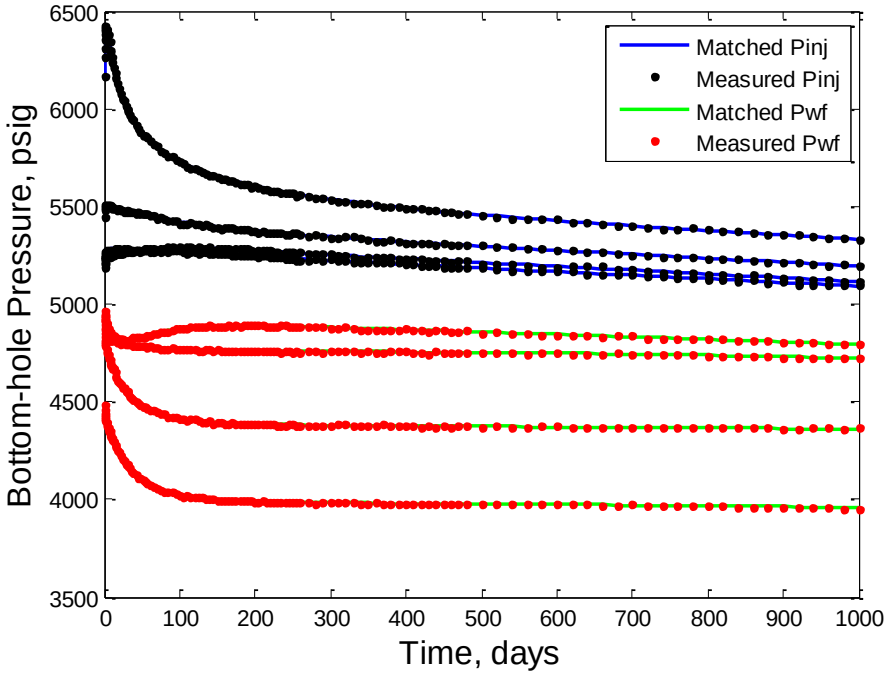

Figure 5.44: Match to measured bottom-hole pressure in all wells for the 32 x 32 reservoir system (wavelet fraction 0.4 – primary case, upscaling performed during history matching)

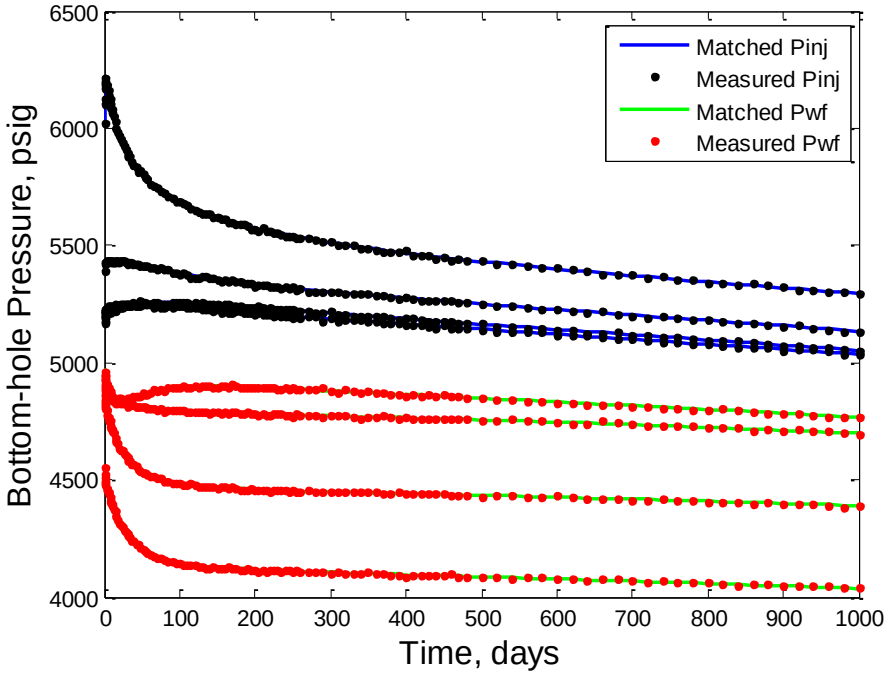

Figure 5.45: Match to measured bottom-hole pressure in all wells for the 32 x 32 reservoir system (wavelet fraction 0.4 – with different mobility, upscaling performed during history matching)

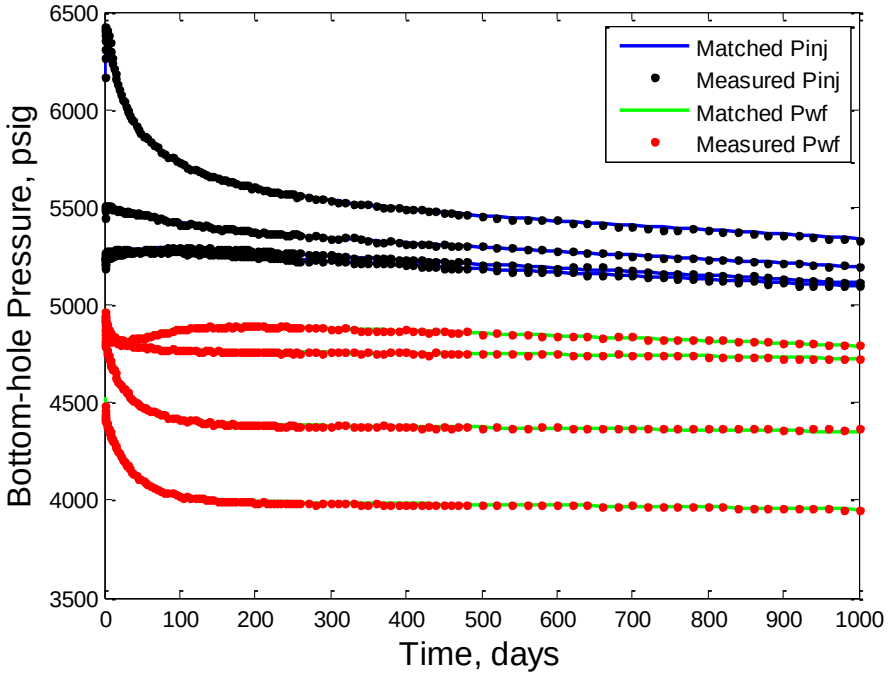

Figure 5.46: Match to measured bottom-hole pressure in all wells for the 32 x 32 reservoir system (wavelet fraction 0.25, upscaling performed during history matching)

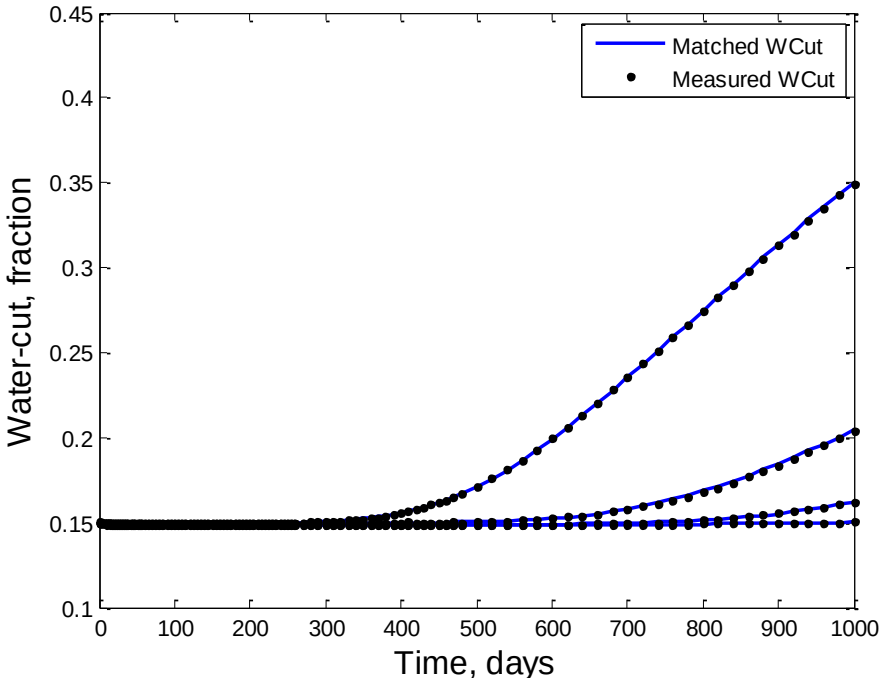

Figure 5.47: Match to water-cut in all producers for the 32 x 32 reservoir system (wavelet fraction 0.6, upscaling performed during history matching)

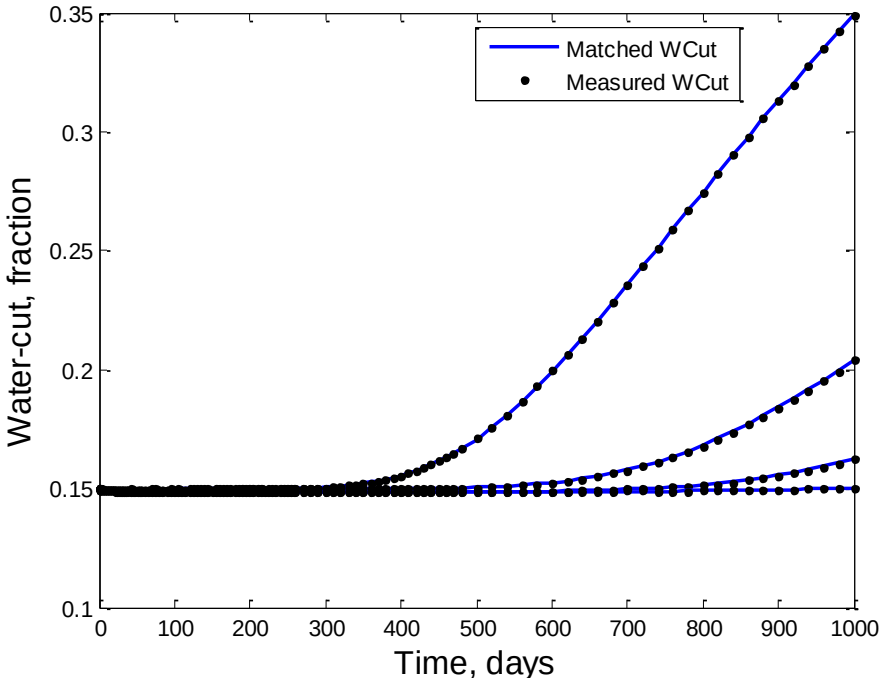

Figure 5.48: Match to water-cut in all producers for the 32 x 32 reservoir system (wavelet fraction 0.4 – primary case, upscaling performed during history matching)

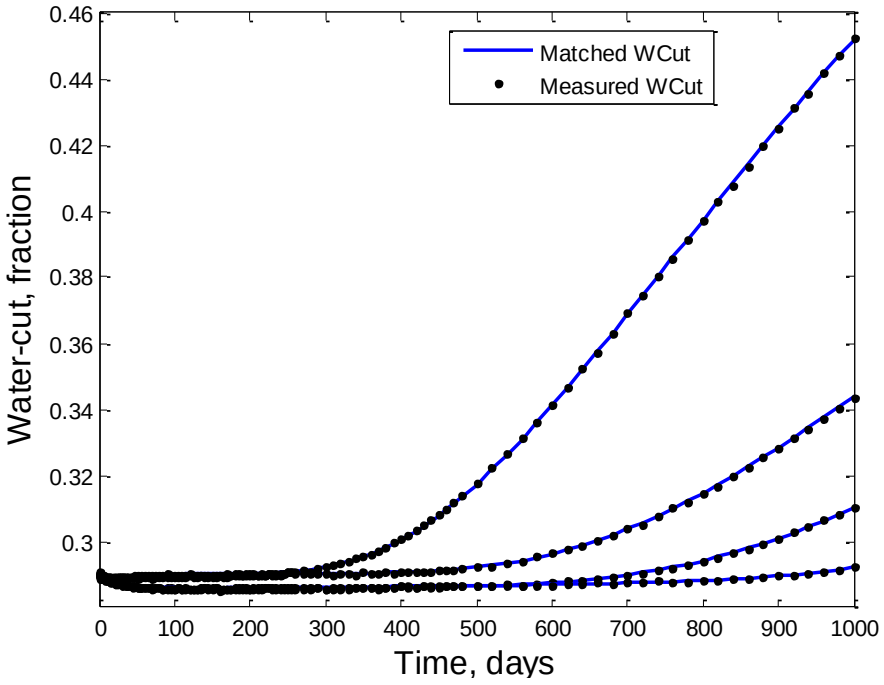

Figure 5.49: Match to water-cut in all producers for the 32 x 32 reservoir system (wavelet fraction 0.4 – with different mobility, upscaling performed during history matching)

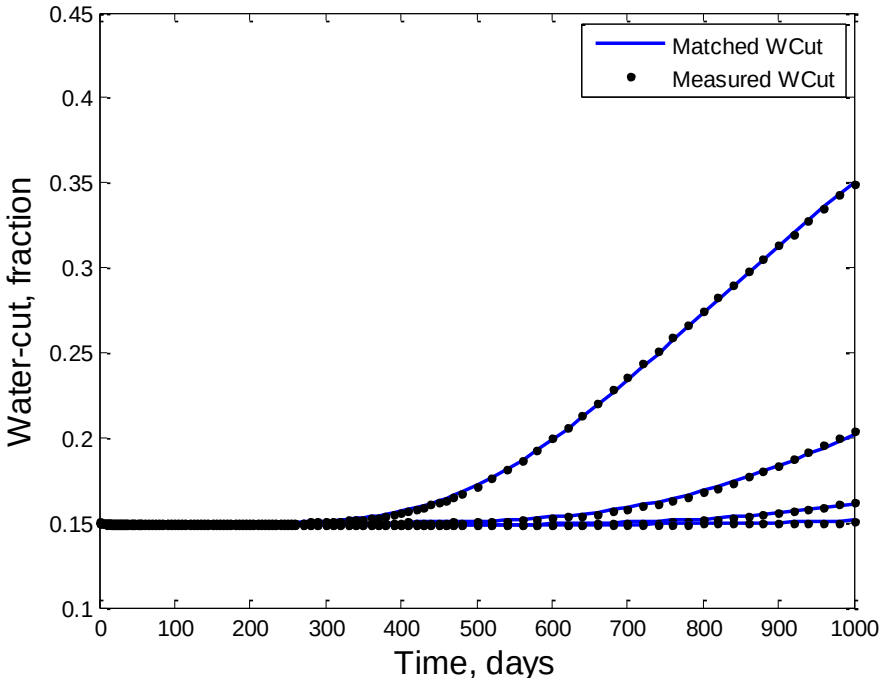

Figure 5.50: Match to water-cut in all producers for the 32 x 32 reservoir system (wavelet fraction 0.25, upscaling performed during history matching)

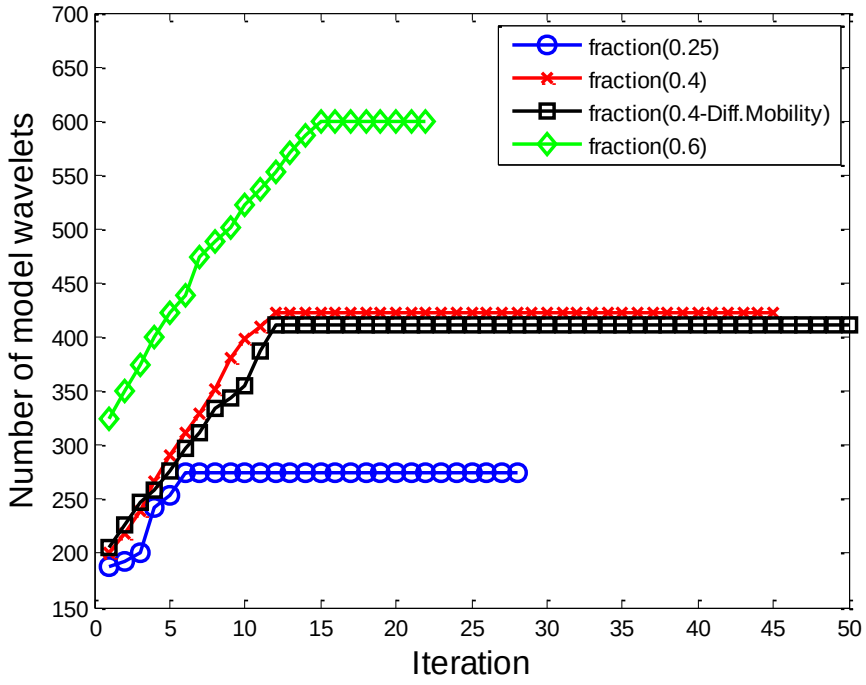

Figure 5.51: Trend of wavelet coefficients for the 32 x 32 reservoir system (all fractions, upscaling performed during history matching)

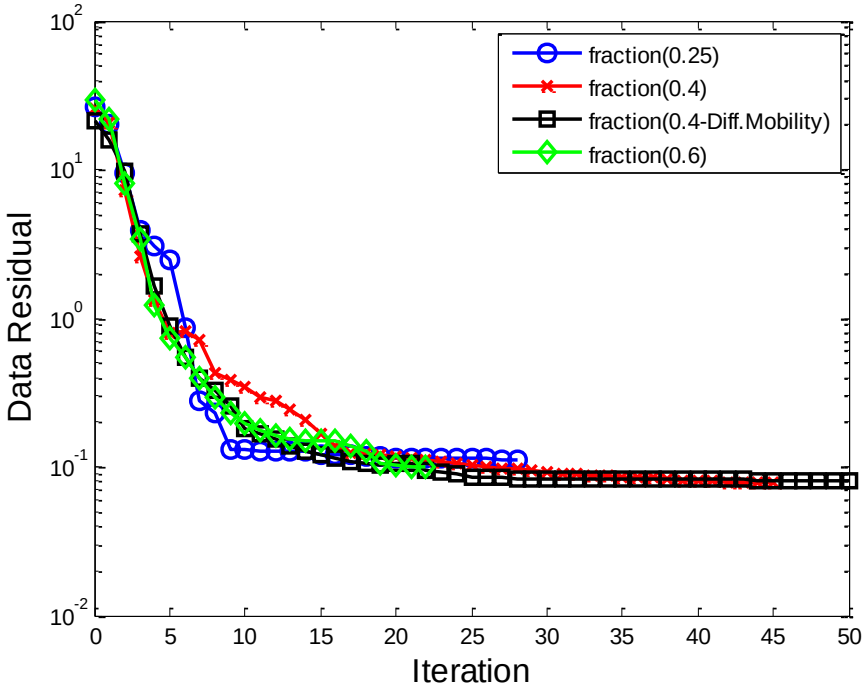

Figure 5.52: Data residual for the 32 x 32 reservoir system (all fractions, upscaling performed during history matching)

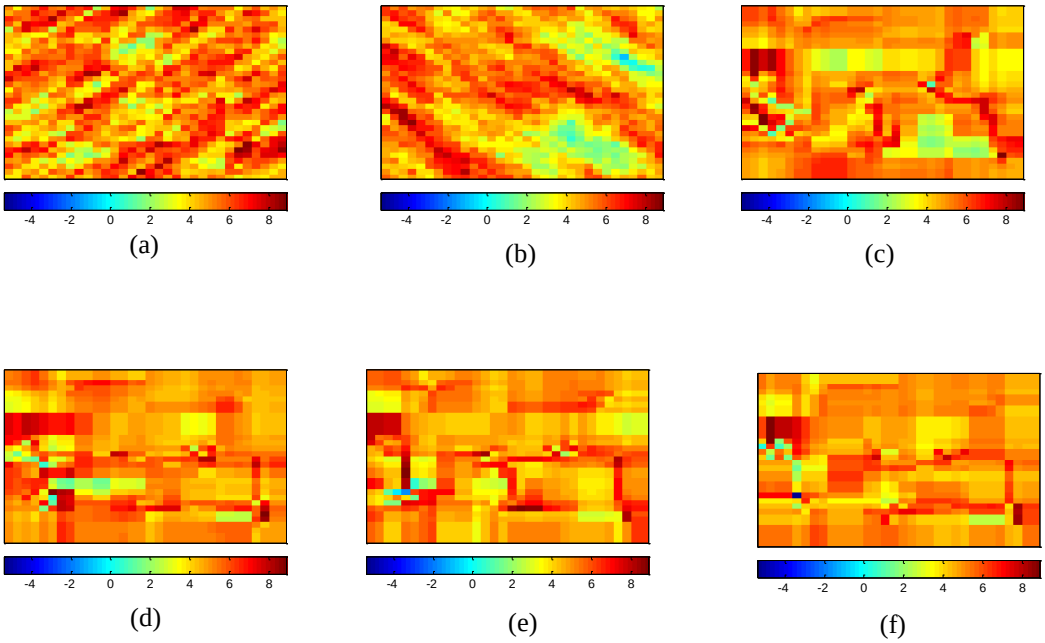

Figure 5.53: *log* permeability distribution for the 32 x 32 reservoir system (a) true (b) initial guess (c) estimate of fraction 0.6 (d) estimate of fraction 0.4 – primary case (e) estimate of fraction 0.4 – different mobility (f) estimate of fraction 0.25 (upscaling performed during history matching)

5.2.3 Reservoir System with 64 x 64 Grids

The 64 x 64 reservoir system is considered with 16 producing wells and 16 injecting wells. The system is analyzed with the wavelet fractions of 0.6, 0.4 and 0.25 used for thresholding. The fine-scale and upscaled history matching is done and the interpretation of results is performed. The resulting permeability distributions from fine-scale and upscaled history matching, for wavelet fraction of 0.4, is used for future prediction of 500 days. The results obtained for the prediction are also analyzed.

Fine-scale Inverse Analysis

The fine-scale match for pressure of all the injectors for all cases is given in Figure 5.54, Figure 5.55 and Figure 5.56. It is observed that the results are excellent with all the

curves providing good match. For all the scenarios, the pressure match of the producing wells is given in Figure 5.57, Figure 5.58 and Figure 5.59. It seems that the well-flowing pressure has also given an excellent match. Water-cut history matching results are then presented in Figure 5.60, Figure 5.61 and Figure 5.62. This history match reveals that we obtain a good water-cut match from all the fractions of wavelets.

The number of wavelets selected at each iteration, for every fraction considered, is displayed in Figure 5.63. The trend of reduction in error with increase in iteration is presented in Figure 5.64; and the permeability distributions are shown in Figure 5.65. It provides the true permeability, the initial guess and resulting permeability distribution estimates for each fraction from history matching.

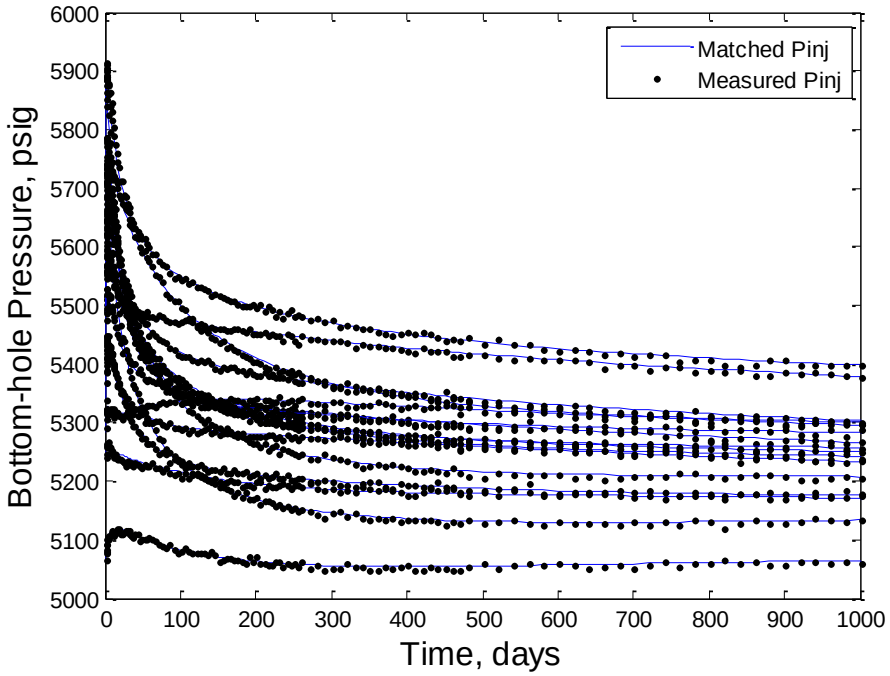

Figure 5.54: Match to measured bottom-hole pressure in all injectors for the 64 x 64 reservoir system (wavelet fraction 0.6, no upscaling performed during history matching)

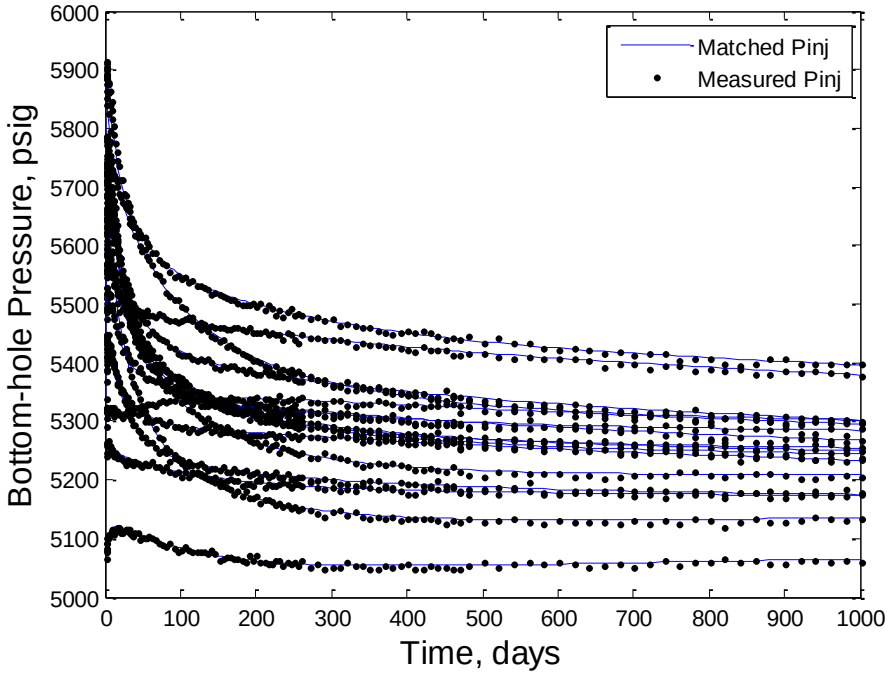

Figure 5.55: Match to measured bottom-hole pressure in all injectors for the 64 x 64 reservoir system (wavelet fraction 0.4, no upscaling performed during history matching)

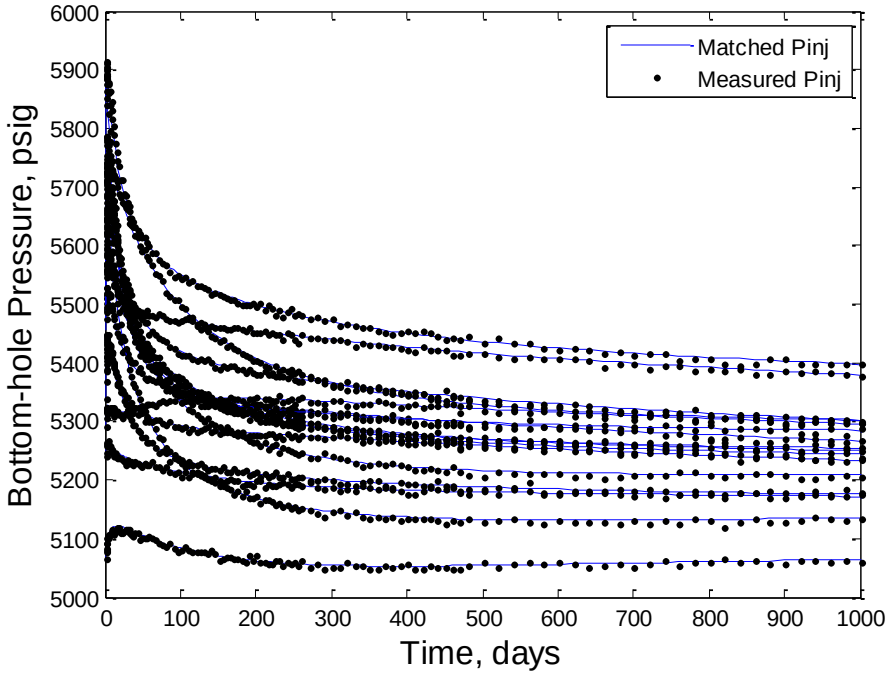

Figure 5.56: Match to measured bottom-hole pressure in all injectors for the 64 x 64 reservoir system (wavelet fraction 0.25, no upscaling performed during history matching)

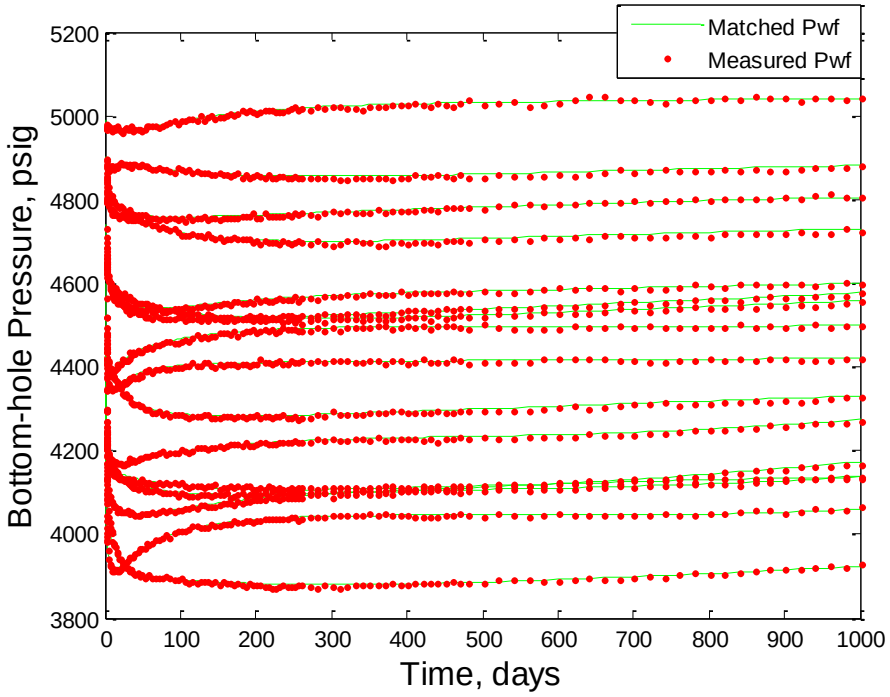

Figure 5.57: Match to measured bottom-hole pressure in all producers for the 64 x 64 reservoir system (wavelet fraction 0.6, no upscaling performed during history matching)

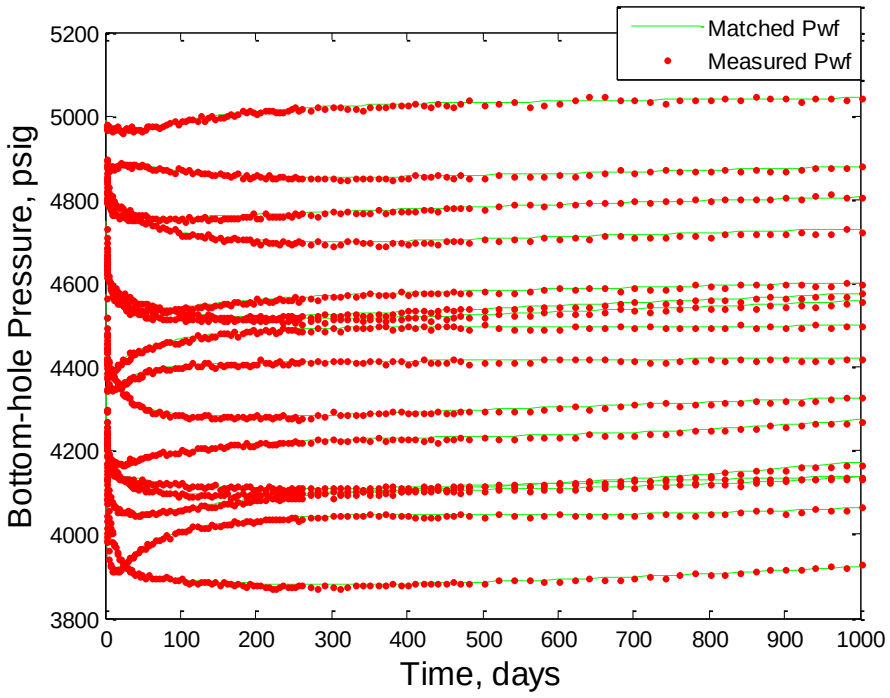

Figure 5.58: Match to measured bottom-hole pressure in all producers for the 64 x 64 reservoir system (wavelet fraction 0.4, no upscaling performed during history matching)

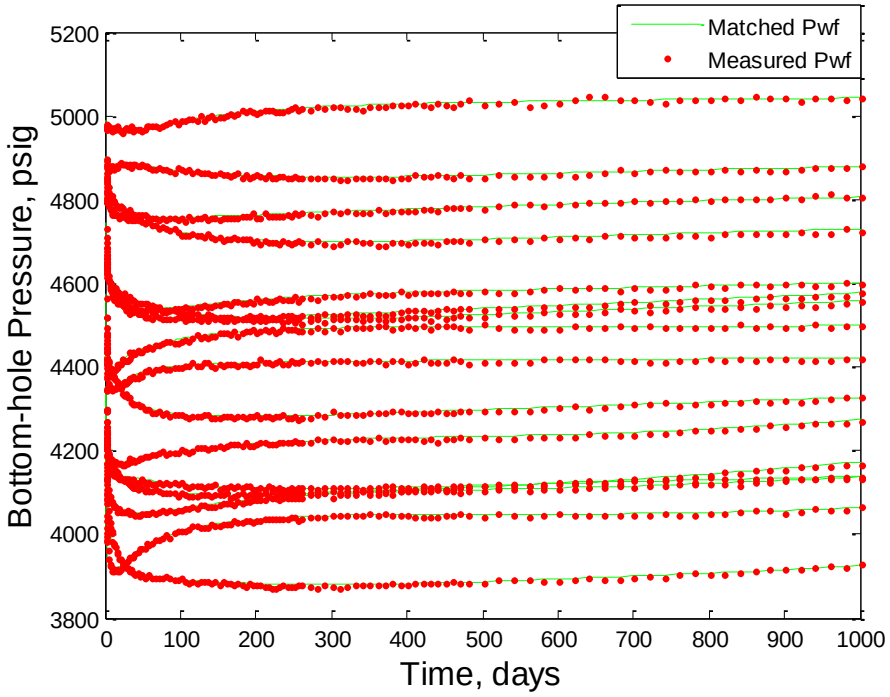

Figure 5.59: Match to measured bottom-hole pressure in all producers for the 64 x 64 reservoir system (wavelet fraction 0.25, no upscaling performed during history matching)

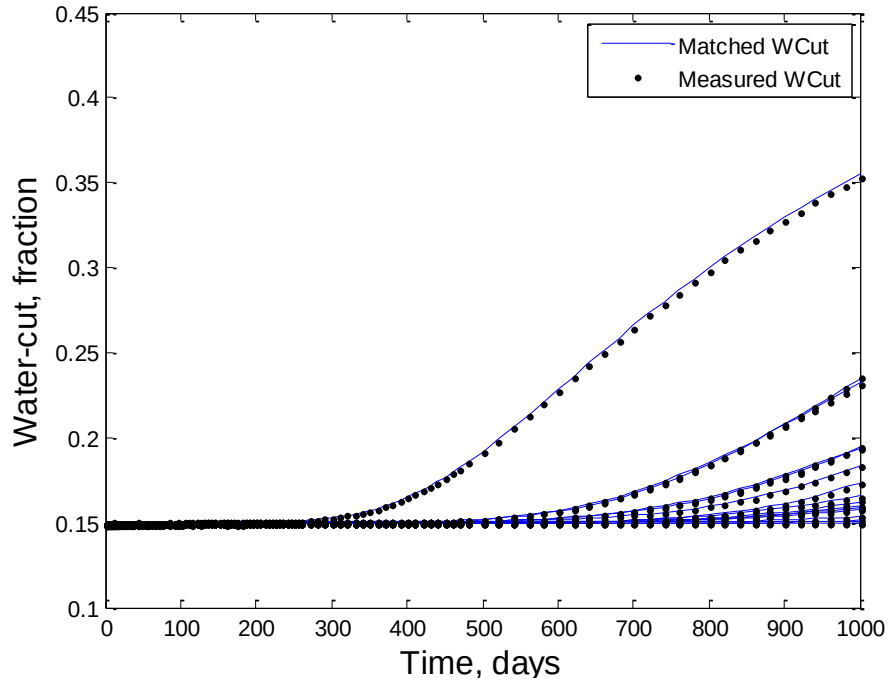

Figure 5.60: Match to water-cut in all producers for the 64 x 64 reservoir system (wavelet fraction 0.6, no upscaling performed during history matching)

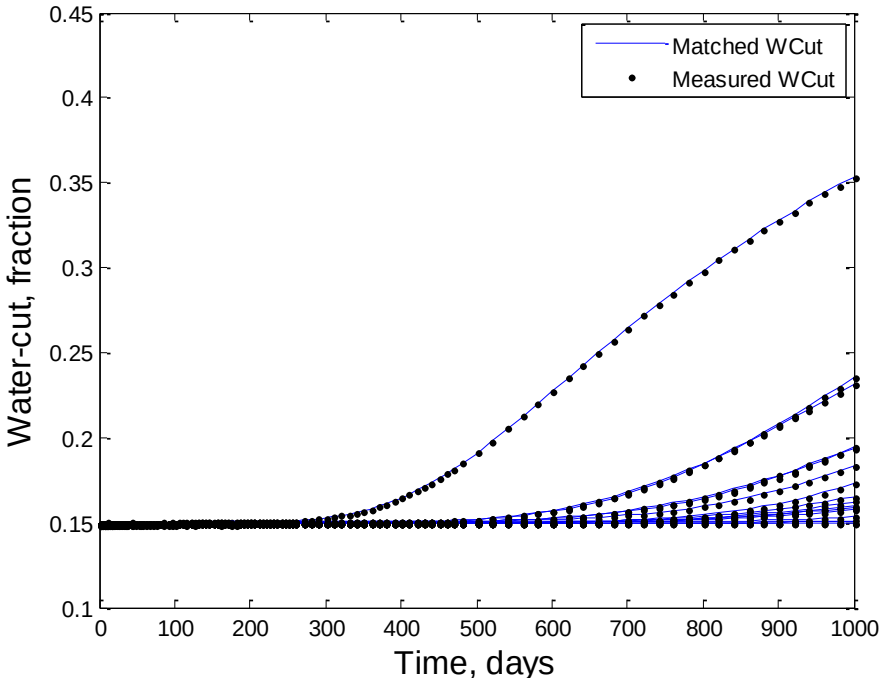

Figure 5.61: Match to water-cut in all producers for the 64 x 64 reservoir system (wavelet fraction 0.4, no upscaling performed during history matching)

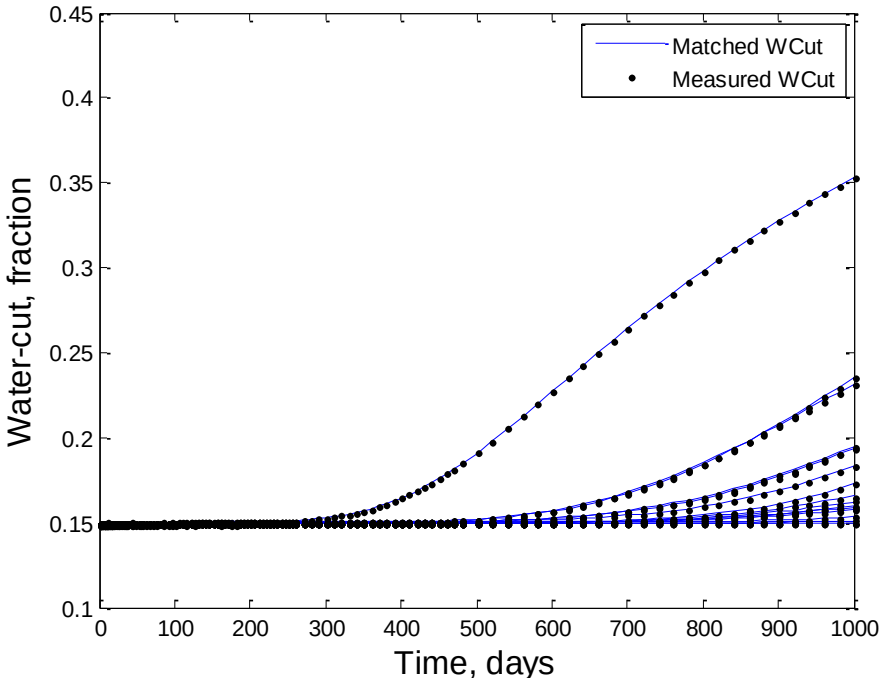

Figure 5.62: Match to water-cut in all producers for the 64 x 64 reservoir system (wavelet fraction 0.25, no upscaling performed during history matching)

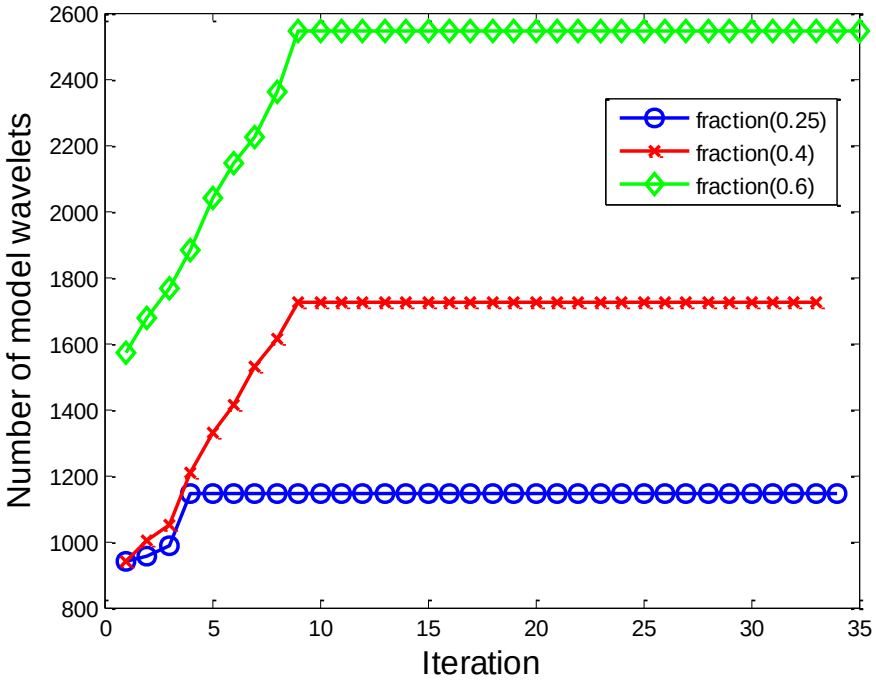

Figure 5.63: Trend of wavelet coefficients for the 64 x 64 reservoir system (all fractions, no upscaling performed during history matching)

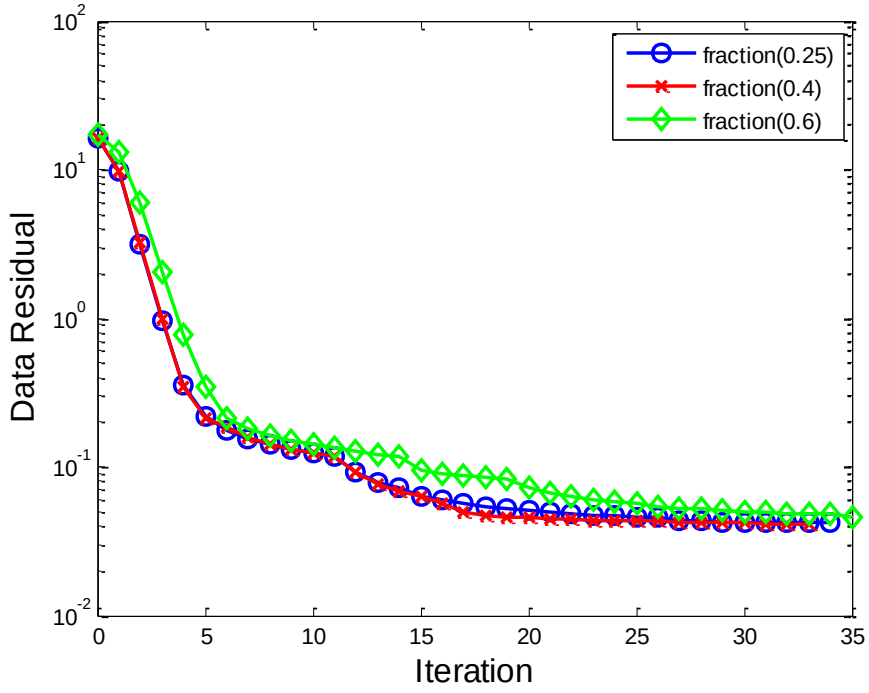

Figure 5.64: Data residual for the 64 x 64 reservoir system (all fractions, no upscaling performed during history matching)

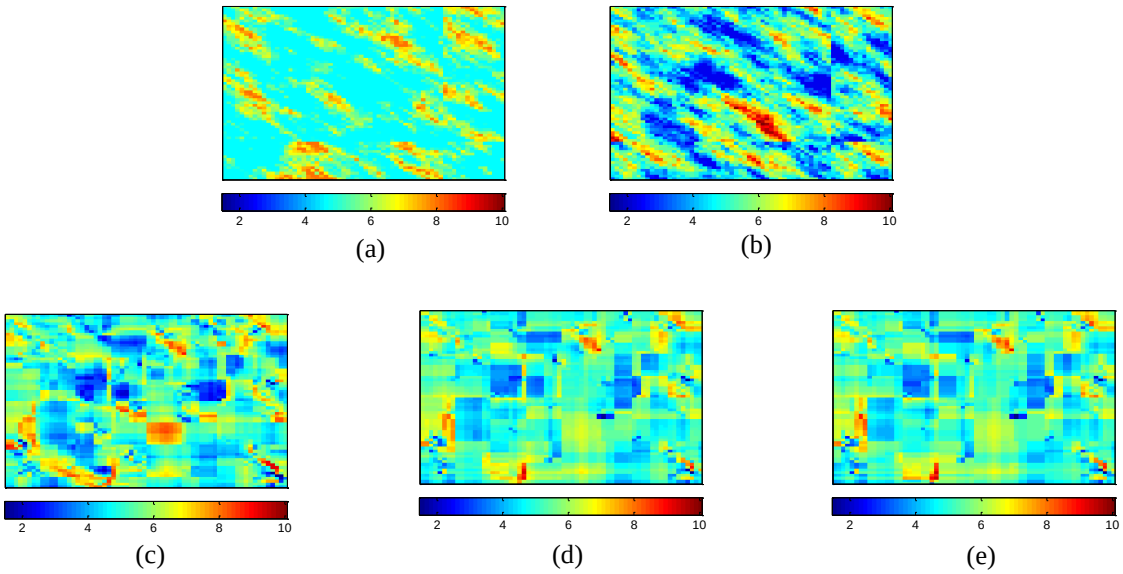

Figure 5.65: *log* permeability distribution for the 64 x 64 reservoir system (a) true (b) initial guess (c) estimate of wavelet fraction 0.6 (d) estimate of wavelet fraction 0.4 (e) estimate of wavelet fraction 0.25 (no upscaling performed during history matching)

Upscaled Inverse Analysis

The upscaling history matching results of pressure in all injectors for fraction of 0.6, 0.4 and 0.25 are shown in Figure 5.66, Figure 5.67, and Figure 5.68 respectively. The analysis tells that we obtained a good match for all the fractions. Subsequently for all cases, the match of calculated and measured bottom-hole pressure of producers is presented in Figure 5.69, Figure 5.70 and Figure 5.71, and it is observed that the results are good. But the pressure match of both injectors and producers suggest that the results for fraction of 0.6 and 0.4 are slightly better as compared to fraction of 0.25. The match for water-cut of all producing wells is displayed in Figure 5.72, Figure 5.73 and Figure 5.74; and it is interpreted that the results are good for all the fractions but the match obtained from fraction of 0.6 is excellent and better than other two fractions. For every fraction that we have used, the trend for number of wavelet coefficient for each iteration is given in Figure 5.75. The decay in error between calculated and measured data, for all

the scenarios, is presented in Figure 5.76. Figure 5.77 presents the distribution of true permeability, initial estimate that we made and the obtained permeability field of all the fractions. The figure shows that the homogenous patches look to increase as we reduce the wavelet fraction.

The data of the cases considered is summarized in Table 5.4. We have total of 6144 production data points and after thresholding, 496 data points have been selected which results in the compression ratio of 12.92. It is a 64 x 64 grid system that means we have total of 4096 reservoir parameter values. The fraction of 0.6 has maximum parameters of 2545 and it is reduced to 1144 when the fraction is reduced to 0.25. Based on these wavelet fractions, the number of parameters selected after reduction for both fine-scale and upscale inverse analysis, are almost same.

Table 5.4: Important statistics for 64 x 64 reservoir system

Details	**Fine-scale**			**Upscale**		
Number of measured data	6144			6144		
Number of wavelets of data	496			496		
Compression ratio	12.92			12.92		
Number of reservoir parameters	4096			4096		
Fraction	0.6	0.4	0.25	0.6	0.4	0.25
Number of wavelets of parameters	1573-2545	942-1725	942-1144	1432-2520	1082-1650	942-1185

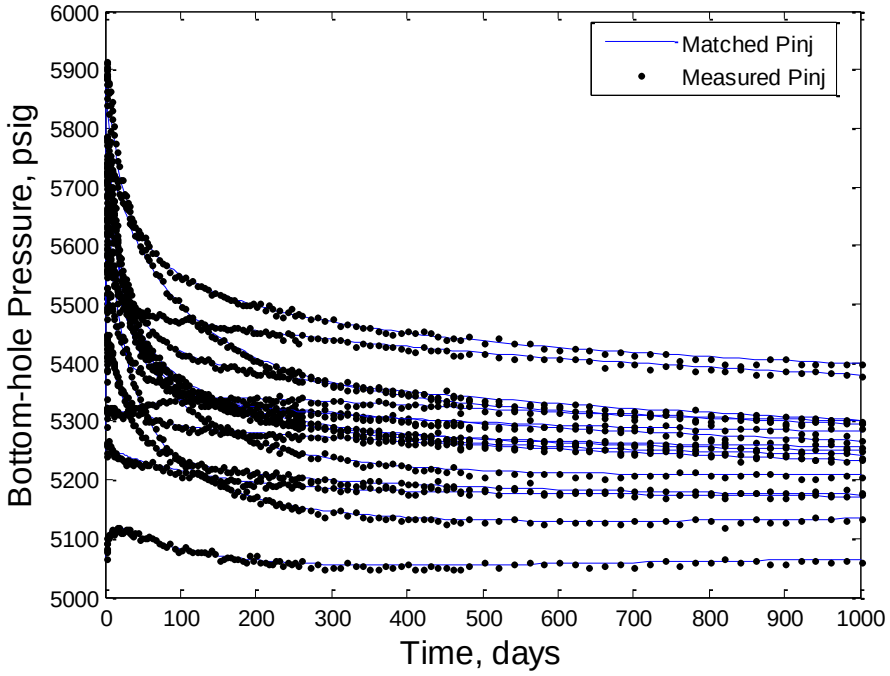

Figure 5.66: Match to measured bottom-hole pressure in all injectors for the 64 x 64 reservoir system (wavelet fraction 0.6, upscaling performed during history matching)

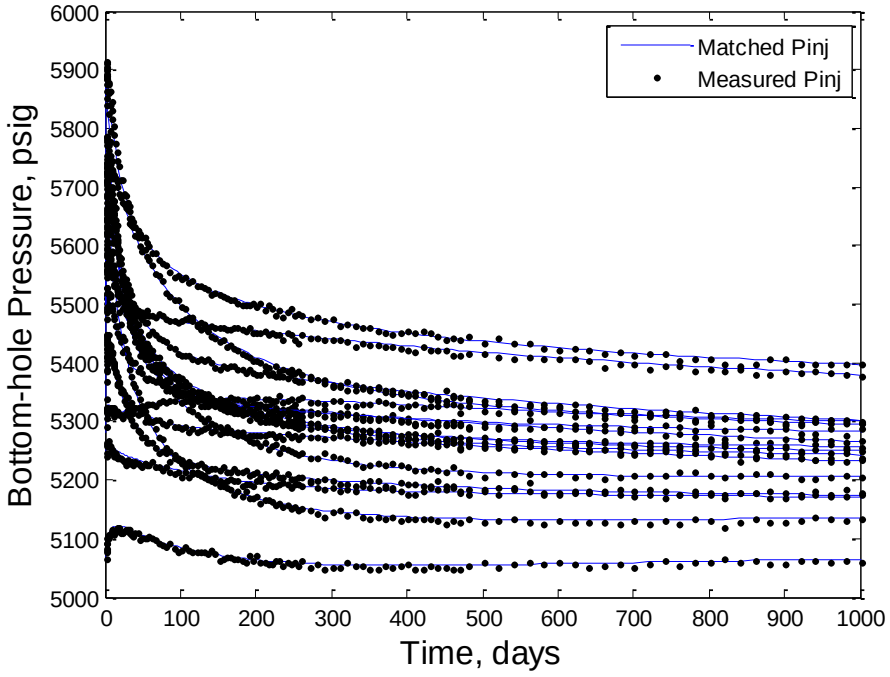

Figure 5.67: Match to measured bottom-hole pressure in all injectors for the 64 x 64 reservoir system (wavelet fraction 0.4, upscaling performed during history matching)

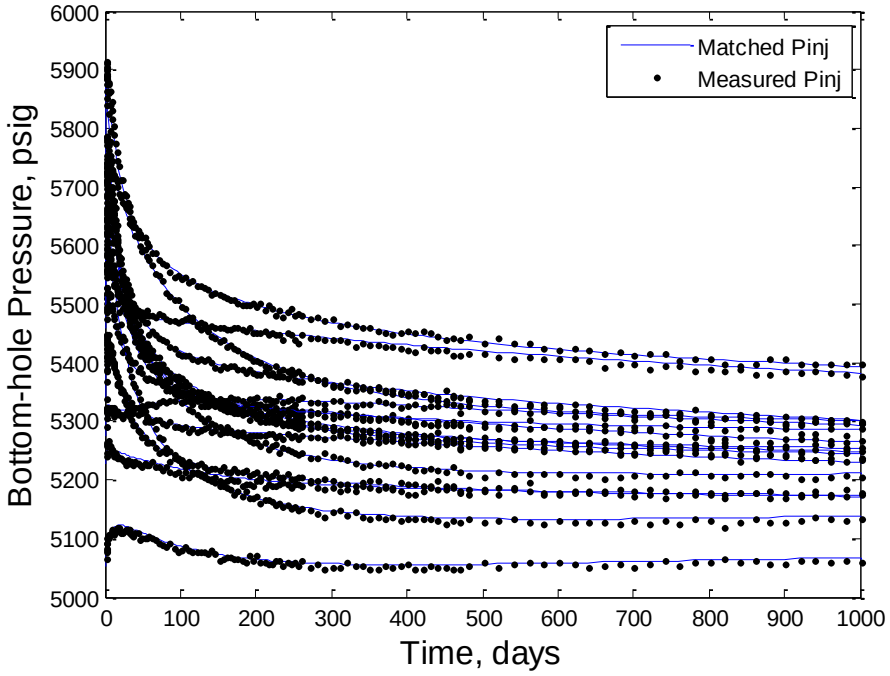

Figure 5.68: Match to measured bottom-hole pressure in all injectors for the 64 x 64 reservoir system (wavelet fraction 0.25, upscaling performed during history matching)

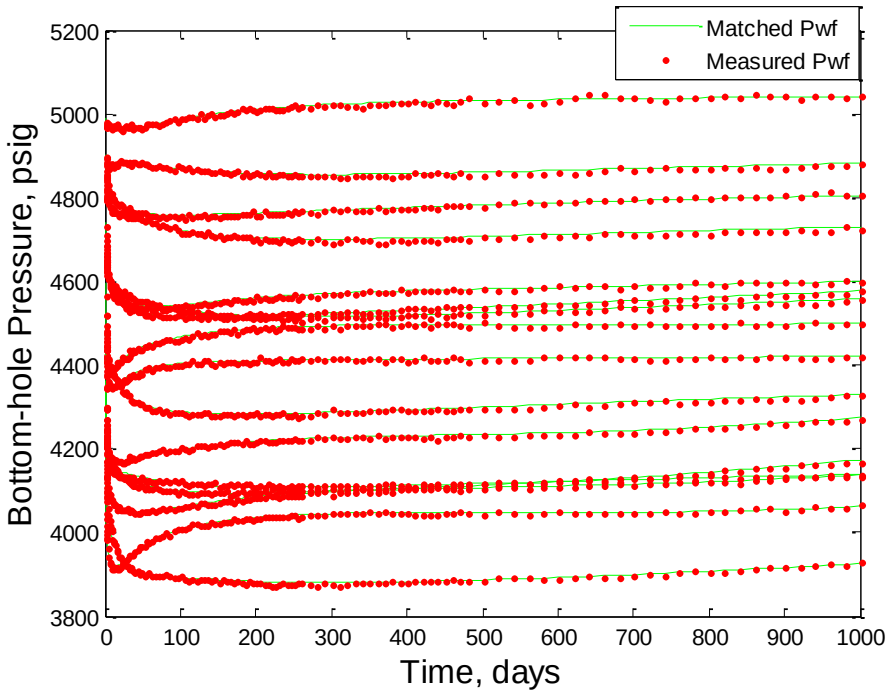

Figure 5.69: Match to measured bottom-hole pressure in all producers for the 64 x 64 reservoir system (wavelet fraction 0.6, upscaling performed during history matching)

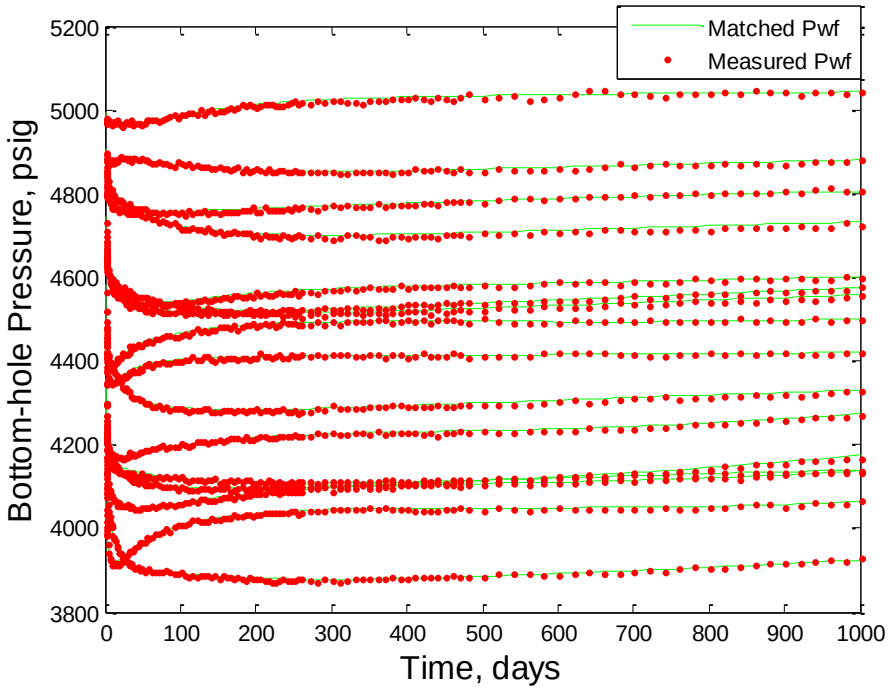

Figure 5.70: Match to measured bottom-hole pressure in all producers for the 64 x 64 reservoir system (wavelet fraction 0.4, upscaling performed during history matching)

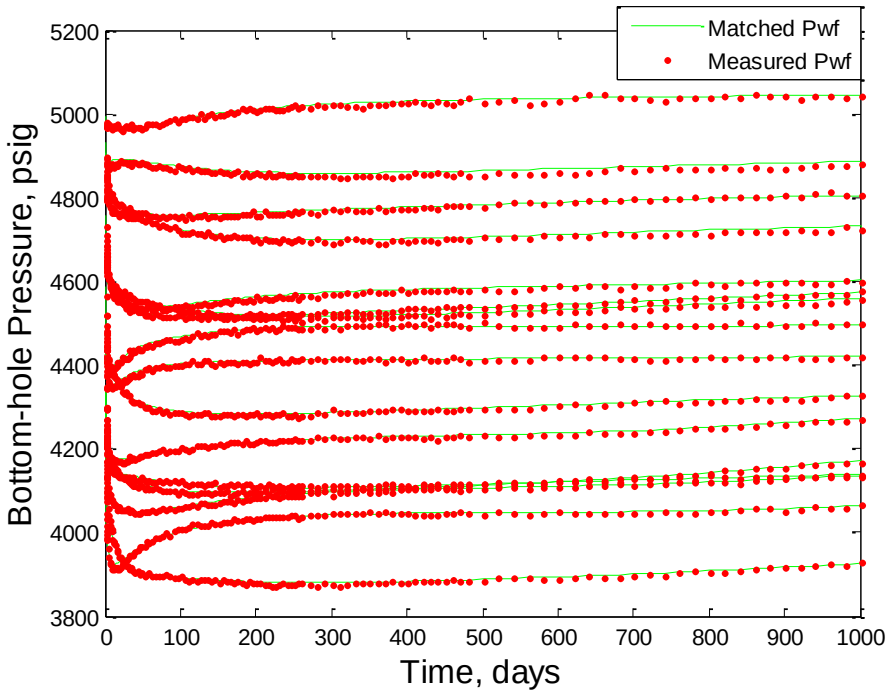

Figure 5.71: Match to measured bottom-hole pressure in all producers for the 64 x 64 reservoir system (wavelet fraction 0.25, upscaling performed during history matching)

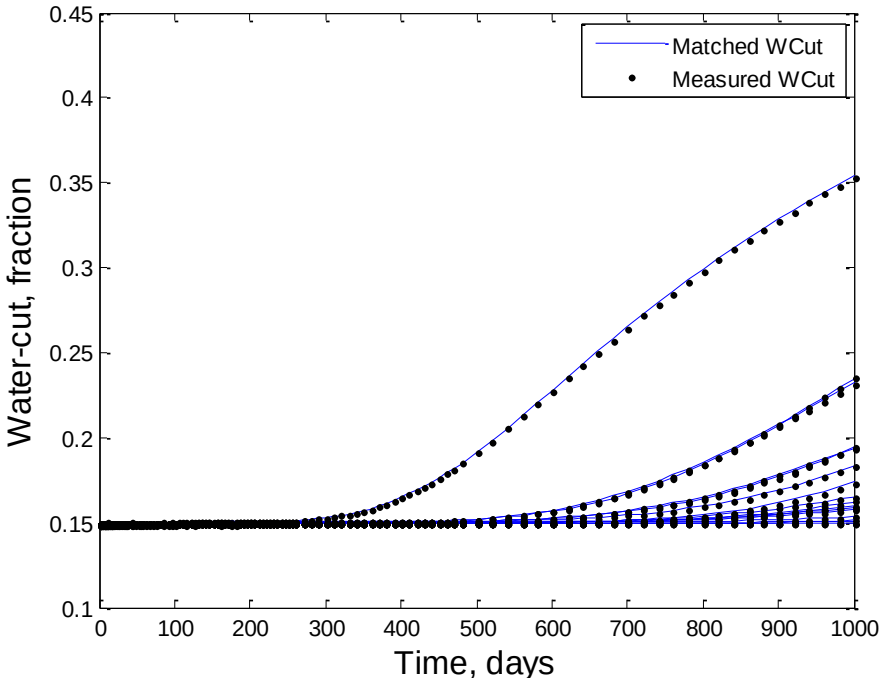

Figure 5.72: Match to water-cut in all producers for the 64 x 64 reservoir system (wavelet fraction 0.6, upscaling performed during history matching)

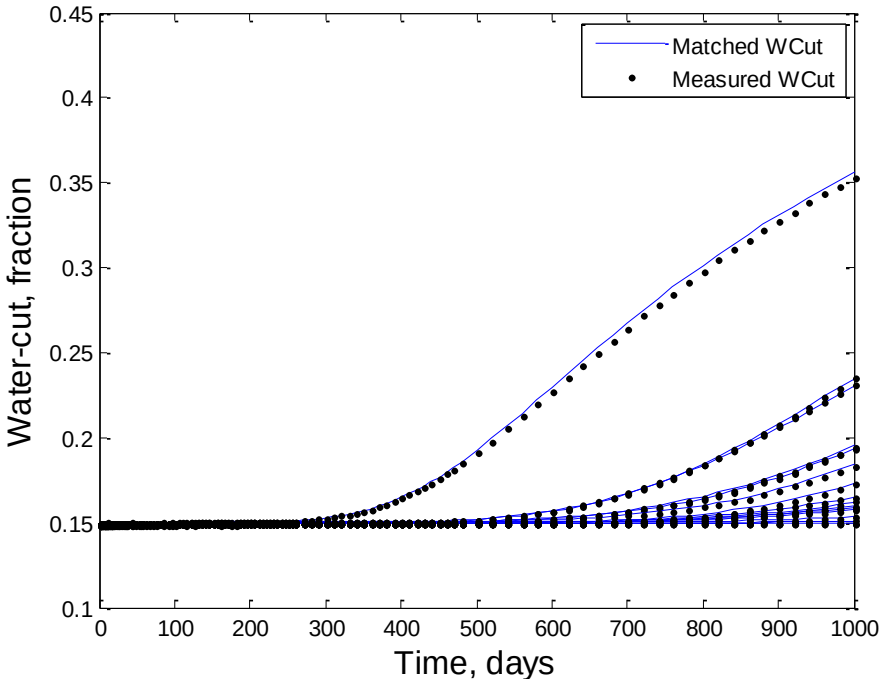

Figure 5.73: Match to water-cut in all producers for the 64 x 64 reservoir system (wavelet fraction 0.4, upscaling performed during history matching)

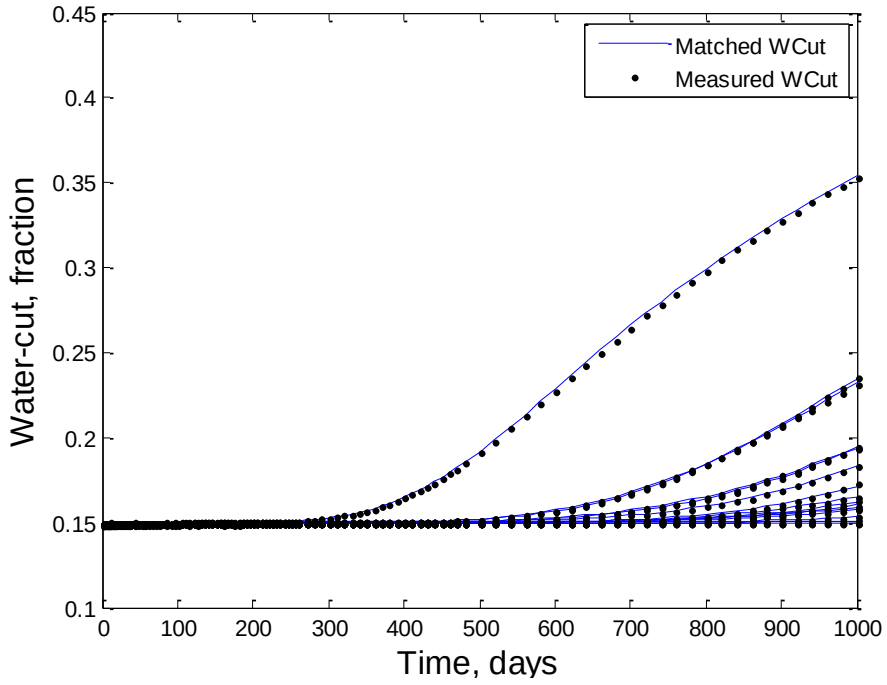

Figure 5.74: Match to water-cut in all producers for the 64 x 64 reservoir system (wavelet fraction 0.25, upscaling performed during history matching)

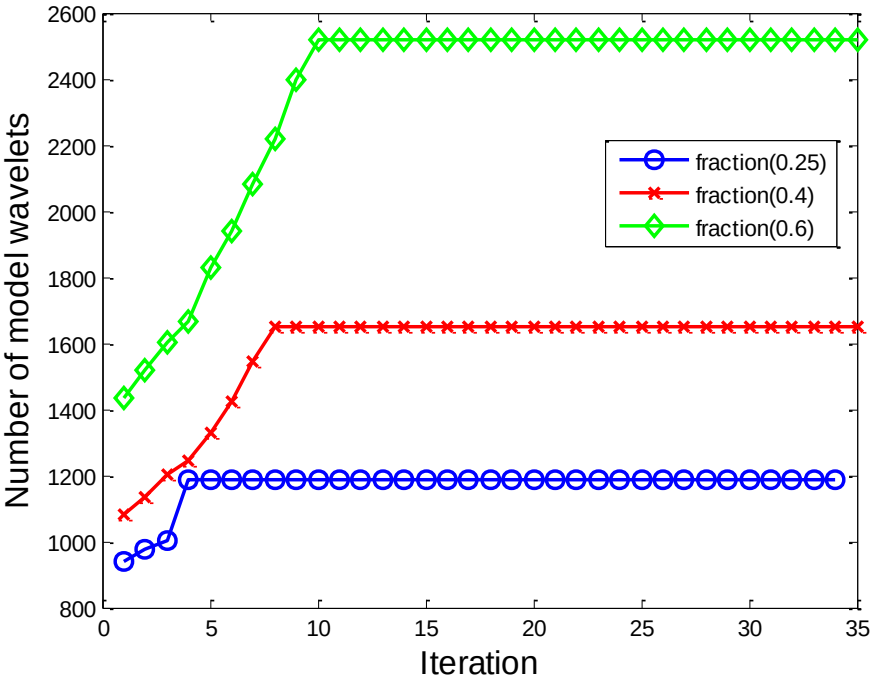

Figure 5.75: Trend of wavelet coefficients for the 64 x 64 reservoir system (all fractions, upscaling performed during history matching)

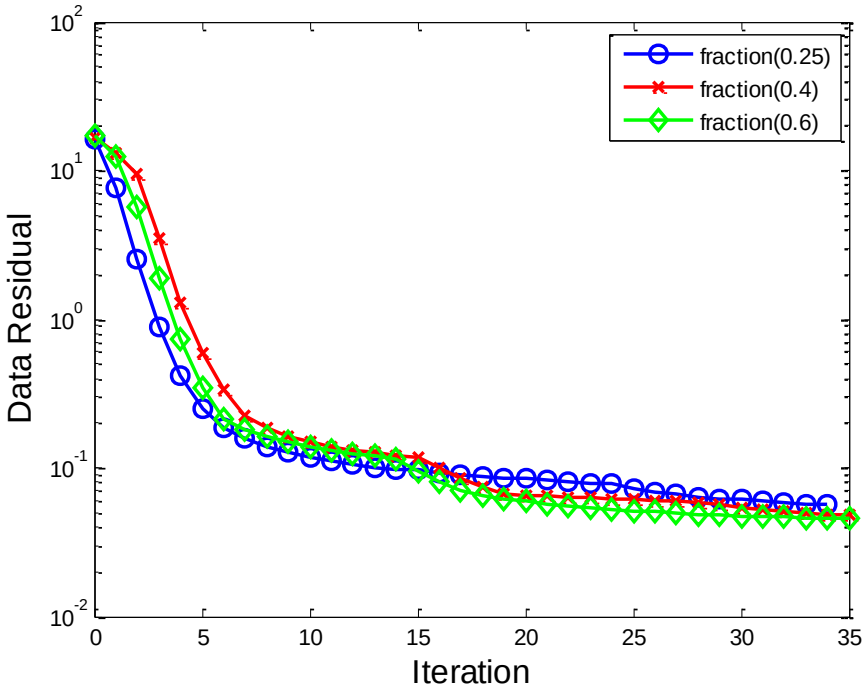

Figure 5.76: Data residual for the 64 x 64 reservoir system (all fractions, upscaling performed during history matching)

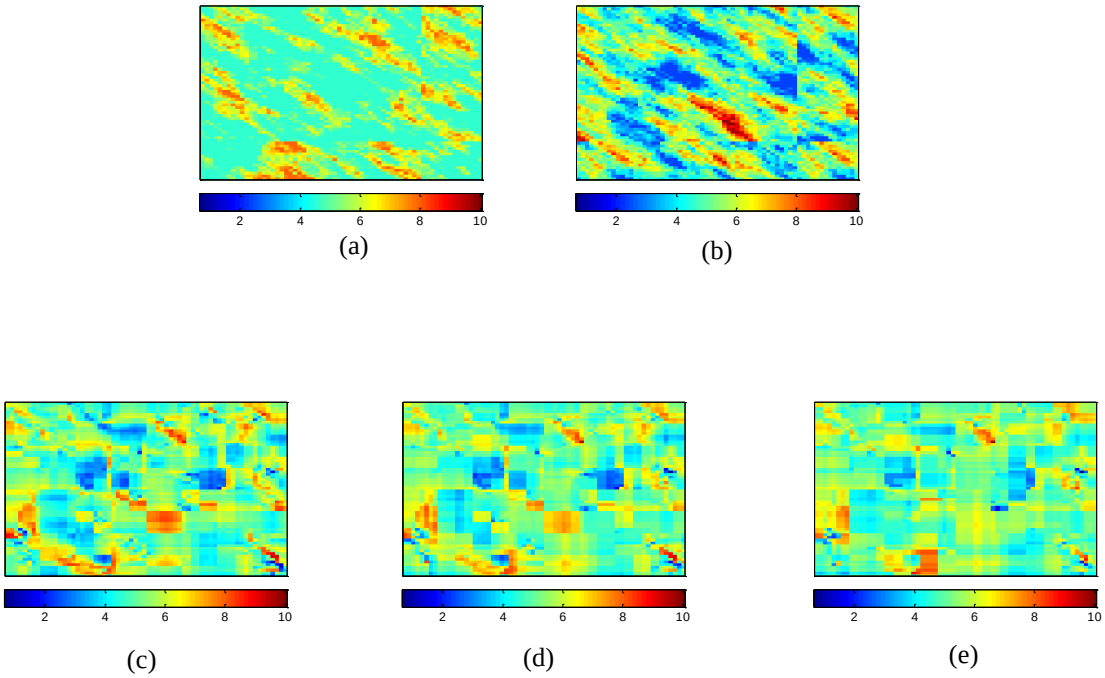

Figure 5.77: *log* permeability distribution for the 64 x 64 reservoir system (a) true (b) initial guess (c) estimate of wavelet fraction 0.6 (d) estimate of wavelet fraction 0.4 (e) estimate of wavelet fraction 0.25 (upscaling performed during history matching)

Future Prediction

One scenario has been considered in which the permeability field obtained after history matching is used to predict the future performance. The case is such that permeability distributions from fine-scale match and upscale match are selected (result of same fraction of 0.4 has been considered for both cases), and this distribution is used to run the forward model in order to perform prediction for 500 days after the time till which we have history matched. The injection pressure obtained from both the fine-scale and upscaled forward model is presented in Figure 5.78, while the pressure of production wells is shown in Figure 5.79.

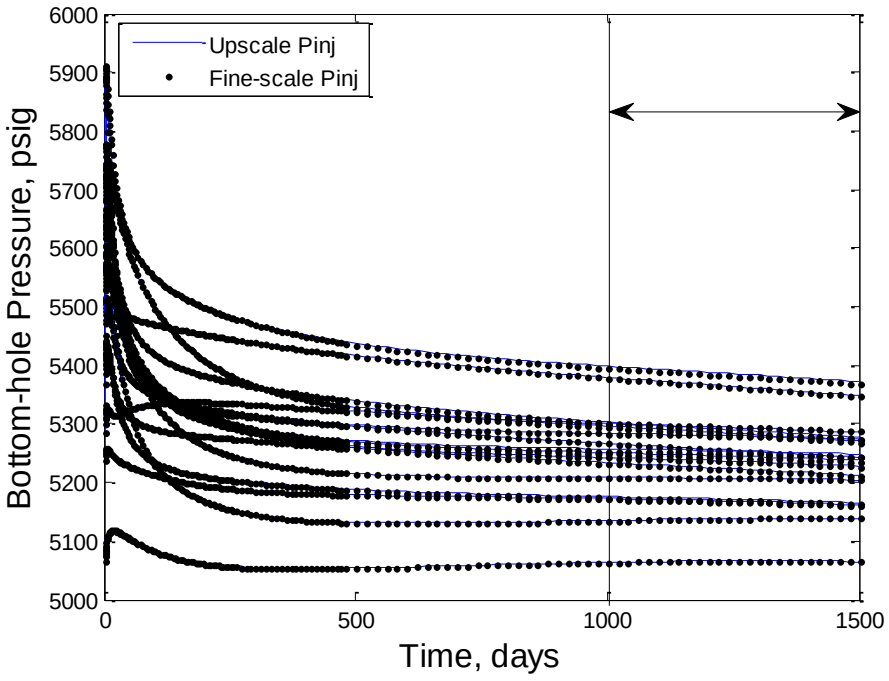

Figure 5.78: Comparison of fine-scale and upscale prediction for pressure of injectors (64 x 64 reservoir system)

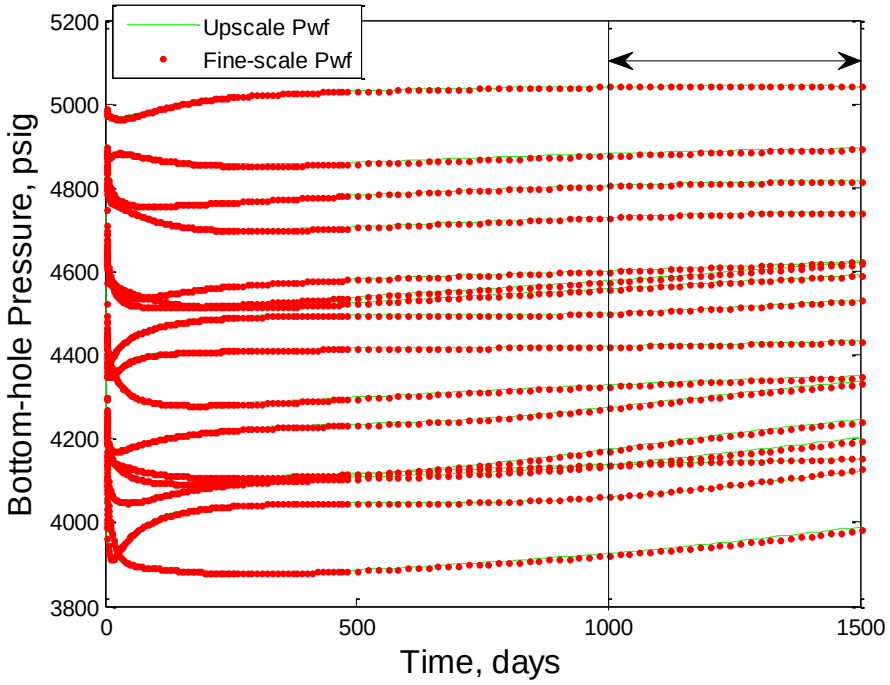

Figure 5.79: Comparison of fine-scale and upscale prediction for pressure of producers (64 x 64 reservoir system)

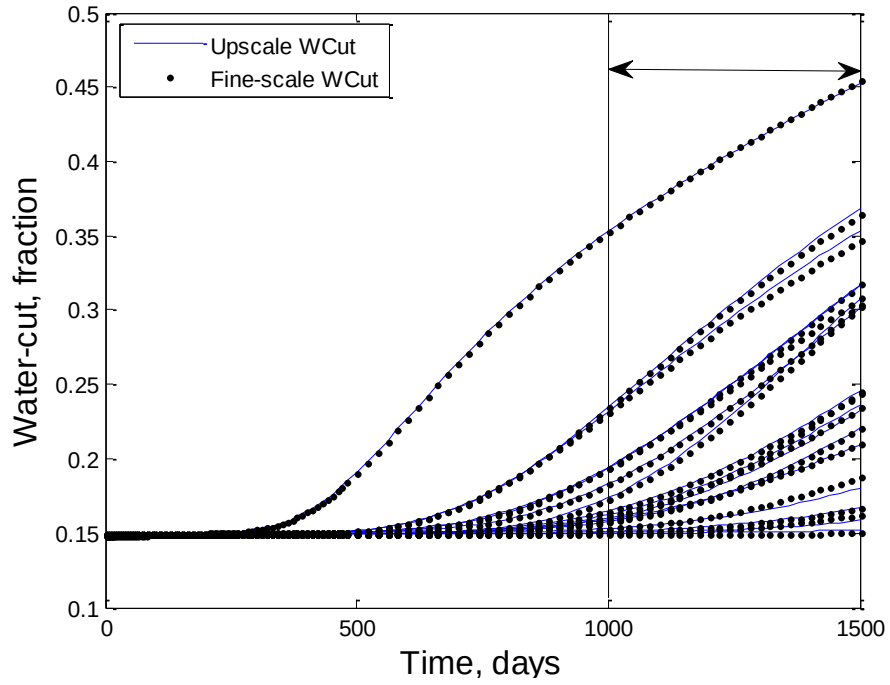

Figure 5.80: Comparison of fine-scale and upscale prediction for water-cut (64 x 64 reservoir system)

The time region of prediction is from 1000 to 1500 days and is identified separately in the figures. It can be observed that an excellent match is obtained for almost all the pressure curves from both fine-scale and upscaled forward model. Trend of water-cur curves from both models is given in Figure 5.80. In this case, we can observe the difference in prediction from both models. The match is not excellent; however we may say that it is acceptable.

5.3 Analysis and Summary

The fine-scale history matching almost provides the same results as presented in the earlier work (Awotunde, 2010). In comparison, the results obtained in this work with history matching using upscaling are acceptable and almost as good as those from fine-scale model. Also, the upscaling methodology used in this work is more efficient in terms of computation time and storage than the one presented in Awotunde and Horne (2012).

We have run the scenarios considering wavelet fractions of 0.6, 0.4 and 0.25. However we have also tried to perform the history matching using wavelet fraction lower than 0.25, but the resulting permeability distribution poses a problem. The heterogeneous permeability distribution with some homogeneous patches that we obtain from sensitivity-based model reduction results in some large upscaled grid blocks with few individual (fine-scale) grid blocks being left out within them. Thus we obtain a large upscaled grid block with few fine-scale grid blocks that are within it but cannot be combined because of different permeability. This results in a pattern having few fine-scale grid blocks within a large upscaled grid block; which is practically; not possible. The other issue comes in the calculation of centroid for such a grid block, because for

centroid the vertices of the grid block should be arranged in clockwise or counter-clockwise order. However in such a grid block there will be additional vertices due to grid blocks that exist within the large grid block and these vertices of fine grids will only be connected to each other but not with the vertices of the upscaled grid block.

For this reason, we have not performed inverse modeling with fractions less than 0.25.

CHAPTER 6

CONCLUSIONS AND RECOMMENDATIONS

6.1 Conclusions

This research work presents the sensitivity-based approach for upscaling the reservoir system. In an earlier work, fine-scale history matching has been performed using wavelets and reduced sensitivity matrix (Awotunde, 2010). The prime objective was to develop an upscaled simulator that is based on the homogeneous structure obtained from sensitivity-based model space reduction during parameter estimation. In upscaling the reservoir model, two constraints were considered; the first in which all grid blocks are combined during the process of upscaling except the grid blocks having wells in them, while in the second constraint the grid blocks having wells and also the grid blocks that have an interaction with the well grid blocks are not merged during upscaling. The following conclusions can be drawn from the results obtained during this work:

1. A good match is obtained for all the fine-scale history matching cases, as was established in earlier research (Awotunde, 2010; Awotunde and Horne, 2010).
2. During upscaling, combining the grid blocks that are adjacent to the well grid blocks does not provide good results. This is evident from the fact the Constraint 2 has provided better results than Constraint 1.
3. The coupling of upscaling can be done with reduced data and model parameters (reduction performed using wavelets) for the purpose of reservoir parameter estimation.

4. The sensitivity-based upscaling during history matching provides reasonable results with sufficient reduction in computation time as compared to fine-scale inverse analysis.
5. It was observed that the results from all three fractions (0.6, 0.4 and 0.25) were reasonably good. However results from 0.25 were beginning to show some slight deviation from the true results, indicating that further reduction may lead to larger deterioration in the performance of the algorithms.
6. It was observed that fine-scale results are just slightly better than the upscaled results for the cases considered.

6.2 Recommendations

Few recommendations that are proposed for future studies:

1. Two-dimensional reservoir systems have been considered in this work; however the method can be performed on three-dimensional reservoirs in future.
2. Different data and model space thresholding techniques can be used and compared.
3. One scenario has been considered with different mobility in this work, however various data can be used for relative permeability and reliability of the matching can be analyzed.
4. The work can be extended for three-phase flow and compositional simulation.

References

1. Anterion, F., Eymard, R., and Karcher, B., "Use of Parameter Gradients for Reservoir History Matching", paper SPE 18433 presented at the 1989 SPE Symposium on Reservoir Simulation, Houston, February 6-8, 1989.

2. Athichanagorn, S., Horne, R. N., and Kikani, J. (2002). Processing and interpretation of long-term data acquired from permanent pressure gauges. *SPE Reservoir Evaluation & Engineering*, 5:384–391.

3. Awotunde, A. and Horne, R. N. (2008, 2011). A multiresolution analysis of the relationship between spatial distribution of reservoir parameters and time distribution of well-test data. Paper SPE 115795 presented at the SPE Annual Technical Conference and Exhibition, Denver, USA, 21-24 September, 2008. SPE Journal, 2011.

4. Awotunde, A. (2010). *Relating Time Series in Data to Spatial Variation in the Reservoir Using Wavelets*. PhD thesis, Stanford University.

5. Awotunde, A. and Horne, R. N. (2010). Multidimensional reservoir description and data integration using time-space wavelet analysis. Paper SPE 133869 presented at the SPE Annual Technical Conference and Exhibition, Florence, Italy, 19-22 September, 2010.

6. Awotunde, A. and Horne, R. N. (2011). A wavelet approach to adjoint state sensitivity computation for steady state differential equations. *Water Resources Research*, Vol. 47, published 1 March, 2011.

7. Awotunde, A. and Horne, R. N. (2010, 2012). An improved adjoint sensitivity computation for multiphase flow using wavelets. Paper SPE 133866 presented at the SPE Annual Technical Conference and Exhibition, Florence, Italy, 19-22 September, 2010. SPE Journal, 2012.

8. Bissel, R., Sharma, Y., and Killough, J. E. "History Matching Using the Method of Gradients: Two Case Studies," paper SPE 28590 presented at the SPE Annual Technical Conference and Exhibition, New Orleans, LA, 25-28 September, 1994.

9. Bissel, R., "History Matching a Reservoir Model by the Positioning of Geological Objects", paper presented at the 5th European Conference on the Mathematics of Oil Recovery, Mining University, Leoben, Austria, September 3-6, 1996.

10. Carrera, J. and Neuman, S. P. (1986). Estimation of aquifer parameters under transient and steady state conditions: 1. maximum likelihood method incorporating prior information. *Water Resources Research*, 22:199–210.

11. Carter, R. D., Kemp, L. F., Piece, A. C., and Williams, D. L. (1974). Performance matching with constraints. *SPE Journal*, 14:187–196. Trans., AIME 257.

12. Chan, K. and Fu, A. W. (1999). Efficient time series matching by wavelets. In *Proceedings of the 15th International Conference on Data Engineering*.

13. Chang, S. G., Yu, B., and Vertterli, M. (2000). Spatially adaptive wavelet thresholding with context modeling for image denoising. *IEEE Transactions on Image Processing*, 9.

14. Chavent, G. M., Dupuy, M., and Lemonnier, P. (1975). History matching by use of optimal theory. *SPE Journal*, 15:74–86.

15. Chen, W. H., Gavalas, G. R., Seinfeld, J. H., and Wasserman, M. L. (1974). A new algorithm for automatic history matching. *SPE Journal*, 14:593–608.

16. Chen, Y. and Durlofsky, L.J. (2006a). Adaptive local-global upscaling for general flow scenarios in heterogeneous formations. Transport in Porous Media 62 (2): 157–185.

17. Chen, Y., Durlofsky, L. J., Gerritsen, M., and Wen, X. H. (2003). A coupled local-global upscaling approach for simulating flow in highly heterogeneous formations. *Advances in Water Resources*, 26:1041–1060.

18. Chen, Y. and Li, Y. (2009). Local-global two-phase upscaling of low and transport in heterogeneous formations. *Multiscale Modeling & Simulation*, 8:125–153.

19. Chen, Y. and Wu, X. H. (2008). Upscaled modeling of well singularity for simulating flow in heterogeneous formations. *Computational Geoscience*, 12:29–45.

20. Chu, L., Reynolds, A. C., and Oliver, D. S. (1995). Computation of sensitivity coefficients for conditioning the permeability field to well-test pressure data. *In Situ*, 19:179–223.

21. Chu, L., Schatzinger, R. A., and Tham, M. K. (1996). Application of wavelet analysis to upscaling of rock properties. Paper SPE 36517 presented at the SPE Annual Technical Conference and Exhibition, Denver, 6-9 October, 1996.

22. Chui, C. K. (1992). *An Introduction to Wavelets*. Academic Press, San Diego, California.

23. Consonni, P., Thiele, M. R., Palagi, C. L., and Aziz, K. (1993). Flexible gridding techniques for coning studies in vertical and horizontal wells. Paper SPE 25563 presented at the Middle East Oil Show, Bahrain.

24. Darman, N. H., Sorbie, K. S., and Pickup, G. E. (1999). The development of pseudo functions for gravity-dominated immiscible gas displacements. Paper SPE 51941 presented at the SPE Reservoir Simulation Symposium, Houston, Texas, USA.

25. Datta-Gupta, A., Vasco, D.W. and Long, J.C.S. "Sensitivity and Spatial Resolution of Transient Pressure and Tracer Data for Heterogeneity Characterization", paper SPE 30589, presented at the 1995 SPE Annual Technical Conference and Exhibition, Dallas, October 22-25, 1995

26. Daubechies, I. (1992). *Ten Lectures on Wavelets*. SIAM-CBMS Series 61, Philadelphia, PA.

27. Ding, Y. (2004). Upscaling on distorted gridblocks for simulation of advanced wells. *Journal of Petroleum Science and Engineering*, 43:87–97.

28. Donoho, D. L. and Johnstone, I. M. (1994). Ideal spatial adaptation by wavelet shrinkage. *Biometrika*, 81:425–455.

29. Durlofsky, L. J., (1991). Numerical calculation of equivalent grid block permeability tensors for heterogeneous porous media. *Water Resources Research*, 27:699–708.

30. Durlofsky, L. J., Milliken, W. J., and Bernath, A. (2000). Scaleup in the near-well region. *SPE Journal*, 5:110–117

31. Durlofsky, L. J., (2005). Upscaling and gridding of fine scale geological models for flow simulation. In *Proceedings of the 8th International Forum on Reservoir Simulation*, Stresa, Italy.

32. Ekrann, S. and Dale, M. (1992). Averaging of relative permeability in heterogeneous reservoirs. In King, P., editor, *The Mathematics of Oil Recovery*. Cambridge University Press, Cambridge.

33. Fuhr, H. (2005). Wavelets. in Skriptzur gleichnamigen Vorlesung an der TU Munchen.

34. Gavalas, G. R., Shah, P. C., and Seinfeld, J. H. (1976). Reservoir history matching by bayesian estimation. *SPE Journal*, 16:337–350.

35. Gerritsen, M. and Lambers, J. (2008). Integration of local-global upscaling and grid adaptivity for simulation of subsurface flow in heterogeneous formations. *Computational Geosciences, 12:193-218*.

36. Gill, P. E., Murry, W., and Wright, M. H. (1981). *Practical Optimization*. Academic Press, New York.

37. Gómez-Hernández, J.J. and Journel, A.G. (1994). Stochastic Characterization of Gridblock Permeabilities. SPEFE 9 (2): 93–99. *SPE-22187-PA*.

38. Gomez-Hernandez, J. J., Sahuquillo, A., and E., C. J. (1998). Stochastic simulation of transmissitivity field conditioned to both transmissitivity and piezometric data, 1, the theory. *Journal of Hydrology*, 203:162–174.

39. Griva, I., Nash, S. G., and Sofer, A. (2009). *Linear and Nonlinear Optimization*. SIAM Press, Philadelphia, PA.

40. Guangming, S., Xiaoping, L., Licheng, J., and Wei, Z. (2002). Adaptive wavelet thresholding for time varying snr signal denoising. *IEEE Trans.*, IV.

41. Holden, L. and Lia, O. (1992). A tensor estimator for homogenization of absolute permeability. *Transport in Porous Media*, 8:37-46.

42. Holden, L. and Nielsen, B.F. (2000). Global upscaling of permeability in heterogeneous reservoirs: the output least squares (OLS) method. Transport in Porous Media 40 (2): 115–143.

43. Hui, M. (2005). *Upscaling of multiphase flow parameters for modeling near-well and miscible displacements*. PhD thesis, Stanford University.

44. Hui, M. and Durlofsky, L. J. (2005). Accurate coarse modeling of well-driven, high-mobility-ratio displacements in heterogeneous reservoirs. *Journal of Petroleum Science and Engineering*, 49:37–56.

45. Jacquard, P. and Jain, C. (1965). Permeability distribution from field pressure data. *SPE Journal*, 5:281–294. Trans., AIME 234.

46. Jansen, F. E. and Kelkar, M. G. (1997). Application of wavelets to production data in describing inter-well relationships. Paper SPE 38876 presented at the SPE Annual Technical Conference and Exhibition, San Antonio, Texas, 5-8 October, 1997.

47. Kind, M. V. and Quinteros, J. (2007). History-matched model validation based on wavelets methods. Paper SPE 108124 presented at the SPE Latin America and Caribbean Petroleum Engineering Conference, Buenos Aires, Argentina, 15-18 April, 2007.

48. King, M.J. and Mansfield, M. (1999). Flow Simulation of Geologic Models. SPEREE 2 (4): 351–367. *SPE Journal Paper 57469-PA*.

49. Landa, J.L. and Horne, R.N. "A Procedure to Integrate Well Test Data, Reservoir Performance History and 4-D Seismic Data Into a Reservoir Description", paper SPE 38653, presented at the 1997 SPE Annual Technical Conference and Exhibition, San Antonio, Texas, 5-8 October.

50. Landa, J.L. '*Reservoir Parameter Estimation Constrained to Pressure Transients, Performance History and Distributed Saturation Data*', Ph.D. dissertation, Stanford University, California, 1997.

51. Levenberg, K. (1944). A method for the solution of certain non-linear problems in least squares. *The Quarterly of Applied Mathematics*, 2:164–168.

52. Li, D., Beckner, B., and Kumar, A. (2001). A New Efficient Averaging Technique for Scaleup of Multimillion-Cell Geological Models. *SPE Journal Paper 72599*.

53. Li, S. and Petzold, L. (2004). Adjoint sensitivity analysis for time-dependent partial differential equations with adaptive mesh refinement. *Journal of Computational Physics*.

54. Lu, P. and Horne, R. N. (2000). A multiresolution approach to reservoir parameter estimation using wavelet analysis. Paper SPE 62985 presented at the SPE Annual Technical Conference and Exhibition, Dallas, USA, 1-4 October, 2000.

55. Lu, P. (2001). *Reservoir Parameter Estimation using Wavelet Analysis*. PhD thesis, Stanford University.

56. Mallat, S. (1989). A theory for multiresolution signal decomposition: The wavelet representation. *IEEE Trans. On Pattern Anal. and Mach Intel.*, II.

57. Mallat, S. (1999). *A Wavelet Tour of Signal Processing*. Academic Press, 2nd edition.

58. Marquardt, D. (1963). An algorithm for least-squares estimation of nonlinear parameters. *SIAM Journal of Applied Mathematics*, 11:431–441.

59. Michalak, A. M. and Kitanidis, P. K. (2004). Estimation of historical groundwater contaminant distribution using the adjoint state method applied to geostatistical inverse modeling. *Water Resources Research*, 40:1–14.

60. Moridis, G. J., Nikolaou, M., and You, Y. (1995). The use of wavelet transform in the solution of two-phase flow. Paper SPE 29144 presented at the Reservoir Simulation Symposium, San Antonio, 12-15 Feb., 1995.

61. Nakashima, T. (2009). *Near-well Upscaling for two and three-phase flows*. PhD thesis, Stanford University.

62. Nakashima, T. and Nomura, M. (2004). New analytical correction for multi-phase flow effect in near well regions of coarse-grid system. Paper SPE 87067 presented at the SPE Asia Pacific Conference on Integrated Modeling for Asset Management, Kuala Lumpur, Malaysia.

63. Nocedal, J. and Wright, S. J. (2006). *Numerical Optimization*. Springer-Verlag, 2nd edition.

64. Oliver, D. S. (1996). Multiple realizations of the permeability field from well test data. Paper SPE 27970 presented at the University of Tulsa Centennial Petroleum Engineering Symposium, Tulsa, Oklahoma, USA.

65. Panda, M. N., Mosher, C. C., and Chopra, A. K. (2000). Application of wavelet transforms to reservoir-data analysis and scaling. *SPE Journal*, 5:92–101.

66. Percival, D. B. (2006). Wavelet methods for time series analysis. A Short Course presented 9 to 13 October 2006 at the Centre for Mathematical Sciences, Lund University, Lund, Sweden.

67. Pickup, G.E., Jensen, J.L., Ringrose, P.S., and Sorbie, K.S. (1992). A method for calculating permeability tensors using perturbed boundary conditions. Proc., European Conference on the Mathematics of Oil Recovery, Delft, The Netherlands, 17-19 June, 1992.

68. Plessix, R. E. (2006). A review of adjoint-state method for computing the gradient of a functional with geophysical applications. *Geophysical Journal International*, 167:495–503.

69. Reynolds, A. C., He, N., Chu, L., and Oliver, D. S. (1996). Reparameterization techniques for generating reservoir descriptions conditioned to variograms and well-test pressure data. *SPE Journal*, pages 413–426.

70. Ringrose, P. S. (2007). Myths and Realities in Upscaling Reservoir Data and Models. Paper SPE 106620 presented at the SPE Europec/EAGE Annual Conference and Exhibition, London, United Kingdom, 11-14 June, 2007.

71. Sahni, I. (2006). *Multiresolution Parameterization and Partitioning of Model Space for Reservoir Characterization*. PhD thesis, Stanford University.

72. Sahni, I. and Horne, R. N. (2005). Multiresolution wavelet analysis for improved reservoir description. Paper SPE Journal 87820.

73. Sahni, I. and Horne, R. N. (2004, 2006). Generating multiple history-matching reservoir-model realizations using wavelets. Paper SPE 89950 presented at the SPE Annual Technical Conference and Exhibition, Houston, USA, 26-29 September, 2004. SPE Journal, 2006.

74. Sahni, I. and Horne, R. N. (2006). Stochastic history matching and data integration for complex reservoirs using a wavelet-based algorithm. Paper SPE 103107 presented at the SPE Annual Technical Conference and Exhibition, Texas, USA, 24-27 September, 2006.

75. Salazar, M. O. and Villa, J. R. (2007). Permeability upscaling techniques for reservoir simulation. Paper SPE 106679 presented at the SPE Latin America and Caribbean Petroleum Engineering Conference, Buenos Aires, Argentina, 15-18 April, 2007.

76. Shah, P. C., Gavalas, G. R., and Seinfeld, J. H. (1978). Error analysis in history matching: The optimal level of parameterization. *SPE Journal*, 18:219–228.

77. Shi-Yi, Z. and Xiao-Gang, L. (2007). Analyzing transient pressure from permanent downhole gauges (pdg) using wavelet method. Paper SPE 107521 presented at the Europec/EAGE Annual Conference and Exhibition, London, 11-14 June, 2007.

78. Soliman, M. Y., Ansah, J., Stephenson, S., and Mandal, B. (2003). Application of wavelet transform to the analysis of pressure-transient data. *SPE Reservoir Engineering & Evaluation*, page 89.

79. Stephen, K. D., Pickup, G. E., and Sorbie, K. S. (2001). The local analysis of changing force balances in immiscible incompressible two-phase °ow. *Transport in Porous Media*, 45:63–88.

80. Sun, N., Sun, N.-Z., Elimelech, M., and Ryan, J. N. (2001). Sensitivity analysis and parameter identifiability for colloid transport in geochemically heterogeneous porous media. *Water Resources Research*, 37:209–222.

81. Sun, N.-Z. and Sun, A. Y. (2005). *Encyclopedia of Hydrological Sciences - 156: Inverse Methods for Parameter Estimations*. John Wiley & Sons, Ltd.

82. Sun, N.-Z. and Yeh, W. G. (1985). Identification of parameter structure in groundwater inverse problems. *Water Resources Research*, 21:869–883.

83. Sun, N.-Z. and Yeh, W. G. (1990a). Coupled inverse problems in groundwater modeling 1. sensitivity analysis and parameter identification. *Water Resources Research*, 26:2507–2525.

84. Sun, N.-Z. and Yeh, W. G. (1990b). Coupled inverse problems in groundwater modeling 2. identifiability and experimental design. *Water Resources Research*, 26:2507–2525.

85. Talukdar, M. S., Banu, H. A., Torsaeter, O. and Kleppe, J. (2000). Applicability and rate sensitivity of several upscaling techniques in fractured reservoir simulation. Paper SPE 59048 presented at the SPE International Petroleum Conference and Exhibition, Villahermosa, Mexico, 1-3 February, 2000.

86. Tan, T. B. and Kalogerakis, N. "A Fully Implicit, Three-Dimensional, Three-Phase Simulator with Automatic History-Matching Capability," paper SPE21205 presented at the 1991 SPE 11th Symposium on Reservoir Simulation, Anaheim, CA, February, 17-20.

87. Tang, Y. N., Chen, Y. M., Chen, W. H., and Wasserman, M. L. (1989). Generalized pulse-spectrum technique for 2-d and 2-phase histroy matching. *Applied Numerical Mathematics*, 5:529–539.

88. Thiele, M.R., Batycky, R.P., and Blunt, M.J., "A Streamline-Based 3D Field-Scale Compositional Reservoir Simulator," paper SPE 38889 presented at the 1997 SPE Annual Technical Conference and Exhibition held in San Antonio, Texas, October 5-8, 1997.

89. Vasco, D.W., Yoon, S., and Datta-Gupta, A., "Integrating Dynamic Data into High-Resolution Reservoir Models Using Streamline-Based Analytic Sensitivity Coefficients," paper SPE 49002 presented at the 1998 SPE Annual Technical Conference and Exhibition, New Orleans, Louisiana, September 27-30, 1998.

90. Wallstrom, T. C., Christie, M. A., Durlofsky, L. J., and Sharp, D. H. (2002). Effective flux boundary conditions for upscaling porous media equations. *Transport in Porous Media*, 46:139–153.

91. Wasserman, M. L., Emanuel, A. S., and Seinfeld, J. H. (1975). Practical application of optimal-control theory to history-matching multiphase simulator models. *SPE Journal*, 15:347–355.

92. Wen, X., Deutsch, C. V., and Cullick, A. S. (1998a). High-resolution reservoir models integrating multiple-well production data. *SPE Journal*, 3:344–355.

93. Wen, X., Deutsch, C. V., and Cullick, A. S. (1998b). Integrating pressure and fractional flow data in reservoir modeling with fast streamline-based inverse method. Paper SPE 48971 presented at the SPE Annual Technical Conference and Exhibition, New Orleans, USA, 27-30 September, 1998.

94. Wen, X. H., Chen, Y., and Durlofsky, L. J. (2006). Efficient 3D Implementation of Local-Global Upscaling for Reservoir Simulation. *SPE Journal Paper 92965*.

95. Wen, X. H., Durlofsky, L. J., and Edwards, M. G. (2003). Use of border regions for improved permeability upscaling. *Mathematical Geology*, 35:443-453.

96. White, C.D. and Horne, R.N. (1987). Computing Absolute Transmissibility in the Presence of Fine-Scale Heterogeneity. Paper SPE 16011 presented at the SPE Symposium on Reservoir Simulation, San Antonio, Texas, 1-4 February, 1987.

97. Wu, X.H., Efendiev, Y.R., and Hou, T.Y. (2002). Analysis of upscaling absolute permeability. Discrete and Continuous Dynamical Systems, Series B 2: 185–204.

98. Yeh, W. (1986). Review of parameter identification procedure in ground water hydrology. *Water Resources Research*, 22:95–108.

99. Yunowo, I. P., Susanto, A., and Soesianto, K. (2005). Application of adaptive wavelets to improve computational performance of krigging. Paper SPE 93197 presented at the Asia Pacific Oil and Gas Conference and Exhibition, Jakarta, Indonesia, 5-7 April, 2005.

100. Zhang, P., Pickup, G. E., and Christie, M. A. (2008). A new practical method for upscaling in highly heterogeneous reservoir models. *SPE Journal*, 13:68–76.

Vitae

Name	**:**	SAAD MEHMOOD
Nationality	**:**	PAKISTANI
Date of Birth	**:**	August 05, 1987
Email	**:**	mehmood.saad@hotmail.com
Address	**:**	L-2394, Block II, Scheme 3, Sector 14A, Metroville III, Gulshan-e-Iqbal, Karachi
Academic Background	**:**	**December 2013 – MS (Petroleum Engineering)** King Fahd University of Petroleum & Minerals Dhahran, Saudi Arabia **May 2013 – 4th Scientific Conference, Makkah** First Prize for Research Paper in Poster Competition (Engineering Graduates Category) **December 2008 – BE (Petroleum Engineering)** NED University of Engineering & Technology Karachi, Pakistan